Distribution Agreement

In presenting this thesis or dissertation as a partial fulfillment of the requirements for an advanced degree from Emory University, I hereby grant to Emory University and its agents the non-exclusive license to archive, make accessible, and display my thesis or dissertation in whole or in part in all forms of media, now or hereafter known, including display on the world wide web. I understand that I may select some access restrictions as part of the online submission of this thesis or dissertation. I retain all ownership rights to the copyright of the thesis or dissertation. I also retain the right to use in future works (such as articles or books) all or part of this thesis or dissertation.

Signature: _____

Joshua A. Owens _____ 7/1/2021 _____
Name Date

Microbiome-driven rewiring of host immunity and metabolism

By

Joshua Aaron Owens
Doctor of Philosophy

Graduate Division of Biological and Biomedical Sciences
Immunology and Molecular Pathogenesis

Rheinallt Jones
Advisor

Timothy Denning
Committee Member

Curtis Henry
Committee Member

Haydn Kissick
Committee Member

Jacob Kohlmeier
Committee Member

Accepted:

Lisa A. Tedesco, Ph.D.
Dean of the James T. Laney School of Graduate Studies

Date

Microbiome-driven rewiring of host immunity and metabolism

By
Joshua Aaron Owens
B.S., Lipscomb University, 2016

Advisor: Dr. Rheinallt Jones
PhD, University of Wales, Bangor

An abstract of
A dissertation submitted to the Faculty of the
James T. Laney School of Graduate Studies of Emory University
in partial fulfillment of the requirements for the degree of
Doctor of Philosophy in the Graduate Division of Biological and Biomedical Sciences
Immunology and Molecular Pathogenesis
2021

Abstract

Microbiome-driven rewiring of host immunity and metabolism
By Joshua Aaron Owens

The human microbiome contains trillions of prokaryotic cells existing in symbiosis with the human host. This relationship has long thought to be neutral or commensal, but recent studies suggest that this relationship is dynamic with far-reaching effects within the human host. Here, we show new evidence that the microbiome and specifically *Lactobacillus rhamnosus* GG is capable of inducing CD8 T-cells. This induction of CD8 T-cells is through a novel toll-like receptor 2 and dendritic cell axis. Utilizing this induction, we can reduce colonic tumor burden in a CD8 T-cell dependent manner. Additionally, we analyzed the small metabolites coming from the gut and the gut microbiome and discovered a novel microbial metabolite known as delta-valerobetaine. We determined that delta-valerobetaine is capable of inhibiting fatty-acid oxidation through depletion of the free fatty acid shuttle molecule, carnitine. Germ-free mice normally lack this molecule and are resistant to obesity from a high fat diet. When we gave physiologically relevant levels of delta-valerobetaine to germ-free mice, it sensitized them to weight gain and obesity on a high fat diet. Furthermore, delta-valerobetaine administration to normal, conventional mice was able to exacerbate the obesity phenotype in these mice compared to controls. In humans, levels of delta-valerobetaine are higher in obese individuals and correlates with increased visceral adipose tissue as well as severity of hepatic steatosis. Altogether, we show that the microbiome can exert beneficial effects on the mucosal immune response to aid in the reduction of tumor burden but also can exert detrimental effects on fatty acid metabolism resulting in increased obesity.

Microbiome-driven rewiring of host immunity and metabolism

By
Joshua Aaron Owens
B.S., Lipscomb University, 2016

Advisor: Dr. Rheinallt Jones
PhD, University of Wales, Bangor

A dissertation submitted to the Faculty of the
James T. Laney School of Graduate Studies of Emory University
in partial fulfillment of the requirements for the degree of
Doctor of Philosophy in the Graduate Division of Biological and Biomedical Sciences
Immunology and Molecular Pathogenesis
2021

Acknowledgements

First and foremost, I would like to thank my family and especially my wife, Erin Owens, for all the support and encouragement over the course of my graduate career. I firmly believe that I would not have made it without her support. Thank you for helping during qualifying exams and listening when I need to vent about the struggles of the lab. Hopefully, I taught you a little bit of science.

Next, I would like to thank all the members of the Jones Lab and the Neish Lab. Every single one of you helped me to become the scientist and the person that I am today. Most importantly, I want to thank Dr. Bejan Saeedi who provided tremendous help, insight, and laughs as we worked through graduate school together. His friendship and mentorship are something I will always cherish and impacted my views on mentorship and the laboratory environment. Additionally, I would like to thank Dr. Ken Liu for all his help and guidance for chapter 3 of this thesis.

Finally, I would like to thank all the members of committee for their insight and encouragement as we progressed through my projects. Above all, I would like to thank Dr. Rheinallt Jones who took me in as his first graduate student. As an advisor, Dr. Jones always had my back and always fought for my advancement. I am deeply honored that I got to work in his laboratory.

This was, by no means, a one-person endeavor. There are countless other people I could thank specifically. I am extremely thankful for this opportunity to switch from a consumer of knowledge to being a producer of knowledge.

Table of Contents

Chapter 1:

Introduction

This introductory chapter serves as a conceptual framework for understanding how the gut microbiome may regulate host physiology. Indeed, numerous studies show how the gut microbiome has been linked to a myriad of diseases including but not limited to obesity, metabolic disorders, cancer, and inflammatory bowel disease. However, the causative molecular mechanisms and functional elements underlying these correlative links are not well understood. In this introductory chapter, a detailed review of the gut microbiome is presented to illustrate how the microbiome can affect host physiology to impact different disease states. Elucidating the causative mechanisms of the microbiome on host physiology remains a critical need as the knowledge of these mechanisms may contribute to new therapeutic options.

1.1 The Microbiome Revolution

The microbiome has been under intense investigation in recent years due to its pronounced effects on a multitude of tissues and diseases in the host. Before this, the microbiome was defined as mere commensals which literally translates from Latin to “at the table”. Because of this, the microbiome was generally assumed to fulfill a mostly non-necessary scavenger function. However, there has been a history of recognition for certain biochemical and biological processes of the gut microbiota such as the metabolism of bile acids and absorption of fat-soluble vitamins. In the past, human pathologists did display a small premonition that the multitude of organisms residing in the gut must be contributing to additional biological functions.

Now, the scientific community has realized the vast array of systemic effects on biology and pathology that are known, correlated, or suggested to be influenced by our collective microbiota. The human microbiome consists of a plethora of different microbial communities colonizing all epithelial surfaces including the gastrointestinal tract, skin, and oropharyngeal-, pulmonary-, and genitourinary- derived surfaces.[1] By any metric, the current interest and number of publications on the microbiome must be deemed a revolution. Indeed, interest in the gut microbiome as a potential therapeutic source is seen through the amount of publications in both the scientific and lay press on the utility of both probiotic and prebiotic interventions.[2] This explosive interest in the microbiome began through advances that lowered the cost of sequencing and increased the availability of sophisticated analytical pipelines. These advances coincided with a vast number of publications from 2005-2010 that showed descriptive data that defined numbers, diversity, and overall microbial community structure in a

plethora of biological and environmental settings.[3] The era of microbiome correlation began, and an almost absurd number of publications illustrated differences in the gut microbiome and many different clinical and pathological diseases.[4] The original cost of sequencing for the human genome cost around 300 million dollars. However, costs have continued to plummet for sequencing platforms and now a human genome can be sequenced for roughly 600 dollars. This dramatic drop in sequencing prices has extended to metagenomic approaches and these approaches have been able to dissect correlative data into finer phenotypic differences. Additionally, mass-spectrometry based metabolomic approaches have expanded and increased the realized impact of microbial influences. Like an iceberg, this may be just the tip of unrealized discoveries of the gut microbiome with investigations ongoing with the complex microenvironment that includes the virome and the mycome.

Additionally, another advance that allowed for identification of the full effects on the microbiome on host health was the advent of germ-free (GF) mouse husbandry methods.[5] This allowed scientists including immunologists, epithelial biologists, physiologists, etc. to analyze GF mice and document the aberrations in biological processes compared to their conventional or microbiome-replete counterparts.[6] These studies illustrated that the collective microbiome exerts influence on several biological systems including immune cell function and development, behavioral phenotypes, metabolic changes, etc.[7–10] Overall, GF and gnotobiotic, or systems with a known microbiota such as mice colonized with defined microbes, approaches have provided definitive experimental details into the interactions between the host and its microbiome.

Collectively, these advances and efforts have matured to the point that all the research and medical community have become fully accepting of the significant role that the microbiota play in host biology. Overall, this introduction will address the role of the microbiome in mucosal immunity, cancer, immunotherapy, metabolism, and metabolic disorders. This introduction will go beyond correlative effects of the microbiome and hypothesize potential causative mechanisms of the microbiome's impact on human health.

1.2 The origin of the microbiome

To truly elucidate the exact effects of the microbiome on the host is to understand the origins of the gut microbiome and its specific composition.[11] The human and murine microbial community is composed of about one thousand species with the composition and density varying greatly along the gastrointestinal tract. Total prokaryotic cell numbers have been reported to reach around 10^{15} organisms which means that there is a ratio of almost 1:1 in terms of prokaryotic cells to eukaryotic cells. The composition of the gut microbiome changes with the host's age; and has its origins from the placenta, amniotic fluid, umbilical cord blood, and meconium being able to start colonization of the fetus *in utero*. The placental microbiota can affect the growth and survival of the fetus and various postnatal pathologies. Consequently, loss of exposure to these microbes and their products *in utero* may have long-term consequences for the development of immune-mediated disease in the offspring.[12,13] Interestingly, a recent study showed that fetal tissue can be colonized by a low amount of viable bacteria including *Lactobacilli* which can influence fetal dendritic cell and T-cell development and activation.[14]

However, this newly developing view is still hotly debated. This is because the uterus was considered to be sterile by medical professionals and is still taught in medical school lectures to be sterile.[15] Nevertheless, even if the womb is truly sterile and devoid of bacteria, that does not prove that bacterially-produced products are not present in the womb and by extension the fetus. However, it is not debated that during birth, there is a vertical transmission of the microbiome where newborns are colonized by the mother's vaginal microbes which mostly consists of *Lactobacillus* and *Prevotella*. These microbial taxa provide a critical foundation of the early gut microbiome as there are approximately 100 bacterial species at birth and this diversity will increase ten-fold through the course of maturation into adulthood.[16]

Conversely, caesarean section (c-section) newborns are first colonized by skin microbes such as *Staphylococcus* and *Corynebacterium.* Though the long-term consequences and the molecular mechanisms of being colonized with these skin microbes as opposed to vaginal microbes is still fully unknown, there are associations with c-section newborns showing increased incidence for some human diseases.[17,18] One disease that c-section newborns are at risk for is allergic disorders.[19] Many hypotheses have been put forward for this correlation but the exact molecular mechanisms remain to be elucidated. Interestingly, c-section newborns have an increased risk of developing acute lymphoblastic leukemia (ALL).[20] ALL occurs when too many immature immune cells are produced in the bone marrow which once again connects the immune response and development with colonization of microbes. Indeed, the observation that colonization of skin microbes as opposed to vaginal microbes such

as lactobacilli and *prevotella* spp. causes incorrect immune responses is intriguing and shows a link between the gut microbiome and the immune response at an early age.

Subsequently after birth, the ingestion of breast milk and perhaps even formula milk influences the colonization process as both *Lactobacillus* spp. and *Bifidobacterium* spp. can be cultured from breast milk.[21,22] Additionally, breast milk and formula milk is full of complex sugars that induce blooms in certain bacterial species and dramatically increases bacterial products in the host. This is due to the ability of bacteria to ferment different products of breast and formula milk.[23,24] Indeed, the fermentation process of lactose and the production of lactic acid from lactobacilli can induce the gut microbiome to produce bacterial products known as short-chain fatty acids (SCFAs).[9] The three major SCFAs include propionate, acetate, and butyrate. Butyrate is the preferred energy source of colonocytes accounting for up to 70% of their energy expenditure.[25] Additionally, butyrate can act as a histone deacetylase (HDAC) inhibitor. Through its inhibition of HDACs, butyrate can augment the chromatin and result in specific transcriptional changes depending on the cell type. For example, butyrate-induced HDAC inhibition in naïve T-cells can cause the differentiation of the cells into regulatory T-cells.[9,26] Indeed, SCFAs produced from breast milk, formula milk, or other dietary substrates can have other far ranging effects and effect many different disease states. This maturation process continues to around 2-3 years of age at which time the microbiome matures to the composition and complexity of an adult microbiome.[27] This mature microbiome does not readily change and takes interventions such as changes to diet or lifestyle, probiotic usage, or fecal microbiota transfer (FMT) to modify.

1.3 The gut microbiome and colonic health

As mentioned, gut colonization is fundamental for the complete tropism of both the small intestine (SI) and the colorectal tract. This important symbiotic relationship has been elucidated through utilizing broad-spectrum antibiotics and germ-free (GF) methodologies. Likened to genetic knockout models, these gnotobiotic models can help to show how the absence of bacteria can have negative consequences on the host. Importantly, these models illustrate the mostly positive complex system of interaction between the gut microbiome and the SI and colon. These interactions include but are not limited to mucus regulation, epithelial junctions, and intestinal stem cell turnover. However, though these effects may be beneficial in the absence of disease, microbial effects on these systems can prove detrimental under settings of colorectal cancer (CRC).

The first barrier between the host and the immense load of luminal bacteria is the mucus layer of the gastrointestinal tract. The mucus layer is composed of a multitude of mucin proteins with MUC2 being the most common mucin in the mucus layer.[28] These mucin proteins are produced by specialized cells known as goblet cells. Goblet cells produce mucins in mass and heavily glycosylate them to prevent degradation by proteases and give them gel-like qualities so that they can fulfill their role as a membrane protecting the epithelium. In the colon, the mucus layer can be divided into two layers: tight and loose layers. The tight mucus layer is mostly devoid of bacteria which serves to protect the stem cells.[29] However, this loose mucus layer provides a niche for certain bacteria called mucus-associated bacteria that differ from bacteria that are found in the lumen.

Mucus-associated bacteria such as *Akkermansia muciniphila* can be detrimental to the host depending on the host's diet. When given a diet that is low in fiber, *Akkermansia muciniphila* causes the degradation of the mucus layer. The thinning of the mucus layer increases the susceptibility and severity of the hosts to colitis, intestinal pathogens, and development of CRC.[30] Despite this negative effect by *Akkermansia muciniphila*, the microbiota is also paramount to the proper function of the mucus layer. For example, GF mice have a thinner mucus layer, have fewer goblet cells, and the mucus layer does not shed in the same manner as conventional mice. Each of these effects were restored when bacterial products were introduced to GF mice.[31] One such class of molecules produced by the microbiota are indoles. It has been shown that certain indoles such as indole-3-aldehyde can stimulate goblet cell differentiation and increase their production of mucus.[32] Altogether, the mucus layer protects the epithelium and gives a niche for certain bacteria that in turn regulate the mucus layer for both their benefit and the host's benefit. But, under settings where the balance is disrupted, these mucus-associated bacteria can aggravate colonic diseases.

Underneath the mucus layer, resides the epithelium which provides the second barrier between the immense bacterial burden and the host. This barrier is maintained by interlocking the epithelial cells through cell-cell interactions known as tight junctions. Tight junctions are composed of cytosolic proteins such as zonula occludins and integral membrane protein such as occludins and claudins. Together, these proteins act as gate keepers that allow only certain molecules to pass through the epithelial barrier in a paracellular fashion. However, as the epithelium is constantly turning over, this barrier is dynamic and constantly changing based off the current stimuli.

Similar to the mucus layer, the microbiota is critical for full barrier function as both GF mice and antibiotic-treated mice exhibit impaired tight junction functionality.[33,34] For example, microbial stimulation of toll-like receptor 2 (TLR2) which acts as a sensor of certain bacteria and their products can cause signaling events through protein kinase C (PKC). This induction of PKC causes increases in barrier resistance through redistribution of tight junction proteins such as zonula occludin-1 (ZO-1).[35] Likewise, certain *Escherichia coli* strains and *Bifidobacterium infantis* Y1 can influence levels of ZO-1 and ZO-2 causing increases to barrier resistance *in vitro*.[36,37] Additionally, certain lactobacilli species can increase barrier resistance *in vivo,* and in general, colonization of germ-free mice results in increased levels of claudins and occludins for increased barrier functionality.[34,38] Conversely, when the microbiome shifts away from a normal composition into dysbiosis, this dysbiotic microbiome can reduce barrier function, increase markers of inflammation in the serum, and drive tumorigenesis.[39] For example, the dysbiotic microbiome from CRC patients was administered to GF mice and was capable of driving tumorigenesis through altering barrier function which exacerbated a pro-inflammatory microenvironment.[40] Therefore, there is a complex relationship between certain microbial community structures and bacteria increasing barrier strength and other members of the microbiome that can alter barrier function for adverse effects.

Most importantly, the function of the mucus layer and the epithelial barrier is dependent on the proliferation and differentiation of intestinal stem cells (ISCs). ISCs repopulate the entirety of the intestinal tract every 2-4 days in mice and every 5-7 days in humans.[41,42] At the base of intestinal crypts, stem cells proliferate and begin to traverse up the crypt. As they traverse, they differentiate into specialized subsets of

cells depending on the stimuli present in the gut at that time. As mentioned above, this constant renewal allows for microbial interventions and the gut microbiome to have dynamic effects on epithelial biology and homeostasis. For example, metabolites produced specifically by the gut microbiome including short-chain fatty acids (SCFAs), lactate, and indoles discussed earlier in this chapter can have dramatic effects on ISC populations which can aid in normal intestinal homeostasis or drive cancer cell growth.

As mentioned, butyrate is the preferred energy source of differentiated colonocytes and metabolism of SCFAs improves epithelial barrier functionality and differentiation.[43] This efficient catabolism of butyrate may be to prevent high levels of butyrate from reaching the base of the crypts as ISC proliferation can be inhibited by butyrate.[44] However, though this reduction in ISC proliferation by butyrate can be beneficial in CRC.[45] Indeed, butyrate has been shown to reduce tumorigenesis as well as tumor cell proliferation through these effects.[46,47] Additionally, lactate is also produced by microbes and has been shown to be protective against colonic injuries and increase stem cell turnover.[48] As mentioned above, lactate can be fermented in butyrate which would also produce anti-tumor effects. Finally, indoles have been shown to activate the Aryl Hydrocarbon Receptor (AhR). Interestingly, depletion of AhR causes unchecked ISC proliferation which implies that indoles are important for maintaining the correct levels of ISC proliferation and there are some reports of indoles and tryptophan metabolism effects in CRC.[49,50] Therefore, metabolites from the gut microbiome tightly regulate ISC proliferation by a mix of both go and stop signals to maintain the tight homeostatic regulation of proliferating ISCs and can be therapeutic targets in the setting of CRC.

Altogether, the gut microbiome through bacterial products and metabolites functions to regulate the mucus layer, the underlying epithelial barrier, and the stem cell compartment. These studies support conclusions ascribing a vital role for the gut microbiome in normal homeostasis of the gut as well as during setting of CRC. However, each human individual is unique with specific genetics, diet, and lifestyle thereby resulting in each individual having a distinct microbiome community structure of their own.[27] As mentioned briefly, certain changes in an individual's microbiome may result in a condition known as microbial "dysbiosis" where a loss in critical symbiotic bacteria and a corresponding bloom in opportunist/pathobiont bacteria are observed.[51] Dysbiosis has been reported in diseases such as inflammatory bowel disease as well as CRC. Interestingly, dysbiosis usually causes low levels of inflammatory responses that are initiated by both the intestinal epithelium and the underlying immune cells that reside in the intestinal sub-mucosa. Not only is there an important role of the microbiome in regulating the epithelium but beyond the epithelium into the mucosal immune response.

1.4 The gut microbiome and mucosal immunity

In recent years, the importance of the gut microbiome as a master regulator of the immune response has begun to be realized. The gut microbiome is necessary for the full maturation of both local and systemic immune defenses, as well as to train the immune response for tolerance toward non-pathogenic agents. Importantly, many reports have shown the link between the microbiome and anti-tumor immune responses. These gut microbiome-specific effects on the mucosal immune response can be observed via broad-spectrum antibiotic usage as well as observing GF mice.[52,53]

For example, GF mice undergoing the Dextran sulfate sodium (DSS) azoxymethane (AOM) model of chemically-induced colorectal cancer have delayed onset of epithelial injury but still produce more tumors than conventional or microbiome-replete animals.[54] Furthermore, studies have illustrated that GF mice are highly susceptible to viral infections such as influenza, bacterial infections such as *Salmonella,* and models of colitis and CRC.[55,56,40] These differences between germ-free/antibiotic animals and microbiome-replete or conventional animals illustrate the robust ability of the microbiome and gut bacteria to modulate many host immune factors.

Many of these responses are due to the known fact that GF mice do not develop a normal immune system in terms of height of the mounted immune response and in terms of the specificity of their repertoire. Recently, some studies have delved into experiments in which mice were born GF and after weaning were allowed to acquire a normal adult mouse microbiome through a process known as conventionalization. This is usually accomplished through mixing of conventional mouse bedding into the cages, and because mice are coprophagic, they will consume the microbe-containing fecal pellets to acquire a microbiome. These ex-GF mice are still more susceptible to infections, colitis models, and tumor models illustrating the key role of gut colonization in early life for the full maturity of the intestinal tissue and the immune system.[57–59]

Immune responses and timelines have been extensively shown before by other studies. Here, we show evidence of the gut microbiome's involvement with innate cells and T-cells in the contexts of homeostatic conditions and cancer. The critical function of the microbiome and immune cells start with myelopoiesis in the bone marrow which is reduced in GF mice. This reduction in myelopoiesis causes increased susceptibility to

systemic bacterial infections.[60] This reduction has been correlated with TLR ligands as well as SCFAs but may begin even before birth as pregnant mice treated with antibiotics display reduced number of innate cells.[60–62] Additionally, the microbiota effects tissue-resident macrophages phenotypes though gene regulation by SCFAs that act as histone deacetylases to change the genetic profile of gut-resident macrophages.[63,64] Additionally, the pool of macrophages in the gut are constantly replenished and maintained due to signaling by the microbiome and that specific maturation and differentiation status is also imparted by the microbiome.[65,66]

These natural effects of the gut microbiome on macrophages can be targeted in bacterial intervention for positive effects in different disease models. Administration of the beneficial microbe, *Lactobacillus rhamnosus* GG (LGG), to mice activated gut-resident macrophages through TLR2 and reduced intestinal injury from radiation.[67] This appears to be common amongst many differ lactobacilli and bifidobacterial strains that activate macrophages in TLR-specific manners.[68–70] Activation of macrophages is critical for settings involving tumors. This is because macrophage activation functions in the clearing of tumor cells and activation of additional immune cells. Altogether, the microbiome, its products, and bacterial interventions can augment macrophage numbers, activation, and differentiation which can be beneficial in settings of colonic injury and CRC.

Another important innate cell subset are dendritic cells (DCs). Both SCFAs such as butyrate and retinoic acid, a vitamin A metabolite, can cause anti-inflammatory programming in gut mucosal DCs.[71–73] These anti-inflammatory properties are less dependent on the action of DCs themselves, but function by expanding the number of

regulatory T-cells (Tregs) in the gut mucosa. Though DC-mediated expansion of Tregs is beneficial in settings of colonic injury, increased numbers of Tregs can be detrimental in CRC. Indeed, reduction in butyrate has been shown to synergize with the effect of radiation treatment for CRC due to increased antigen presentation and CD8 T-cell activation by DCs.[74] This is of particular interest as the gut microbiome has been linked to immunotherapy responses.[75–77] Of note, the response rate appears to be due to microbiome-specific effects on DCs and T-cells.[78,79] However, there appears to be many mechanisms at play as to how the microbiome is regulating DCs and T-cells with a mix of SCFAs and other metabolites, TLRs, c-GAS-STING, and T-cell cross-reactivity.[26,78–82]

Moving beyond innate cells, the gut microbiome, depending on the specific stimuli, can expand almost all subsets of CD4 T-cells such as Th17s, Tregs, Th1s, and Th2s. GF mice are known to have little to no Th17s, lowered Tregs, and a Th1/Th2 imbalance. For example, members of the gut microbiome such as segmented filamentous bacteria (SFB) are known to adhere to the epithelium and cause the induction of Th17 CD4 T-cells.[83,84] This increase in Th17 cells and correspondingly Th17-driven inflammation has been painted as a negative ramification of the microbiome; however, depletion of the main Th17 cytokine, IL-17a, can exacerbate inflammation and inflammatory bowel disease.[85,86] In CRC, Th17 cells can be beneficial and help to reduce tumor burden.[87] These differing roles and benefits illustrates the fine-tuned role of the microbiome in regulating levels of Th17s for homeostasis and its potential role as a therapeutic in cancer.

Continuing, CD4 T-cells can also differentiate into the Th1 subset. Th1 cells produce cytokines that aid CD8 T-cell proliferation and activation. The bacterium,

Lactobacillus acidophilus has been shown to expand Th1s and their cytokines such as IFN-g and decrease Th2s and their cytokines such as IL-4 to increase survival in a breast tumor model.[88] This appears to be a common effect upon lactic acid bacteria as at least 10 strains were able to recapitulate this phenotype of expanding Th1 cytokines and decreasing Th2 cytokines.[89] Interestingly, Th1 cells aid CD8 T-cells and have been shown to correlate with better immunotherapy rates. This suggests that bacteria that increase levels of Th1s would exert greater anti-tumor immune responses and aid in immunotherapy.

Additionally, the gut microbiome can regulate Tregs through the production of the SCFA, butyrate. Butyrate acts as a histone deacetylase which cause increased transcriptional access of the FoxP3 promoter causing transcriptional changes of CD4 cells to differentiate into Tregs.[26,73] This effect can also be accomplished through the production of lactate by lactic acid bacteria through direct modulation of CD4 T-cell metabolism as well as lactate being bio-converted by other gut microbes into butyrate.[9,90] As mentioned, increased number of Tregs can be detrimental in settings of CRC but might depend on the specific stage of the tumor.[91] Therefore, the metabolites coming from the microbiome can have profound effects on the presence of Tregs and explains why GF mice have limited Tregs compared to conventional animals.

Until recently, the microbiome had not been shown to have effects on CD8 T-cells; however, studies are now reporting the dramatic effects of the microbiome on CD8 T-cells. Indeed, a recent study showed that a consortium of bacteria is able to expand IFN-g producing CD8 T-cells.[78] CD8 T-cells are vital for immunotherapy against tumors. Interestingly, the gut microbiome has been linked to immunotherapy response

rates. For example, several high impact publications have shown links between the community structure of the gut microbiome and whether patients with melanoma will respond to immunotherapy.[75–77] These studies did not propose a molecular mechanism describing how the microbiome may be increasing immunotherapy response rates but evidence suggests that it may be through expansion of CD8 T-cells.

This link between the gut microbiome and immunotherapy has led researchers to ask questions on how modification of the microbiome such as through the usage of antibiotics might exert effects in cancer and anti-tumor immune responses. For example, epidemiological studies have shown that long-term use of antibiotics during early and mid-adulthood increase the risk of colorectal adenoma development.[92,93] As previously mentioned, the gut microbiome is almost always a double-edged sword as there is also evidence that a subset of gut microbes can promote CRC. After surgical resection of CRC tumors, the gut microbiome in conjunction with a western style diet, or a diet containing high fat levels, has been shown to promote tumor growth.[94] Indeed, the most well-known bacteria that can increase tumorigenesis in CRC is *Fusobacterium nucleatum*. *F. nucleatum* has been shown to be the dominant bacterial strain within CRC tumors and can potentiate their growth and negatively impacts anti-tumor immune responses.[95–99] Therefore, in cases with *F. nucleatum*, antibiotics could be beneficial to the patient.

Another way to modulate the microbiome besides antibiotics is through the usage of beneficial bacteria known as ‘probiotics’. Probiotics represent the most common supplement therapy used during intestinal issues. In 2002, the joint Food and Agriculture Organization of the United Nations/World Health Organization (FAO/WHO)

worked together to define probiotics as "live microogranisms, which when consumed in adequate amounts, confer a health benefit on the host."[100] For immunotherapy, it has been shown that administration of certain Bifidobacterium strains as well as a consortium of different bacterial strains can improve anti-PD-1 and anti-CTLA-4 immunotherapy in melanoma.[78,79] For CRC, it has been shown that several strains of both Bifidobacterium and Lactobacilli can be beneficial in preventing CRC development.[101–103] However, little research exists examining the extent to which bacterial supplementation can modulate CRC tumors once established and whether these bacteria impact the anti-tumor immune response or immunotherapy rates. This raises the fundamental question of what the exact role of the microbiome is in orchestrating an anti-tumor immune response? Ideally, microbial interventions would exert a positive effect on CD8 T-cells. This induction of CD8 T-cells would not only drive anti-tumor immune responses but could potentially synergize with immunotherapy that is targeted to CD8 T-cells. **(Figure 1.1)** Some studies have hypothesized that the link between the microbiome and immunotherapy is not only through microbial recognition but through microbially-produced metabolites and microbially-induced changes to the metabolite pool. These changes to the metabolome are not only critical for cancer but for other important human diseases.

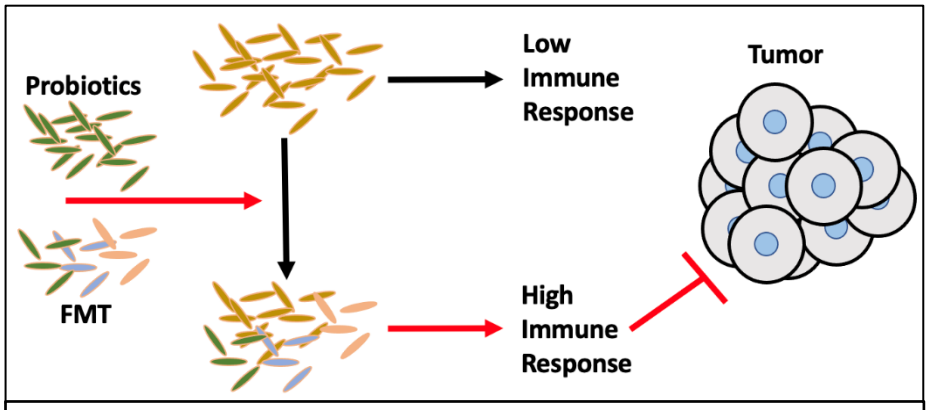

Figure 1.1: Microbial Intervention and Immune Responses.
Hypothesis of microbiome effects on anti-tumor immunity.

1.4 Metabolism and Microbes

The observation that regulation of metabolism is critical for the survival and development of an animal is well-known. When there is loss of the host's ability to regulate metabolism, it results in metabolic disease. One major metabolic disease is obesity. Obesity is defined as abnormal or excessive fat accumulation in the adipose tissue. Metabolic hormones such as insulin, glucagon, and noradrenaline control the extracellular uptake and intracellular release of the main energy sources: carbohydrates, proteins, and fats. Fatty acids (FAs) are either esterified, metabolized into secondary messengers, or beta-oxidized in the mitochondria. A first critical step in fatty acid oxidation (FAO) is the transport of long-chain FAs (LCFAs) into the mitochondrial matrix. This step is controlled by carnitine palmitoyltransferase (CPT) and is composed of three proteins: CPT1, acylcarnitine translocase, and CPT2.[104] Once inside the mitochondria, FAs will generate acetyl-CoA and will then be able to be metabolized through the TCA cycle. One way FAO is regulated is through malonyl-CoA, which is an intermediate in FA synthesis and can inhibit CPT1.[105] This first step of FAO also serves as the rate-limiting step in mitochondrial oxidation of FAs. This means that both FAO and lipogenesis cannot occur at the same time. Therefore, any molecule that can inhibit carnitine shuttling will effectively cut off FAO and cause an accumulation of fat through lipogenesis.

Interestingly, the microbiome has been correlated to lipogenesis, obesity, FAO, and host metabolism. This critical role was established when the microbiome from an obese and lean twin were transferred into GF mice and the mice recapitulated the metabolic phenotype of the microbiome they recieved.[106] The microbiota can also

exacerbate metabolic phenotypes as GF mice on a high-fat diet display reduced obesity, adiposity, glucose intolerance, and insulin resistance when compared to conventional counterparts.[107,108] These metabolic modulatory effects by the microbiome may occur through a variety of ways including SCFAs, secondary bile acids, and other unknown bacterial metabolites.

One major set of bacterial metabolites are SCFAs. As previously mentioned, SCFAs can cause a variety of effects but are mainly used as a fuel source. Butyrate is preferentially metabolized by colonocytes and propionate is mainly metabolized in the liver by hepatocytes.[109] Administration of the SCFA acetate has been shown to reduce weight and improve glucose tolerance in obese rats.[110] Indeed, diets rich in butyrate cause increased thermogenesis and energy expenditure and cause resistance to obesity.[111] Some of the beneficial effects are due to the fact that both butyrate and propionate are known inducers of hepatic and intestinal gluconeogenesis which is sensed by a gut-brain neural circuit that causes an increase in insulin sensitivity and glucose tolerance.[112] Though despite these beneficial effects, it is reported that obese individuals have more SCFAs than lean individuals.[113] Altogether, SCFAs play an important role in regulating host metabolism and metabolic disease.

Another major bacterial metabolite is secondary bile acids. Bile acids are amphipathic molecules that are produced from cholesterol in the liver and are deposited into the small intestine via the bile duct to aid in the emulsification and absorption of dietary fat. Through deconjugation and dehydroxylation, the gut microbiome can convert these primary bile acids into secondary bile acids. These conversions control bile acids hydrophobicity and entero-hepatic cycle as well as their solubility and ability to be

reabsorbed.[114] These conversions can also effect metabolism as primary bile acids are ligands for the farnesoid X receptor (FXR). FXR signaling can suppress hepatic gluconeogenesis and lipogenesis, enhance fatty acid oxidation and clearance of triglyceride-rich lipoprotein, and improve hepatic insulin sensitivity.[115–117] Therefore, by controlling the pool of bile acids, the gut microbiome can regulate bile acid-mediated signaling on the host's metabolism.

Finally, there exists a multitude of different bacterial derived metabolites that could potentially exert uncharacterized roles on host metabolism. Indeed, utilizing metabolomic approaches, one study undertook a comparative analysis of GF mice and conventional mice and determined that up to 10% of all circulating blood metabolites are microbially produced or induced.[118] Furthermore, it was discovered that there are hundreds of these uncharacterized metabolites produced by the microbiome with many of these metabolites having both uncharacterized structure and function. Based on these reports, there exists a critical need to better under these metabolites and what role they play in host metabolism and metabolic diseases.

1.5 Hypotheses

With the above information, we wanted to determine if certain bacterial strains or products could regulate mucosal immunity or metabolism. First, we investigated if specific bacterial species could modulate mucosal immunity. Interestingly, it was reported that melanoma patients that did not respond to immunotherapy have an absence of lactobacilli in their microbiome.[75–77] We therefore reasoned that certain lactobacilli may be regulating immune cells. To that end, we investigated *Lactobacillus*

rhamnosus GG (LGG) as it is a well-established and well-used probiotic strain. Previous work on LGG showed that LGG is capable of activating neutrophils and dendritic cells *in vitro* as well as being able to reduce the severity of influenza and increase efficacy of influenza vaccinations.[119–121] Additionally, when LGG is administered is a preventative or prophylactic manner, LGG is able to reduce tumor burden in different colonic tumor mouse models.[101,103,122] However, no immunological mechanism has been proposed explaining how LGG can modulate tumor burden in these models and no detailed study has ascertained what are LGG's immunological effects on T-cells *in vivo*. Altogether, we hypothesized that LGG may function in modulating mucosal immune responses and activation of an anti-tumor immune response.

In addition, we wanted to understand how the microbiome in general was augmenting and controlling host metabolism. It is well-established that a correlation exists between the microbiome and host metabolism, but few definitive metabolites and pathways have been identified. To better understand what role the overall microbiome had on metabolism, we took a litter of GF mice, and upon weaning, the mice were divided into two groups. One group was maintained in GF conditions, while the other was placed into dirty bedding from conventional mice and colonized by a conventional microbiome. At six weeks of age, the mice were sacrificed, and livers removed for metabolomic analysis and RNA-seq. RNA-seq and metabolomic analysis of liver tissue revealed dramatic changes in fatty acid metabolism. Interestingly, one metabolite was abundantly expressed in conventional mice but absent in GF mice. We hypothesized that this metabolite, later identified as delta-Valerobetaine (VB), was produced by microbes and functioned in the regulation of fatty acid metabolism.

1.6 Statement of Research Objectives

The overall objective of this dissertation research was to obtain an understanding and potential causative mechanism of how the microbiome regulates mucosal immune responses and host metabolism. Chapters 2 and 3 of this thesis describe investigations to test the previously mentioned hypotheses. Chapter 2 is a published manuscript in the journal of *Cellular and Molecular Gastroenterology and Hepatology* that describes my work where I identified a mechanism of how one member of the microbiome, LGG, is capable of inducing a mucosal immune response that can attenuate colonic tumor burden in an immune-mediated manner. Chapter 3 is a manuscript that is currently under secondary review for consideration of publication in *Nature Metabolism* which describes an investigation to elucidate the role of the microbial metabolite, delta-Valerobetaine, on the regulation of fatty acid oxidation and its role in obesity. Chapter 4 is a detailed discussion of both chapters 2 and 3 and consists of a dialogue addressing the significance of the data in the greater scheme of host cell and microbe interactions in the gut, and on experimental science.

Chapter 2

Lactobacillus rhamnosus GG orchestrates an anti-tumor immune response

Joshua A Owens[1], Bejan J Saeedi[2], Crystal R Naudin[1], Sarah Hunter-Chang[2], Maria E Barbian[1], Richard U Eboka[2], Lauren Askew[1], Trevor M Darby[1], Brian S Robinson[2], and Rheinallt M Jones[1,3,]

[1] Division of Gastroenterology, Hepatology, and Nutrition, Department of Pediatrics, [2] Department of Pathology, [3] Emory Microbiome Research Center, Emory University School of Medicine, Atlanta GA, 30322.

Synopsis: This chapter was previously published in the journal of Cellular and Molecular Gastroenterology and Hepatology. This chapter establishes a causative mechanism as to how a member of the microbiome, *Lactobacillus rhamnosus* GG, can activate certain aspects of the immune response that can initiate an anti-tumor immune response.

Summary

Background and Aims: In colorectal cancer, about 95% of patients are refractory to immunotherapy due to low anti-tumor immune responses. Therefore, these is an exigent need to develop treatments that increase anti-tumor immune responses and decrease tumor burden to enhance immunotherapy.

Methods: The gut microbiome has been described as a master modulator of immune responses. We administered the human commensal, *Lactobacillus rhamnosus* GG (LGG) to mice and characterized the changes in the gut immune landscape. Because the presence of lactobacilli in the gut microbiome has been linked with decreased tumor burden and anti-tumor immune responses, we also supplemented LGG to a genetic and a chemical model of murine intestinal cancer. For clinical relevance, we therapeutically administered LGG after tumors had formed. We also tested for the requirement of CD8 T-cells in LGG-mediated modulation of gut tumor burden.

Results: We detected elevated colonic CD8 T-cell responses specifically in LGG supplemented mice. The CD8 T-cell induction was dependent on dendritic cell activation mediated via Toll-like receptor-2 (TLR2), thereby describing a novel mechanism where a member of the human microbiome induces an intestinal CD8 T-cell response. We also show that LGG decreased tumor burden in the murine gut cancer models by a CD8 T-cell-dependent manner.

Conclusions: These data support the potential use of LGG to augment anti-tumor immune responses in colorectal cancer patients and ultimately for increasing the breadth and efficacy of immunotherapy.

2.1: Introduction

Over 1700 Americans per day succumbed to a cancer-related death in 2019.[123] Of these deaths, colorectal cancer (CRC) is the second highest cause of cancer-related mortality in the United States although the incidence and mortality rates have stabilized over the last few years.[124] However, globally, the incidence and mortality of CRC is increasing and cases of CRC are predicted to rise by 60% by 2030.[125] With this negative outlook, innovative approaches and improvements to currently approved therapeutics are needed for enhanced treatment of CRC.

Recently, the advent of immunotherapy has revolutionized the fight against cancer. However, for CRC, only 10% of patients are approved for immunotherapy and more than 50% of these patients are refractory to treatment.[126,127] The major determinant for CRC patients being approved for immunotherapy is microsatellite instability (MSI). This approval is because MSI-high tumors have increased levels of genomic instability. Genomic instability leads to abundant mutations which culminates in a high output of tumor neoantigens. Because of increased tumor neoantigens, MSI-high tumors have greater immune cell infiltrate compared to their MSI-low counterparts. Tumors that have a heightened immune cell infiltrate correlate with greater responses in immunotherapy and better clinical outcomes.[128–134] Therefore, one strategy for CRC treatment involves triggering MSI-low tumors to develop higher anti-tumor immune cell infiltrate such as their MSI-high counterparts. On the other hand, the immune cell infiltrate within MSI-high tumors can reach a point in which they no longer effectively clear tumor cells, reaching a state known as exhaustion.[135] These exhausted immune cells are targeted in immunotherapy to restore their cytotoxic function and trigger anti-tumor immune

responses. Unfortunately, immunotherapy response rates in MSI-high tumors still remain around 50%.[126,127] Therefore, there exists a critical challenge to increase the percentage of patients that respond to immunotherapy intervention.

Recently, the gut microbiome community structure has been linked to immunotherapy response rates.[75–77] Interestingly, the microbiome of non-responding immunotherapy patients lack lactobacilli, whereas lactobacilli were shown to be present in the microbiome of responding patients.[75] In addition, other studies that investigated the influence of *Lactobacillus rhamnosus* GG (LGG) on gut health and disease report that LGG and other lactobacilli promote an anti-inflammatory response in the intestine by regulating IL-10 levels and promoting regulatory T-cells activity.[9,136,137] At first, these reports seem discordant since increasing immunotherapy response rates would imply pro-inflammatory responses, whereas modulating regulatory T-cells would suggest anti-inflammatory responses. Nevertheless, LGG was also reported to modulate the immune landscape in a pro-inflammatory manner, including increased M1 macrophage polarization, increased antibody production, modulation of dendritic cell activity, and reducing viral burden during influenza infections.[119,121,138,139] Due to these data, we hypothesized that members of the gut microbiome, specifically lactobacilli such as *Lactobacillus rhamnosus* GG may hold promise in augmenting colonic immune responses and colonic anti-tumor responses.

To date, clinically plausible approaches to modulate the microbiome to induce increased CD8 T-cell infiltration into tumors, and by extension decreased tumor burden remains to be thoroughly explored. In addition, the cell and molecular signaling cascades that the microbiome triggers within gut mucosal immune cells is still largely unclear. To

address this gap in knowledge, we investigated the extent to which the human commensal, *Lactobacillus rhamnosus* GG (LGG), could modulate CD8 T-cell responses, the mechanism by which this occurs, and the therapeutic efficacy of this commensal bacterium in reducing colonic tumors in an immune-mediated manner.

Herein, we show that supplementation of mice with LGG expands the prevalence of CD8 T-cells in the colonic mucosa. This expansion results through signaling cascades dependent on toll-like receptor-2 (TLR2) on dendritic cells. We show that LGG administered as a therapeutic to colonic tumors can drive CD8 T-cells to initiate anti-tumor immune responses. This response was dependent on CD8 T-cells for greatest attenuation of colonic tumor burden. Therefore, we show that LGG can induce CD8 T-cell driven anti-tumor immune responses and demonstrate the potential of LGG holding clinical promise as a co-therapeutic to be administered in conjunction with currently approved immunotherapy.

2.2: Methods

Animals

C57BL/6 mice (Stock #000664) were obtained from Jackson Laboratories and maintained in Emory's Whitehead Vivarium or Emory's Gnotobiotic Animal Core located in Emory's Health Science Research Building Vivarium. BATF3 knockout mice (Stock #013755), TLR2 knockout mice (Stock #004650), Villin Cre mice (Stock #004586), and $MSH2^{loxP}$ mice (Stock #016231) were also obtained from Jackson Laboratories. All experiments were carried out with approval of the Institutional Animal Care and Use Committee.

Bacterial cultures and growth conditions

Lactobacillus rhamnosus GG (LGG, ATCC 53103) was grown in MRS broth at 37ºC without shaking for 16 hours prior to administration. *Bacillus cereus* (BC, lab strain) was grown in brain heart infusion media with shaking at 37ºC for 16 hours prior to administration.[140] Bacteria were centrifuged at 3000g for 5 minutes, the supernatant aspirated, and the pellet washed with one volume Hank's Buffered Salt Solution (HBSS). This was repeated for a total of 3 washes. The bacteria were then resuspended to a final concentration of $2x10^9$ CFU/mL.

Administration of Bacteria

Mice were gavaged with commensals as described previously.[141] Briefly *Lactobacillus rhamnosus* GG (LGG), *Bacillus cereus* (BC), or vehicle control, HBSS, were orally gavaged to mice every day in the mid-afternoon at a dose of $2x10^8$ CFUs at a volume of 100uL with control mice receiving 100uL of HBSS.

CFSE-Labeling of Bacteria

Bacteria were grown as mentioned above. However, after the third wash, bacteria were resuspended in 10mL of Cell-Trace CFSE (ThermoFischer) diluted 1:1000 in HBSS per manufacturer's instructions (Heat-killed LGG was heat-killed prior to CFSE staining). Bacteria in CFSE solution were incubated at 37C in the dark for 20 minutes then centrifuged at 3000g for 5 mins at RT to pellet which will be visually yellow. Bacteria were washed three times with HBSS to remove any unbound dye. Additionally, to control for any unbound dye, an empty 15mL tube underwent the CFSE protocol and was administered to the HBSS group. Fluorescence was checked by a plate reader or FCM to verify fluorescence at 488nm.

Isolation of Colonic Lamina Propria Lymphocytes

We performed protocols as previously described.[142] Briefly, colons were extracted by cutting between the proximal colon and the cecum and between the distal colon and the anal verge. Colons were teased apart from the mesentery and flushed of luminal contents. Normally, colons were opened longitudinally and then cut in half longitudinally with half going to isolation of colonic LPLs and the other half for immunofluorescence. Colon was weighed, and then cut into small 1cm pieces and placed into a 50mL conical tube with epithelial digestion buffer consisting of 1x HBSS with 5% FBS, 5mM EDTA, and 10mM HEPES. Tubes were placed into a shaker at 200rpm for 20 minutes at 37ºC. A wire-mesh strainer was used to separate pieces of colon from buffer with a collection tube collecting epithelial cells and intraepithelial lymphocytes. This step was repeated for a total of 40 minutes of digestion. After the second straining, colonic pieces were briefly washed with

RPMI-1640 media. The pieces were then minced with a clean razorblade and placed into a new 50mL conical tube with lamina propria digestion buffer consisting of RPMI-1640 media with 10% FBS, 1mg/mL collagenase type IV, and 50ug/mL DNAse I. Tubes were placed into a shaker at 200rpm for 15 minutes at 37ºC. Afterwards, contents were emptied into a 70-micron cell strainer and contents pushed through with a syringe stopper. Cells were then pelleted by centrifugation at 300g for 5 min at 4ºC and resuspended in 1mL of complete media. Immune Cells were isolated from total cell populations by a percoll gradient: 90% percoll overlaid with 30% percoll. Cells were placed on top and centrifuged at 670g for 30 minutes at RT with acceleration and brakes set to slow. Immune cells are found as a band at the 90:30 interface with remaining cells such as fat at the top. These cells at the top were aspirated while leaving immune cells undisturbed. Fresh media was added to dilute percoll gradient and spun down at 300g for 5 min at 4ºC. Pelleted cells were resuspended in media and pushed through a 40-micron filter and either were immediately analyzed by flow cytometry or were frozen down in complete media with 10% DMSO.

Antibody Array

C57Bl/6 mice were obtained from Jackson Laboratories and maintained in specific-pathogen free conditions inside Emory's Gnotobiotic Animal Core. Mice were orally gavaged every day with LGG, BC, or HBSS for 2 weeks and kept inside an ISOcageP Bioexclusion system (Techniplast) maintained in a BSL-2 facility. Upon sacrifice, flash-frozen whole colons were given to RayBiotech Inc. (Peachtree Corners, GA) for protein extraction and cytokine analysis using Quantibody Mouse Cytokine Array Q4000.

BMDCs generation and bacterial incubation

BMDCs were generated and activated as previously described.[119,143] In short, the femur and tibia were removed from either WT or *TLR2*-/- mice with the bone marrow being removed in a sterile hood. Red blood cells were lysed and $5x10^5$ progenitor cells/mL were resuspended and plated in RPMI 1640 supplemented with 10% FBS and 10ng/mL GM-CSF (Biolegend). BMDCs were cultured for 6 days at 37ºC in 5% CO_2 with replenishing of complete media and cytokines on days 2 and 4. On day 6, BMDCs were removed and re-plated at $5x10^5$ cells/well. After two hours, BMDCs were incubated with a concentration of 10:1 BC, LGG, heat-killed LGG, or HBSS for four hours. At four hours, 200ug/mL of gentamycin was added to kill all extracellular bacteria and cells were washed three times with HBSS. Fresh media was then given and BMDCs were incubated for an additional 20 hours. BMDCs were then stained and analyzed by FCM for expression of CD80 and CD86.

Flow Cytometry

Flow Cytometry was carried out as previously described.[142] Briefly, a single cell suspension of colon, lymph node, or spleen was placed in a round-bottom 96-well plate and centrifuged at 300g for 5 min at 4ºC. Supernatant was flicked off and cells were resuspended in 100uL of antibody master mix. Antibody master mix contained desired antibodies run on two different panels (The first consisted of: APC-CD3, PerCP-CD4, BV605-CD8, PE-CD44, BV650-CD62L, BV510-CD25, B421-CXCR3, PE-TR-CD28, FITC-Granzyme-B. The second consisted of: BV421-CD11b, PE-CD11c, A700-F4/80, PerCP-MHCII, BV650-Ly6G, APC-CD19, PE-TR-CD80, BV510-CD86, and BV711-

CD103, all from Biolegend) at 1:100 dilution and LIVE/DEAD Fixable near-IR staining kit at 1:1000 dilution (ThermoFischer) in FACS Buffer containing 1X PBS with 5% FBS and .5mM EDTA. Cells were stained for 1 hour at 4C in the dark. After, cells were centrifuged and washed with FACS Buffer for a total of three times. Additionally, for granzyme B staining, we used the True-Nuclear Transcription Factor Buffer Set (Biolegend) according to manufacturer's instructions. After staining, cells were resuspended in a final concentration of 200uL of FACS Buffer and analyzed by a LSRII Flow Cytometer (BDbiosciences). Data was analyzed using Flow Jo Software. Gating Strategy for T-cells consisted of Cells/SingleCells/LiveCells/CD3+ and then analyzed for CD4 and CD8 with subsequent effector status and other molecules. Gating Strategy for DCs consisted of Cells/SingleCells/LiveCells/CD3-CD19-/MHCII+/CD11c+ and then analyzed for activation or for CFSE uptake. Cell numbers were calculated using Precision Count Beads (Biolegend). Compensation was done via single color controls using UltraComp eBeads Compensation Beads (ThermoFischer) and for CFSE compensation was performed with stained and unstained bacteria with compensation matrices created in Flow Jo Software.

Immunofluorescence

Colon samples for immunofluorescence were swiss-rolled and fixed in 10% formalin and then processed and embedded in paraffin. 5-micron sections were cut and underwent a deparaffination process followed by a citrate antigen retrieval step before being permeabilized in 0.5% triton-X 100 in PBS and blocked with 5% normal goat serum. The CD8 monoclonal rat antibody (eBioscience) was used at 1:100 in PBS with 0.1% Triton-

X and 5% NGS. Samples were incubated in primary antibody overnight at 4ºC. Samples were then washed three times and incubated for 1 hour in fluorochrome-conjugated secondary antibody. Samples were again washed and incubated with DAPI at a concentration of 1:10000 in PBS for 5 minutes. Samples were mounted using Prolong diamond antifade and imaged on an Olympus FV1000 confocal microscope at 20X. At least 3 sections and three different images were taken for each sample.

Histology

Colon samples were swiss-rolled upon sacrifice and fixed in 10% formalin and then processed and embedded in paraffin. 5-micron sections were cut and underwent hematoxylin and eosin staining as performed by Emory University's Cancer Tissue and Pathology core. Stained slides were examined by a board-certified pathologist for dysplasia and calculated percentage of the dysplastic epithelium of the section by eye.

Transcriptional analysis

For transcriptional analysis, 1cm of the proximal colon was dissected and snap frozen in liquid nitrogen. Colon was then homogenized by mechanical disruption using a MagnaLyser (Roche) with ceramic MagnaLyser beads (Roche) with 1mL of Trizol. RNA was prepared according to Trizol manufacturer's instructions. cDNA was synthesized using iScript cDNA synthesis kit (BioRad) and manufacturer's instruction were carried out using 1ug of RNA. RT-PCR was performed using SybrGreen supermix (BioRad) with a two-step amplification protocol while using the following primers: CXCL9-F: CGAGGCACGATCCACTACAA, CXCL9-R: CCGGATCTAGGCAGGTTTGA; CXCL10-F:

TGCGTGGCTTCACTCCAGTT, CXCL10-R: TCCTGCCCACGTGTTGAGAT; IL-12p40-F: TCTTCAAAGGCTTCATCTGCAA, IL-12p40-R: ACAGCACCAGCTTCTTCATCA; TLR2-F: GGGCTTCACTTCTCTGCTTT, TLR2-R: TCCTCTGAGATTTGACGCTTTG. Data was analyzed using the 2^{ddCt} method.

Intestinal MSH2 Cancer Model

We performed the well-characterized genetic MSH2 colonic cancer model.[23] Briefly, intestinal specific depletion of exon 12 of MSH2 was generated by crossing $MSH2^{loxP}$ with Villin Cre mice until homozygosity. Genotypes were confirmed by PCR (Transnetyx) and mice were then aged to approximately 7 months. At this point, mice began receiving either HBSS, LGG, or BC daily by oral gavage for 6 weeks.

DSS-AOM Model

We performed the well-characterized chemical model of Dextran Sulfate Sodium (DSS)-Azoxymethane (AOM).[145] Briefly, we intraperitoneally injected AOM at a dose of 60mg/kg from a solution of 10mg/ml which equated to roughly 100-150uL of AOM for mice ranging from 20g-25g. Mice were 7-8 weeks old at time of injection. Three days after injection of AOM, drinking water was replaced with 2% DSS for 7 days. After induction of colitis, mice were allowed to recover for two weeks on normal drinking water. Colitis was induced by DSS for a total of three times. After the third round of colitis, mice were allowed to recover for two weeks on normal drinking water before undergoing endoscopy to verify tumor burden. At this point, intervention with either monoclonal antibodies or bacteria was introduced for 4-6 weeks depending on the experiment.

Endoscope

All procedures and post-anesthesia care were performed in accordance within IACUC guidelines. Each mouse was anesthetized with 3% isoflurane and maintained with 1.5% isoflurane in an oxygen/air mixture by using a gas anesthesia mask. Body temperature was maintained during the procedure at 37°C with a homeothermic blanket (Harvard Apparatus, Holliston, MA). For monitoring of tumor burden, a high-resolution mouse video endoscopic system was utilized (Karl Storz Endoskope, Tuttlingen, Germany). The system consists of a miniature endoscope (1.9 mm outer diameter), a xenon light source, a triple chip camera, and an air pump for regulated inflation of the mouse colon (Karl Storz, Tuttlingen, Germany). The endoscopic procedure was viewed on a color monitor and digitally recorded for post-procedure review with recording of ileocecal valve all the way to the anus of each mouse. Videos were reviewed by a board-certified pathologist and tumor burden was established by their identification of individual tumors in the videos of each mouse.

Depletion of CD8 T-Cells

CD8 T-cells were depleted by intra-peritoneal injection of CD8a mAb (BioXCell, clone:YTS 169.4). 200ug of mAb CD8a or isotype control (BioXCell, Rat IgG2b, clone:LTF-2) was given two days before administration of bacteria and was administered every 6-7 days afterwards.

Quantification and Statistics

Graphs are shown as mean ± SEM. Statistical analyses were performed using GraphPad Prism software. For comparisons of two groups, the unpaired Student's T-Test was used. For comparisons of groups of 3 or more, one-way ANOVA was used, followed by Dunnett's multiple comparison test. For incidence of rectal prolapse, the Martel-Cox test was used. Statistical parameters are stated within the figure legends. All authors had access to the study data and reviewed and approved the final manuscript.

2.3: Results

LGG orchestrates a colonic CD8 T-cell response

As LGG has been reported to have both pro- and anti-inflammatory properties, we first investigated if oral administration of LGG could modulate the murine colonic immune response by performing an expansive antibody array. We administered either LGG, a control non-probiotic Gram-positive bacterium known as *Bacillus cereus* (BC), or a vehicle control of Hank's Buffered Salt Solution (HBSS) daily by oral gavage for two weeks to 6-week-old specific pathogen free (SPF) C57BL/6 mice and then performed an antibody array on protein extracted from total colonic tissue. Specifically, in LGG treated mice, we detected several increased levels of several cytokines including IL-12 and IFN-γ **(Figure 2.1A)**. We also detected altered levels of chemokines such as CXCL11 specifically in LGG treated mice which pointed to an altered immune response and potentially a modified T-cell response **(Figure 2.1B and C)**. As there exists several reports of anti-inflammatory properties of LGG, we wanted to confirm these findings and elucidate LGG's effect on the immune response in greater detail. Therefore, we took another cohort of C57BL/6 mice and administered either LGG, BC, or HBSS daily for one week. Mice were sacrificed and the colonic lamina propria lymphocytes were analyzed by flow cytometry (FCM). We detected a significant increase in total numbers of CD8 T-cells as well as effector and cytotoxic CD8 T-cells in LGG treated mice **(Figure 2.1D-G)**. Furthermore, we detected an increase in total CD4 T-cells and CD4 effectors T-cells indicating that both subsets increased with LGG treatment **(Figure 2.2C and D)**. In addition, analysis for transcript enrichment of chemokines and cytokines by LGG as observed in the antibody array confirmed a significant increase in

IL-12 and chemokines that function in CD8 T-cell trafficking, namely CXCL9/10. **(Figure 2.1H-J)**. Similar to the increase in CXCL9/10, we detected an increase in the number of colonic CXCR3+ CD8 T-cells that bind CXCL9/10 in LGG treated mice **(Figure 2.1K)**. Importantly, we did not observe any significant changes in CD8 T-cell numbers in the spleens of LGG-treated mice **(Figure 2.2A and B)**, showing that LGG only induces a CD8 T-cell immune response localized to the gut. In order to determine if a specific element from live LGG is necessary to elicit the CD8 T-cell response, we administered LGG that was heat-killed for 10 minutes at 60ºC to mice for 1 week. We found that heat-killed LGG was also able to increase total colonic CD8 T-cells and effector CD8 T-cells **(Figure 2.1L and M)**. These data establish that LGG is capable of inducing colonic CD8 T-cells and this induction occurs even in response to heat-killed LGG.

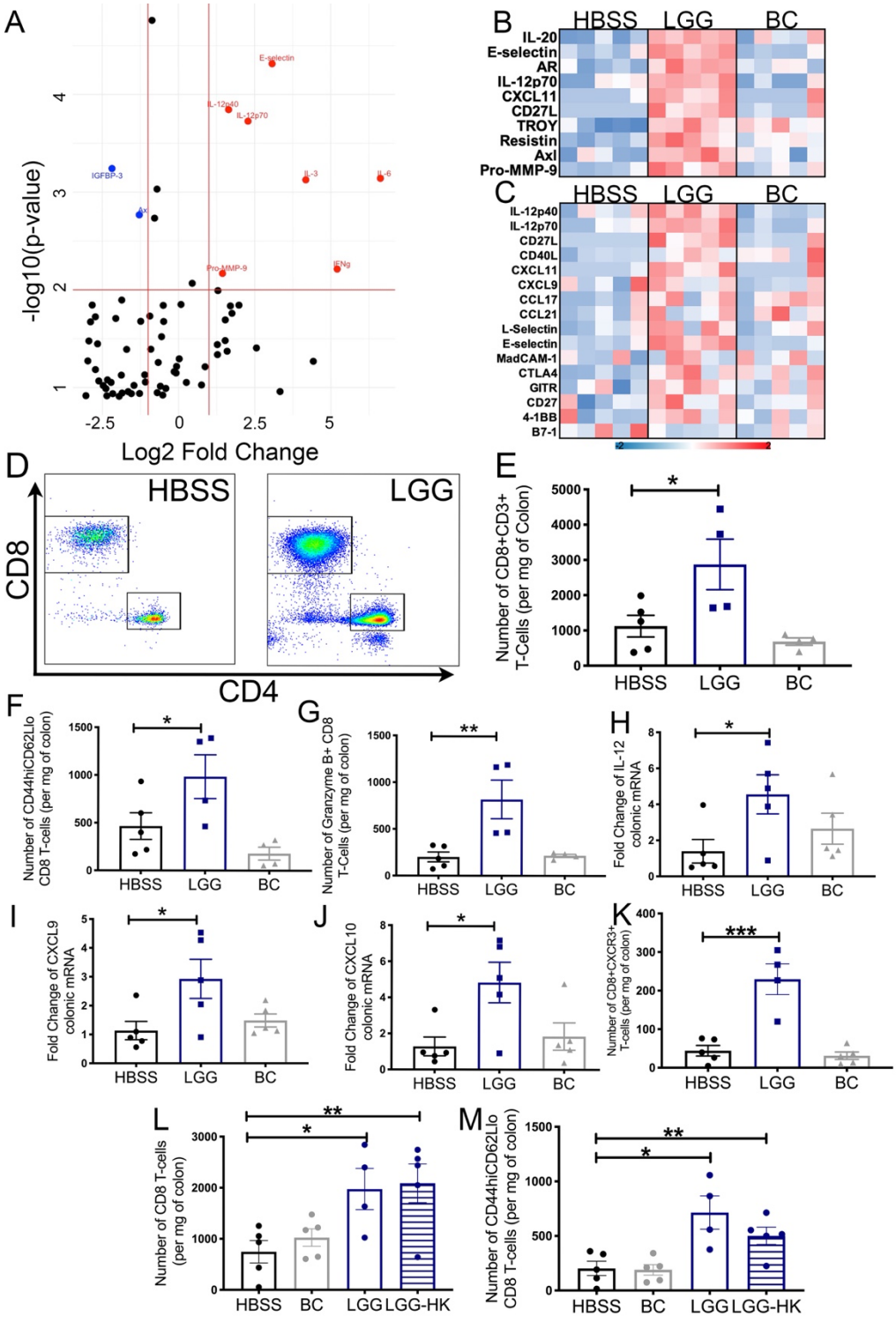

Figure 2.1: *Lactobacillus rhamnosus* GG orchestrates a colonic CD8 T-cell response. (A) SPF C57BL/6J mice were supplemented with HBSS, *Bacillus cereus* (BC), or *Lactobacillus rhamnosus* GG (LGG) or by oral gavage daily for 2 weeks before

colons harvested and analyzed for protein abundance using the Quantibody® Mouse Cytokine Array 4000 (Raybiotech Inc, Peachtree Corners GA). Image shows Volcano plot representation of cytokines that were significantly more abundant in colonic tissues of LGG supplemented mice compared to colons of mice supplemented BC. Axes represent Log2 fold change (x-axis) against -log10(p-value) (y-axis). **(B)** Heatmap representation of the top 10 differentially abundant proteins in LGG mice compared to HBSS supplemented mice detected in the colonic tissue of mice described in (A), **(C)** Heatmap representation of the top 16 differentially expressed immune-mediated proteins detected in the colonic tissue of the three groups, **(D)** Flow cytometry analysis for the detection of immune cells in the colonic epithelium of C57BL/6J mice administered either HBSS, LGG, or BC for 1 week. Representative FCM plots shown of T-cells, **(E)** Quantification of CD8 T-cells in (D), **(F)** Quantification of effector CD8 T-cells in (D), **(G)** Quantification of granzyme-B expressing CD8 T-cells in (D), **(H)** RT-PCR analysis for the detection of *il-12* transcripts in the colonic tissue of mice in (D), **(I)** detection of *cxcl9* transcripts in the colonic tissue of mice in (D), **(J)** detection of *cxcl10* transcripts in the colonic tissue of mice in (D), **(K)** Quantification of CXCR3+ CD8 T-cells for analysis described in (D). **(L)** Flow cytometry analysis for the detection of immune cells in the colonic epithelium of C57BL/6J mice administered either HBSS, BC, LGG, or heat killed (H-K) LGG for 1 week. Chart represents quantification of the number of CD8 T cells in the colonic tissues of these mice. **(M)** Quantification of effector CD8 T-cells in mice described in (L). Statistical significance was tested by One-Way ANOVA for all experiments. *=$p<0.05$, **=$p<0.01$, ***=$p<0.001$. n=4/5 for all experiments.

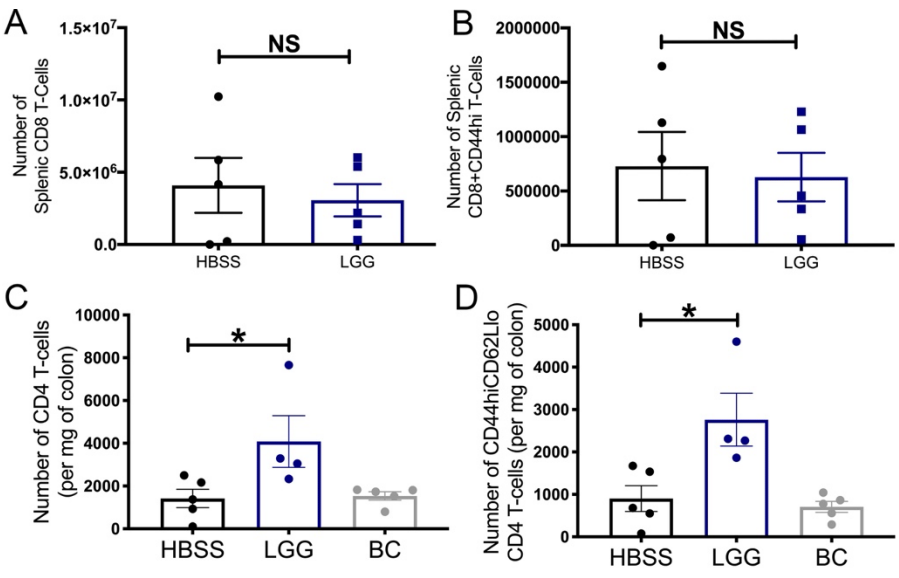

Figure 2.2: LGG effects CD4 T-cells but immunomodulatory effect is location-specific. C57BL/6J male mice were treated with HBSS or *Lactobacillus rhamnosus* GG (LGG) for one week. At sacrifice, spleens were removed and analyzed by FCM for numbers of CD8 T-cells **(A)** and number of effector CD8 T-cells **(B)**. C57BL/6J male mice from Figure 1D-K were analyzed by FCM for number of CD4 T-cells **(C)** and number of effector CD4 T-cells **(D)**. Statistical significance was tested by Unpaired-Student's T-test or One-Way ANOVA. *=$p<0.05$, ns= not significant. n=5.

LGG primes and requires Dendritic Cells for increased CD8 T-cell responses

A previous study showed that LGG could activate dendritic cells (DCs) *in vitro*.[119] We first corroborated this finding by showing that LGG can activate bone-marrow derived DCs (BMDCs) *in vitro* **(Figure 2.3A)**. Because DCs function in the expansion of CD8 T-cells, we investigated whether this response to LGG also occurs *in vivo*. We administered C57BL/6 mice daily for one week with either LGG, BC, or HBSS and isolated the mesenteric lymph node (mLn) which collects the lymphatic fluid from the colon and the small intestine. We detected a significant increase in total number of DCs in the mLn of LGG treated mice **(Figure 2.3B and C)**. However, we did not detect changes to the number of other immune cells including macrophages, neutrophils, and B-cells in LGG treated mice **(Figure 2.4)**. Although we did not further characterize these cell types, it is noteworthy that other reports have shown that LGG can influence the activation of these cells.[67,139,146] As heat-killed LGG could activate CD8 T-cells, we tested whether heat-killed LGG was capable of inducing changes to DCs *in vitro* and *in vivo*. First, we generated BMDCs from C57BL/6 mice and incubated them with either HBSS, BC, LGG, or heat-killed LGG. FCM analysis detected significant DC activation following incubation with both LGG and heat-killed LGG **(Figure 2.3D)**. Importantly, we investigated how LGG was activating DCs *in vivo* and whether direct contact with LGG by surveilling gut DCs was required. To determine this, in a new cohort of C57BL/6 mice, we administered either HBSS or fluorescently tagged (carboxyfluorescein succinimidyl ester, CFSE) BC, LGG, or heat-killed LGG. CFSE covalently links with lysine residues and other amines effectively labeling the bacteria. This approach would allow tagging and tracking of DCs that had sampled and taken up the CFSE-labeled

bacteria after the DC had egressed from the gut to the mLn. Analysis of treated mLns by FCM detected both LGG and heat-killed LGG increased DC numbers and activation **(Figure 2.3E and F)**. Critically, LGG and heat-killed LGG activated DCs were positive for CFSE meaning indicating that these DCs had indeed interacted with LGG before trafficking to the mLn **(Figure 2.3G)**. Based on these data, we hypothesized that LGG requires DCs to increase CD8 T-cell numbers in the colon. Therefore, to test this, we treated a cohort of WT C57BL/6 or *BATF3*-/- mice that lack conventional DCs with HBSS or LGG and found that LGG did not increase the number of CD8 T-cells in *BATF3*-/- mice compared to wild-type (WT) controls **(Figure 2.3H-J)**. Altogether, these data support the conclusion that that LGG drives CD8 T-cell expansion and responses via a DC-dependent mechanism.

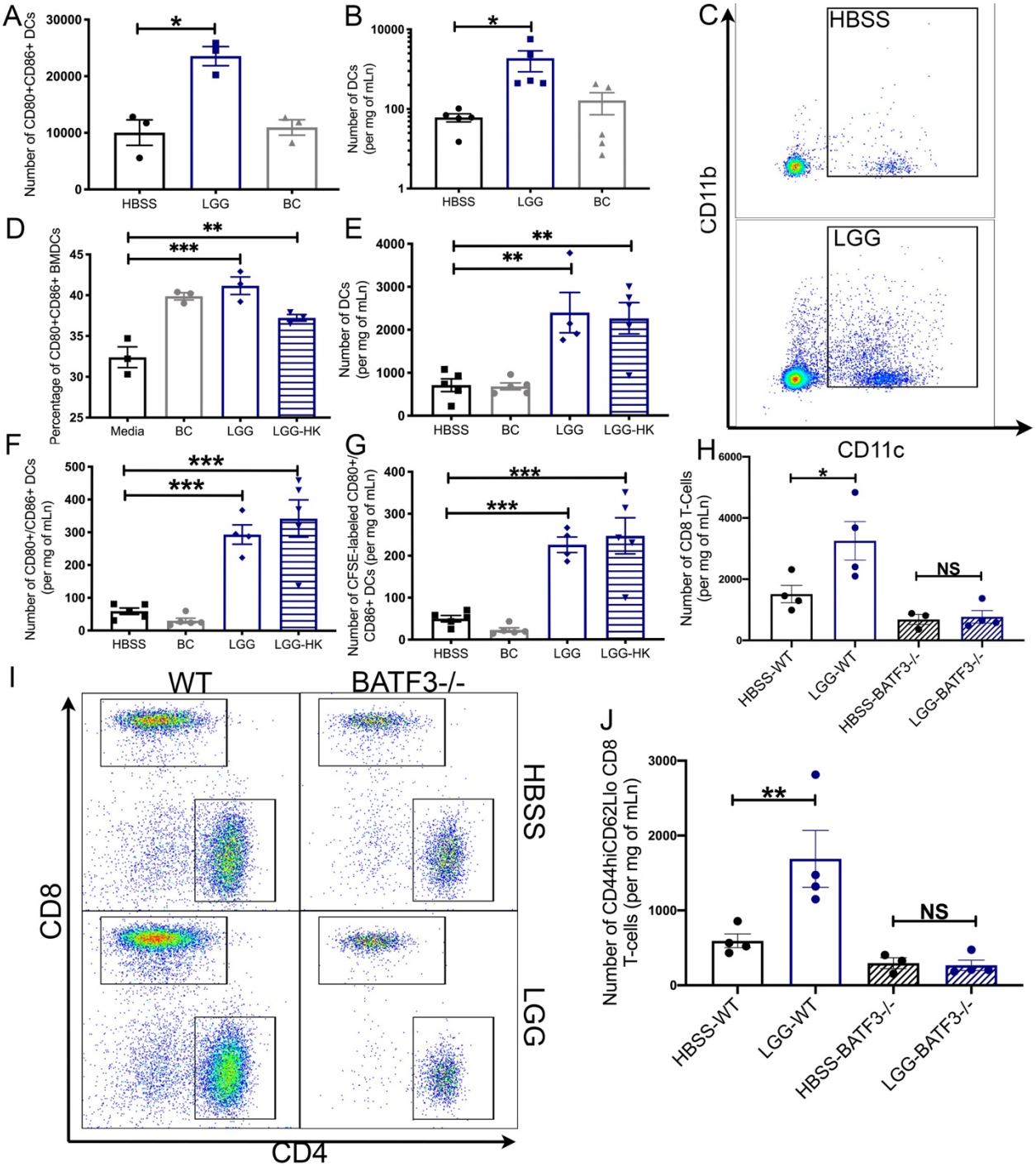

Figure 2.3: *Lactobacillus rhamnosus* GG primes and requires Dendritic Cells for enhanced CD8 T-cell responses. (A) Detection by flow cytometry of the number of CD80+/CD86+ Dendritic cells (DCs) in C57BL/6 mouse bone marrow-derived DCs

(**BMDCs**) following incubation with either HBSS, *Bacillus cereus* (BC), or *Lactobacillus rhamnosus* GG (LGG) for 24 hours. **(B)** Quantification of CD11B+ and CD11C+ DCs in the mesenteric lymph node (mLn) of C57BL/6J mice supplemented for 1-week with either HBSS, LGG, or BC, **(C)** Representative flow cytometry analysis chart for experiment described in (B). **(D)** Frequency of CD80+/CD86+ DCs in C57BL/6 mouse **BMDCs** following incubation with either HBSS, BC, LGG, or heat killed (HK) LGG for 24 hours. **(E)** Quantification of CD11b and CD11c+ DCs in the mLn of C57BL/6J mice supplemented for 1-week with carboxyfluorescein succinimidyl ester (CFSE) labeled HBSS, BC, LGG, or HK-LGG. **(F)** Number of CD80+CD86+ DCs in mLn of mice described in (E). **(G)** Number of CFSE+CD80+CD86+ DCs in mLn of mice described in (E). **(H)** Flow cytometry analysis for the detection of CD8 T-cells in the mLn of B6.129S(C)-*Batf3*^{tm1Kmm}/J (BATF3-/-) or Wild-type (C57BL/6) mice administered either HBSS or LGG by oral gavage for 1-week. **(I)** Representative flow cytometry analysis of mice described in (H). **(J)** Quantification of effector CD8 T-cells of mice described in (H). Statistical significance was tested by One-Way ANOVA for all experiments. *=$p<0.05$, **=$p<0.01$, ***=$p<0.001$. n=3 for all BMDCs experiments. n=5 for (B), n=4/5 for (E-G), and n= 3/4 for (H-J).

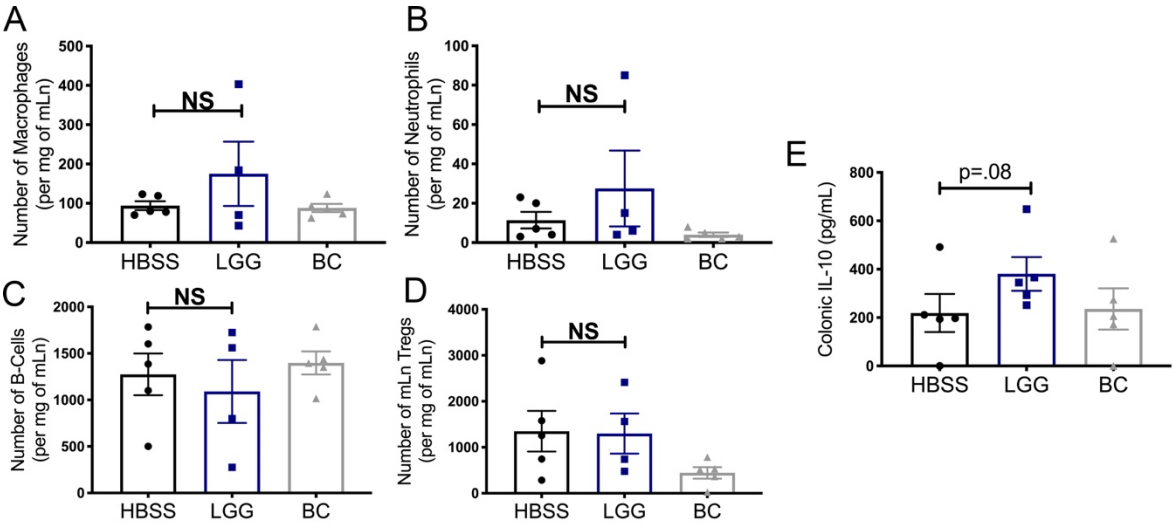

Figure 2.4: LGG does not increase all immune cells. C57BL/6 mice from Figure 2.3D-G which were administered HBSS, *Lactobacillus rhamnosus* GG (LGG), or *Bacillus cereus* (BC) for one week were also analyzed by FCM for number of macrophages **(A)**, number of neutrophils **(B)**, number of B-cells **(C)**, and number of Tregs **(D)**. Antibody array data from Figure 2.1 was reanalyzed to look for colonic IL-10 levels **(E)**. Statistical significance was tested by One-Way ANOVA. NS=not significant

LGG requires TLR2 signaling for DC priming and CD8 T-cell activation

Because we had determined that DCs were required for LGG's effect on CD8 T-cells and the observation that heat-killed LGG still retained the effect, we investigated which elements within DCs are involved in sensing LGG and activating DCs. Previous reports had demonstrated that some of LGG's effect on the colonic epithelium occurred via TLR2 signaling.[20,22] Corroborating these reports, we detected transcript enrichment of *tlr2* in colonic tissue of mice fed LGG **(Figure 2.5A)**. To first test the requirement of TLRs for LGG-induced CD8 T cell expansion, we administered LGG, BC, or HBSS daily to *MyD88*-/- mice for one week. Analysis of colonic lamina propria lymphocytes detected no changes in total or cytotoxic CD8 T-cell numbers in *MyD88*-/- mice in response to LGG compared to WT controls **(Figure 2.6)**. This suggests that MyD88 is indeed required for LGG-induced CD8 T-cell expansion. However, many TLRs and even IL-1 family cytokines can signal through MyD88. Thus, to test if TLRs and specifically TLR2 was required, we generated BMDCs from both WT and *TLR2*-/- mice and incubated them with LGG, BC, or HBSS for 24 hours. We detected increased activation of WT BMDCs with LGG incubation, but this effect was abrogated in *TLR2*-/- BMDCs **(Figure 2.5B)**. To elucidate this further, we daily administered LGG or HBSS to *TLR2*-/- or WT C57BL/6 mice for one week. Analysis by FCM showed no changes to number or activation of DCs nor changes to total or effector CD8 T-cell numbers in LGG treated *TLR2*-/- mice **(Figure 2.5C-H)**. Altogether, these data point to the conclusion that LGG is sensed by TLR2 on DCs, which thereafter increases DC number and activation, culminating in the activation of a CD8 T-cell response.

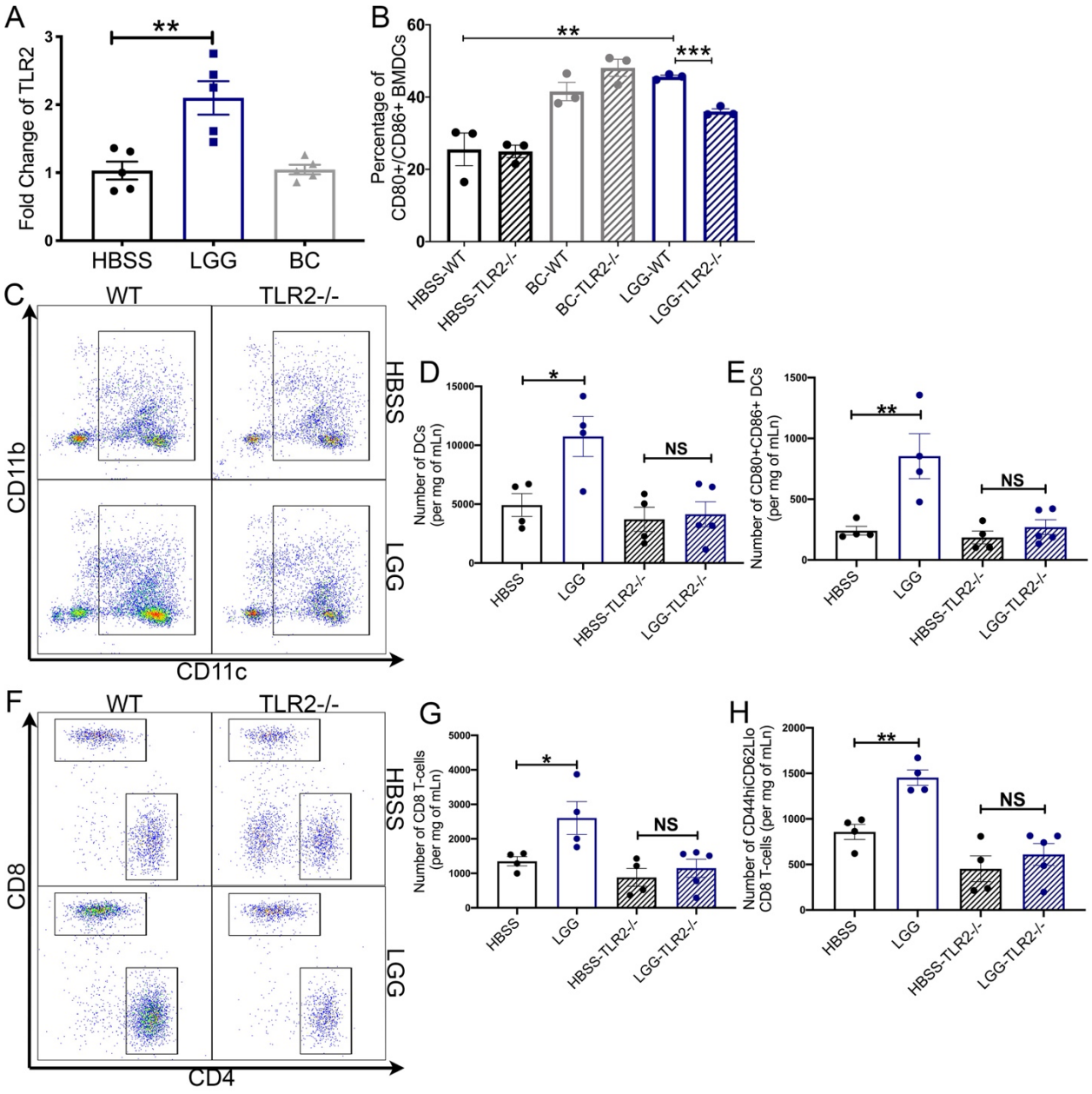

Figure 2.5: *Lactobacillus rhamnosus* GG requires TLR2 signaling for DC priming and activation of CD8 T-cells. (A) RT-PCR analysis for the detection of *tlr-2* transcripts in the colonic tissue of C57BL/6 mice supplemented with HBSS, *Bacillus cereus* (BC), or *Lactobacillus rhamnosus* GG (LGG) or by oral gavage daily for 2 weeks. **(B)** Detection of CD80+/CD86+ Dendritic cells (DCs) bone marrow-derived DCs (**BMDCs**) derived from either wild type (C57BL/6) mice, or from TLR2-/- (B6.129-

Tlr2^{tm1Kir}/J) mice following incubation with either HBSS, *Bacillus cereus* (BC), or *Lactobacillus rhamnosus* GG (LGG) for 24 hours. **(C)** Representative flow cytometry plots from the analysis of MLNs from wild type (C57BL/6) mice, or from TLR2-/- (B6.129-*Tlr2*^{tm1Kir}/J) mice supplemented with HBSS or LGG for 1 week. **(D)** Quantification of DCs in the mLn of mice described in (C). **(E)** Number of CD80+CD86+ DCs in MLNs of mice described in (C). **(F)** Quantification of T cells in mice described in (C). **(G)** Quantification of CD8 T-cells in mice described in (C). **(H)** Quantification of effector CD8 T-cells in mice described in (C). One-Way ANOVA was used for statistical analysis and represented as *=p<.05, **=p<.01, ***=p<.001. n=5 for 3a, n=3 for 3b, and n= 4/5 for TLR2-/- experiments.

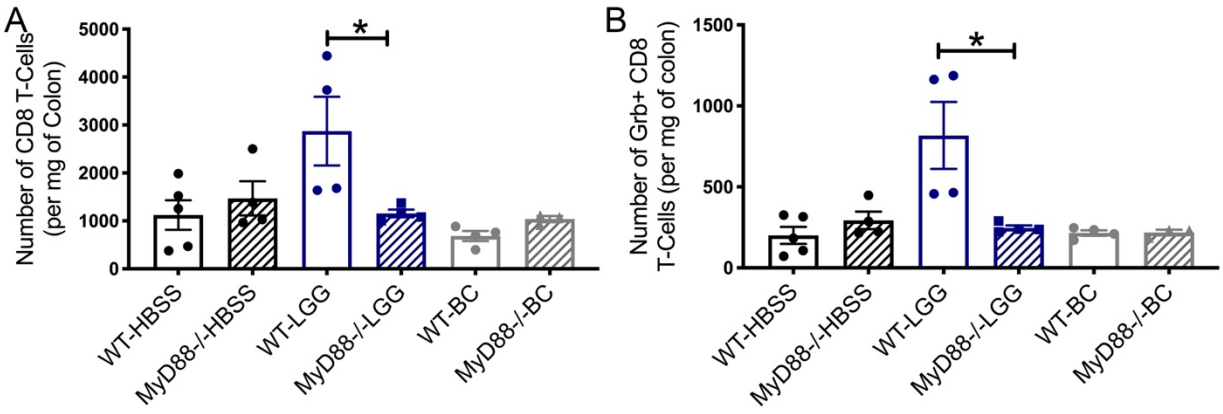

Figure 2.6: MyD88 is required for LGG's effect on CD8 T-cells. C57BL/6 WT or *MyD88*-/- mice were treated with HBSS, *Lactobacillus rhamnosus* GG (LGG), or *Bacillus cereus* (BC) for one week. At sacrifice, colonic lamina propria lymphocytes were extracted and analyzed by FCM for quantification of the number of colonic CD3+CD8+ T-cells **(A)** and the number of granzyme-B expressing CD8 T-cells **(B)**. Statistical significance was tested by One-Way ANOVA. *=p<.05

LGG supplementation decreases colonic tumor burden in a genetic cancer model

In CRC, the CD8 T-cell immune response performs a critical function both in microsatellite instability high colonic tumors, and in inherited Lynch Syndrome CRC.[148] To examine if LGG supplementation influences colonic tumor burden in these contexts, we used a model of Lynch Syndrome where intestinal specific MSH2 knockout mice are generated.[23] Both male and female intestinal specific MSH2 knockout mice were raised until 7 months of age and then subjected to 6 weeks of either HBSS, LGG, or BC supplementation. After 6 weeks, LGG-supplemeted animals exhibited significantly lower colonic tumor burden compared to HBSS- or BC-supplemented mice (**Figure 2.7A**). In addition, colons of LGG-treated mice were significantly longer than controls (**Figure 2.7B**). However, total tumor counts were generally low in the MSH2 model, and overall histological analysis by H&E could not detected significant changes in LGG-treated mice, probably due to the low tumor burden present (**Figure 2.7C**). Nevertheless, we detected significantly increased mLn weight and increased total and effector CD8 T-cells in the mLn of LGG-supplemented mice compared to controls (**Figure 2.7D-F**). Together, these data illustrated that LGG expanded the CD8 T-cell population and significantly reduced tumor burden in a genetic model of intestinal cancer.

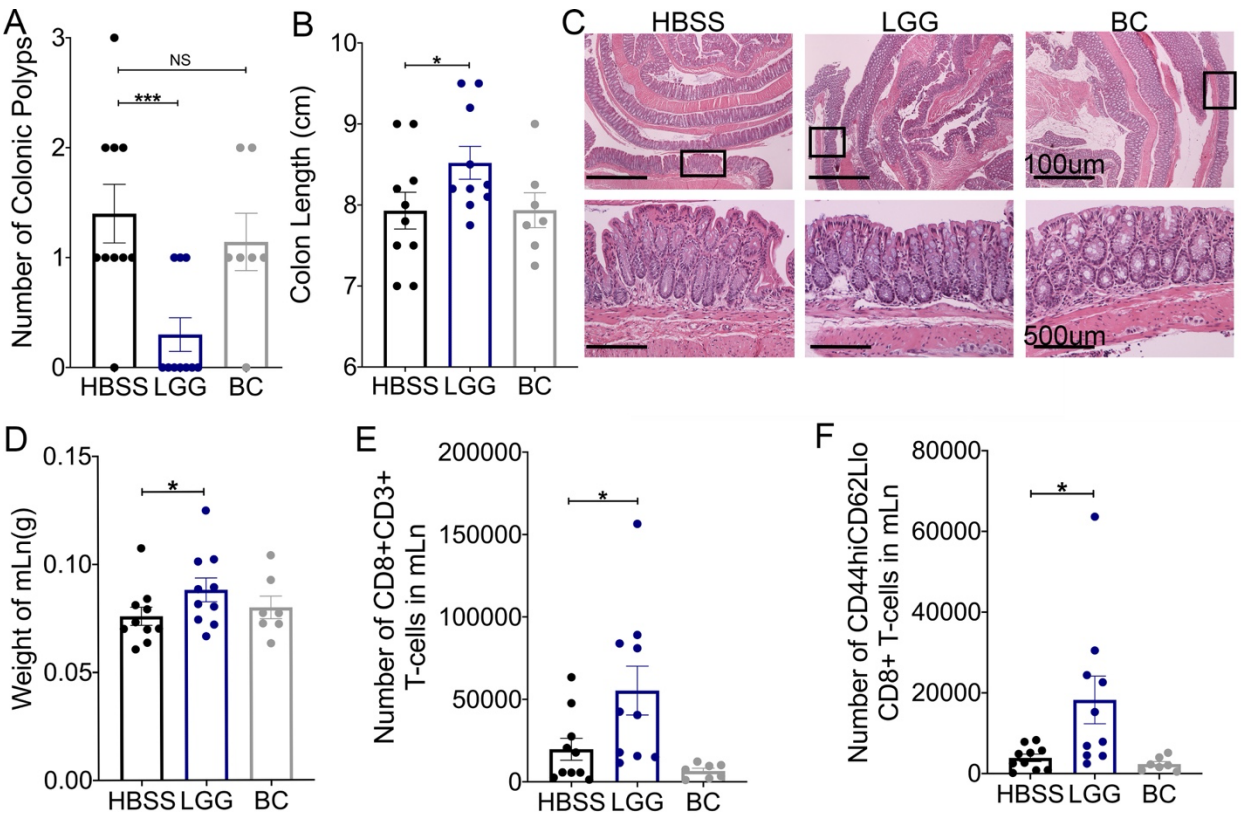

Figure 2.7: LGG supplementation decreases colonic tumor burden in a genetic cancer model. (A) Intestinal specific MSH2 knockout mice were generated by crossing Villin-Cre mice with MSH2^{loxP} until homozygosity. Intestinal specific MSH2 knockout mice were raised to 7 months of age, whereupon the were supplemented with Hank's Buffered Salt Solution (HBSS), *Lactobacillus rhamnosus* GG (LGG), or *Bacillus cereus* (BC) by oral gavage for 6 weeks. After 6 weeks of supplementation, quantification of tumor burden was determined following removal and opening the colon longitudinally. **(B)** Colon lengths of mice described in (A) measured from rectum to cecum before removing colonic contents or any other manipulation. **(C)** Hematoxylin and Eosin (H&E) sections of swiss-rolled colonic tissue with representative images of low-powered (Upper Panels) and high-powered view (Lower Panels). Areas within lower panels indicated by rectangle within the upper panels. **(D)** Weights of Mesenteric lymph nodes

(mLn) in mice described in (A). **(E)** Flow cytometry analysis for the detection total CD8 T-cell numbers in mLn of mice described in (A). **(F)** Quantification of total effector CD8 T-cells from samples described in (E). One-Way ANOVA was used for statistical significance with *= p<.05 and ***=p<.001 n=10/10/7 for HBSS, LGG, and BC respectively. Groups were made up of approximately half male and female mice with 5/5/3 male mice for HBSS, LGG, and BC respectively.

Therapeutic LGG administration attenuates tumors in a chemical colonic cancer model

Because the intestinal specific MSH2 knockout mice did not generate many tumors, we deemed that the model was not optimal to examine LGG-induced modulation of T-cells infiltration into tumors. As an alternative and complementary approach, we induced colonic tumors in mice through the well-established Dextran Sulfate Sodium (DSS)-Azoxymethane (AOM) chemical model of colitis-associated carcinoma. Previous studies on LGG in CRC models have always administered the bacteria prophylactically.[101,122,149,150] By contrast, we daily administered LGG, BC, or HBSS after tumors had been established as outlined in the experimental design **(Figure 2.8A)**. In LGG treated animals, we observed significantly lower clinical manifestation of disease including less rectal bleeding or rectal prolapse **(Figure 2.8B)**. At sacrifice, we observed fewer visible colonic tumors in LGG-treated mice **(Figure 2.8C)**. Furthermore, hematoxylin and eosin (H&E) staining and subsequent histological analysis revealed less dysplastic epithelium in LGG-treated colons **(Figure 2.8D and E)**. Importantly, immunofluorescent analysis for CD8 T-cells detected significantly more intra-tumoral or intra-dysplastic epithelial CD8 T-cells in LGG-treated samples as compared to controls demonstrating an LGG-induced boost to cytotoxic CD8 T-cell anti-tumor response **(Figure 2.8F and G)**. Together, these data show that therapeutic administration of LGG reduced tumor burden in a mouse model of CRC and induced the recruitment of CD8 T-cells into the tumor microenvironment.

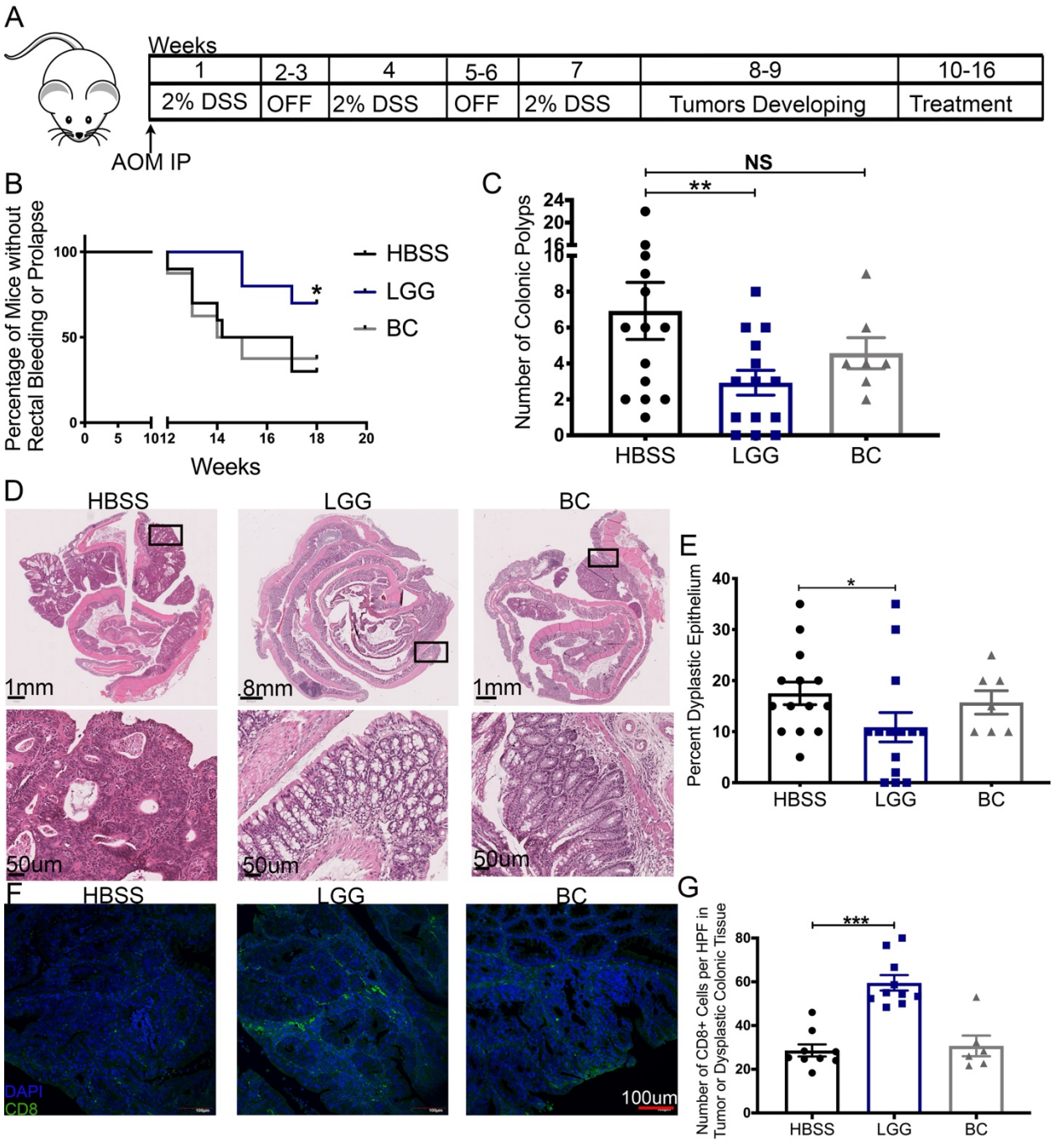

Figure 2.8: Therapeutic administration of LGG attenuates colonic tumor burden.

(A) Graphical representation of the experimental outline for the induction of colonic tumors in C57BL/6 mice. Seven to eight-week-old male mice were injected with azoxymethane (AOM) before being subjected to three rounds of 1-week exposure to 2%

Dextran sodium sulfate **(DSS)** and 2-week recovery period. After three cycles of DSS, and between weeks 8 and 10 of the experiment tumors begin to form within the colonic epithelium of treated mice. At week 10, groups of mice were supplemented with HBSS, *Bacillus cereus* (BC), or *Lactobacillus rhamnosus* GG (LGG) or by oral gavage daily for a total of 6 weeks. Mice were sacrificed at week 16 **(B)** Incidence of rectal bleeding or rectal prolapse between weeks 10 and weeks 16 (the treatment period) of mice described in (A). **(C)** Quantification of tumor burden at sacrifice at week 16 following removal of colon and opening the colon longitudinally with visual examination of the colon of groups of mice described in (A). **(D)** Hematoxylin and eosin (H&E) sections of swiss-rolled colonic tissue at 16 weeks of mice described in (A) with representative images of entire colon (Upper Panels) and high-powered view (Lower Panels) of the area shown in rectangle of upper panels. **(E)** Quantification of dysplastic epithelium in mice at 16 weeks of mice described in (A). **(F)** Immunofluorescence analysis for the detection of CD8 T-cells (green) DNA (Blue) within colonic polyps at 16 weeks of mice described in (A). **(G)** Quantification of CD8 T-cells (green) within colonic polyps at 16 weeks of mice described in (F). One-Way ANOVA and Martel-Cox utilized for statistics and represented as *=p<.05, **=p<.01, ***=p<.001. n= 14/7/14 for HBSS, BC, and LGG respectively.

LGG requires CD8 T-cells to elicit reduction of colonic tumor burden

Previous studies reported that LGG utilizes epithelial-specific mechanisms for reduced tumor burden when administered preventatively. However, due to our observation of higher infiltrating CD8 T-cells, we tested whether LGG requires CD8 T-cells for its attenuation of colonic tumors when administered therapeutically. To this end, we again performed a DSS-AOM experiment, but in conjunction with bacterial administration, we intraperitoneally (IP) injected anti-CD8 antibodies or isotype control antibodies to deplete CD8 T-cells **(Figure 2.9A)**. First, we verified that an IP injection of anti-CD8 antibodies would be able to deplete CD8 T-cells in the colon and mLn **(Figure 2.10)**. Additionally, to mitigate variability in tumor burden induced by DSS-AOM between groups, we performed colonic endoscopy on all mice before treatment to establish baseline tumor burden. Furthermore, LGG treatment was shortened to four weeks because humoral responses against IP injected antibodies may be detected after four weeks. At sacrifice, we observed that LGG significantly reduces tumor burden as compared to HBSS controls in isotype control treated mice. However, this effect was significantly reduced when CD8 T-cells are depleted **(Figure 2.9B and C)**. H&E staining and histological analysis corroborated results and detected fewer dysplastic epithelium when LGG was administered with isotype controls **(Figure 2.9D and E)**. Likewise, immunofluorescent analysis for CD8 T-cells confirmed our findings that LGG increases intra-tumoral or intra-dysplastic epithelial CD8 T-cells in mice treated with isotype controls and confirmed the depletion of CD8 T-cells within tumors in anti-CD8 antibody groups **(Figure 2.9F and G)**. Interestingly, LGG was able to somewhat reduce tumor burden even when CD8 T-cells were depleted but to a significantly lesser extent

compared to LGG with CD8 T-cells present. This lesser response in the absence of CD8 T-cells may be due to reported influences of LGG on tumor burden via epithelial-mediated mechanisms [149–151]. Together, these data suggest that the novel immune mechanism initiated by LGG described in this manuscript plays a dominant role in reducing colonic tumor burden when administered therapeutically.

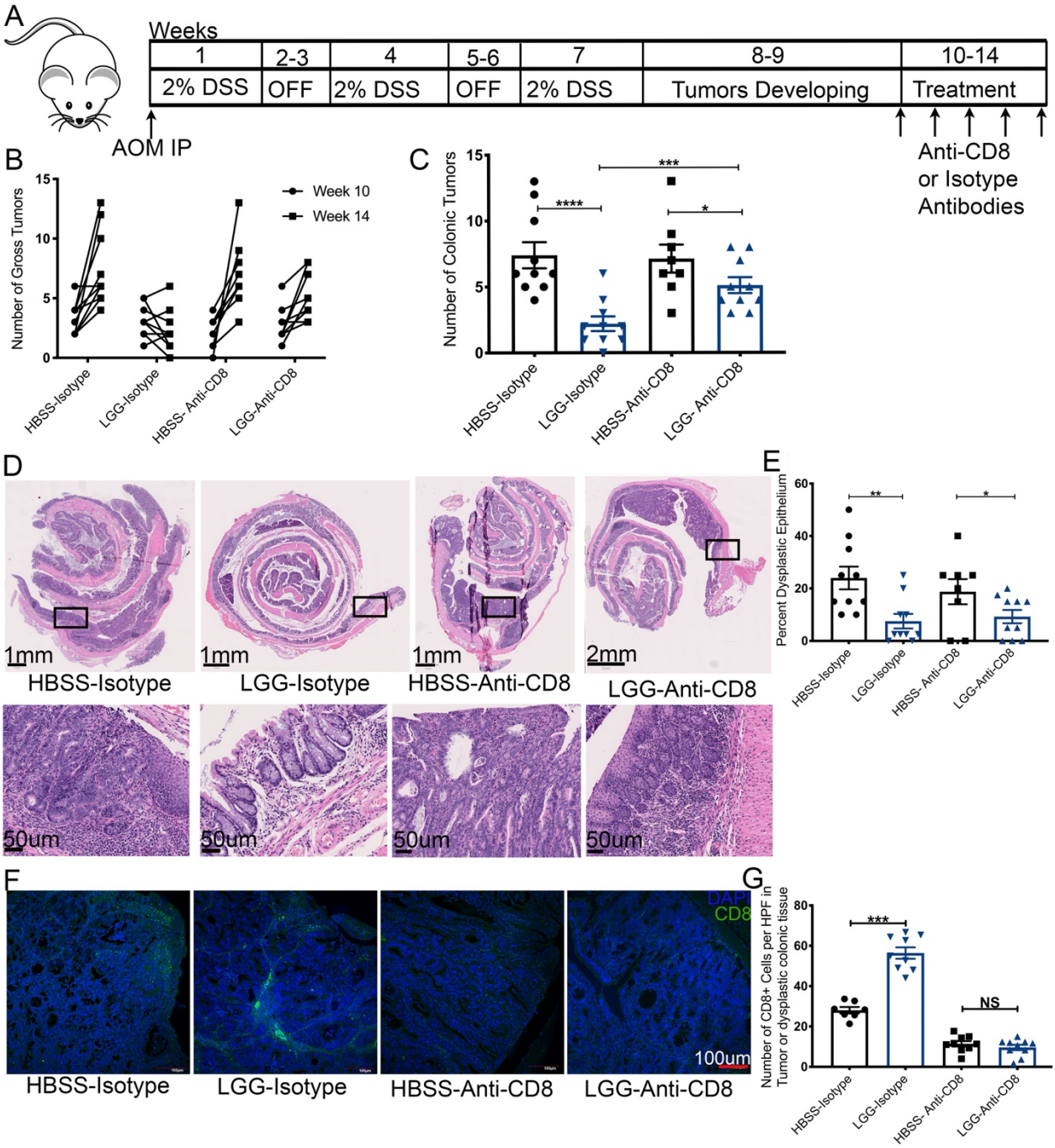

Figure 2.9: LGG requires CD8 T-cells to elicit strong reduction of colonic tumors.

(A) Graphical representation of the experimental outline for the induction of colonic tumors in C57BL/6 mice. Seven to eight-week-old mice were injected with azoxymethane (AOM) before being subjected to three rounds of 1-week exposure to 2% Dextran sodium sulfate (**DSS)** and 2-week recovery period. After three cycles of DSS,

and between weeks 8 and 10 of the experiment tumors begin to form within the colonic epithelium of treated mice. Tumors were quantified by miniature colonoscope at week 10, before the start of treatment period at week 10, where groups of mice were supplemented with HBSS, *Bacillus cereus* (BC), or *Lactobacillus rhamnosus* GG (LGG) or by oral gavage daily for a total of 4 weeks period. Tumors were further quantified by miniature colonoscope at week 14, at the end of the 4-week treatment period. In addition, during the 4-week treatment period, groups of mice were administered either an anti-CD8 or an isotype control weekly for 4 weeks. Mice were sacrificed at week 14. **(B)** Numeration of tumor burden as detected by mature colonoscopy at weeks 10 and week 14 of mice described in (A). **(C)** Quantification of tumor burden at sacrifice at week 14 following removal of colon and opening the colon longitudinally with visual examination of the colons of groups of mice described in (A). **(D)** Hematoxylin and eosin (H&E) sections of swiss-rolled colonic tissue at 14 weeks of mice described in (A) with representative images of entire colon (Upper Panels) and high-powered view (Lower Panels) of the area shown in rectangle of upper panels. **(E)** Quantification of dysplastic epithelium in mice at 14 weeks of mice described in (A). **(F)** Immunofluorescence analysis for the detection of CD8 T-cells (green) DNA (Blue) within colonic polyps at 14 weeks of mice described in (A). **(G)** Quantification of CD8 T-cells (green) within colonic polyps at 14 weeks of mice described in (F). One-Way ANOVA utilized for statistics and represented as *=p<.05, **=p<.01, ***=p<.001. n= 9/9/8/10 for HBSS-Isotype, LGG-Isotype, HBSS-anti-CD8, and LGG-anti-CD8 respectively.

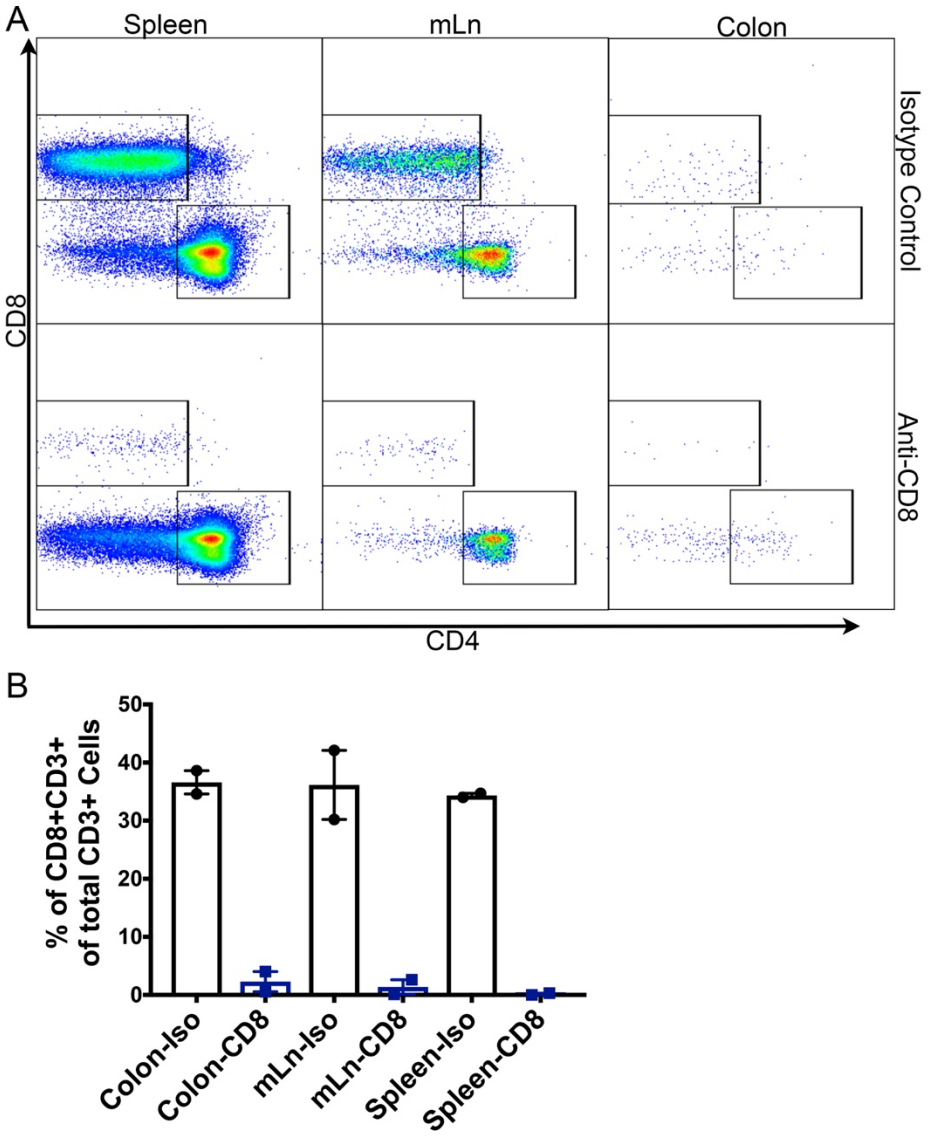

Figure 2.10: Verification of CD8 Depletion by IP antibody injection in mice. C57BL/6J mice were given 200ug of CD8 antibody or 200ug of Isotype Control antibody by IP and then sacrificed two days later. Colon, mLn, and Spleen were analyzed by FCM for CD8 T-cells with representative plots shown **(A)** and quantification of CD8 T-cells relative to total T-cells **(B)**. Statistical significance was tested by Student's Unpaired T-test.

2.4: Discussion

An increasing body of scientific literature reports on the role of the microbiome in cancer development, in cancer therapy, and in augmenting currently approved treatment modalities. In particular, a trio of manuscripts reported that the gut microbiome influences efficacy of anti-PD-1 in metastatic melanoma patients.[75–77] They reported that contrasting commensal microbial communities exist within anti–PD-1 responding patients and non-responding patients. Data from these reports showed an absence of lactobacilli in anti–PD-1 non-responding patients whereas lactobacilli was present in responding patients. Furthermore, a subsequent manuscript reported that a defined set of commensal microorganisms isolated from human feces were capable of inducing CD8 T-cells in the intestine.[78] These reports established the principle that members of the commensal microbiota can elicit immunomodulatory effects for the benefit of patients undergoing cancer treatment. Based on these published data as scientific premise, we reasoned that dietary supplementation with a human commensal probiotic that harbors the capacity to elicit expansion of intestinal CD8 T-cells may be efficacious at inhibiting tumor growth.

We reported a novel mechanism whereby a constituent of the human gut microbiome and a widely used probiotic, LGG, activated a CD8 T-cell response. We showed that administration of LGG to mice expanded the number of total and effector CD8 T-cells in a response localized to the intestine. Indeed, LGG can also expand CD4 T-cells showing that both cell types are influenced by LGG. Moreover, the expansion of CD4 T-cells may function in promoting the efficacy of the CD8 T-cells response as we saw increased IL-12 by antibody array and RT-PCR. IL-12 is known to regulate

granzyme-B expression which we observed was increased in CD8 T-cells from LGG-treated animals. This expansion was dependent on DCs, and more specifically, required TLR2 expression on DCs to expand T-cells. In contrast to previous reports that treated LGG prophylactically[101,149,151], we showed that LGG given therapeutically in a mouse model of colonic tumors can confer an anti-tumor response. To show that LGG-induced expansion of CD8 T-cells was required for the anti-tumor response, we depleted CD8 T-cells in conjunction with LGG administration and observed an attenuation of LGG's anti-tumor effect. These data support the notion that supplementation with LGG holds the promise of augmenting cancer therapy when administered in combination with currently approved therapeutics.

Published literature speculated that metabolites released by the microbiome may be the mechanisms whereby certain gut microbes elicit their effects on T-cells.[78] Indeed, our research group reported that LGG can modify the hepatic transcriptome and other distal host sites via the generation of gut microbe-derived metabolites.[9,140] However, we show conclusive evidence that LGG-induced expansion of T-cells requires TLR2 expression by DCs. Indeed, a recent report shows that enhanced immunotherapy by the microbiome requires TLR2 and may be due to the same mechanism described in this study.[152] Moreover, in heathy mice and in mice subjected to the DSS-AOM and MSH2 models, LGG increased the CD8 T-cell response by about two-fold with no detectable negative pathological damage to the normal colonic epithelium. Importantly, this effect was preserved when heat-killed LGG was administered indicating that the metabolic activity of LGG was not required for this response. In addition, *in vitro* studies where BMDCs were exposed to pure cultures of LGG detected TLR2-dependent activation of

DCs. These data point to the conclusion that TLR2's sentinel action allows DCs to sense a heat-resistant LGG microbe-associated molecular pattern (MAMP), and that this is the most likely stimulatory mechanism of DCs in our studies. Therefore, we speculate that under healthy conditions, LGG-activated DCs will likely sample LGG-derived proteins and products. As well as other bacterial proteins and products generated by the extant microbiome and the healthy colonic epithelium. Notably, despite the ensuing increase of CD8 T-cells that we detected, no pathological tissue damage was observed, possibly due to the inhibitory mechanisms against normal host factors. Indeed, we did detect a non-significant increase in IL-10 by antibody array which may aid in preventing immunopathological damage in healthy mice. Alternatively, when tumors are present, LGG-activated DCs will also sample mutated host proteins, and the responding CD8 T-cells will initiate an anti-tumor response. In this situation, we do not discount the possibility that LGG and the extant microbiome may synergize and augment T-cell activation and the anti-tumor response. Nevertheless, we show that LGG induced a potent anti-tumorigenic response, without any negative effects during the DSS-AOM model and during homeostatic conditions. We propose that these data serve as pre-clinical evidence for the rational use of LGG in relevant clinical situations.

The data reported here contrasts with some published reports on immune response to lactobacilli, but importantly are consistent with several published data investigating the immunomodulatory activity of LGG.[17-23,41] Previous reports on the anti-inflammatory influences of LGG showed that LGG expanded regulatory T-cell populations in the gut and in the bone marrow.[9] In that report, it was shown that LGG-induced anti-inflammatory mechanisms via the generation of the short-chain fatty acid,

butyrate. Interestingly, it was reported that LGG itself does not produce butyrate, but provides a substrate (lactic acid) to other members of the microbiome such as Clostridia sp. that convert lactate to butyrate.[9] Of note, in the current study, we administered LGG daily but did not detect any changes in the levels of IL-10 or number of regulatory T-cells in our models. However, direct contact of LGG with immune cells *in vitro* induce pro-inflammatory responses, which illustrate that LGG can evoke pro-inflammatory responses in certain contexts. In our hands, observations of LGG's immunomodulation consistently showed a pro-inflammatory context under both homeostatic conditions and colonic cancer but these effects might change depending on the disease context. Additionally, many reports illustrating that lactobacilli and LGG are protective in settings of chronic inflammation show that this protection is mediated through effects on the colonic epithelium.[10,147,153] Therefore, LGG's effects on the epithelium must be considered as well to fully understand all dynamics at play.

Since contrasting commensal microbial communities exist within anti–PD-1 responding patients and nonresponding patients, and because responding patients have a more robust microbiome-induced CD8 T-cell response[75], it is practical to speculate about the extent to which further supplementation with LGG or any other CD8 T-cell inducing bacteria may enhance immunotherapy efficacy and breath. Due to heterogeneity in microbiome community structures across cultural and ethnic populations, employing 16S rDNA-based methodology to identify a human microbiome community structure that induces an elevated basal CD8 T-cell response in all individuals may be challenging. This would be further confounded, if, as was previously reported, a consortium of bacteria is necessary to expand CD8 T-cell numbers in the

intestine.[78] Until keystone bacterial species that expand CD8 T-cell numbers in the intestine are identified and are faithfully detectable, the lack of clearly defined microbiome that enhances CD8 T-cell responses will continue to be a barrier to progress in this field. Nevertheless, as dietary supplementation with LGG is relatively cheap and easy to administer, the question may be asked if it would be recommended that all patients undergoing immunotherapy for colonic cancer should be supplemented with LGG or a similar CD8 T-cell enhancing bacterium or consortium of bacteria. Indeed, a report showed that *Lactobacillus acidophilus* lysates can synergize with anti-CTLA4 immunotherapy in mice if administered immediately after colitis.[154] This could be considered for non-responding immunotherapy patients, especially as there appears to be little to no negative effects of LGG supplementation in our mouse models of tumorigenesis as well as no evidence of increased bacteremia by lactobacilli over the last few decades despite the increasingly widespread use of probiotic supplements that include lactobacilli.[155]

2.5: Conclusion

Together, we show data to support the use of bacteria-based modalities to treat CRC. This approach of using probiotics was previously reported to limit tumor burden only when the beneficial bacteria was administered prophylactically.[101,122,149–151] We show data that therapeutic administration of LGG limits tumor burden, thereby offering a potential interventional therapy for CRC in conjunction with other modalities. Before the use of beneficial commensal bacteria in clinical trials, it is necessary to fully understand the host mechanisms at play. Our identification of the mechanism of how LGG elicits its efficacious effects on CRC adds to the growing body of scientific evidence for utilization of probiotics in cancer treatment and may directly inform decisions related to dosing and timing for the use of LGG in CRC clinical trials.

Chapter 3

Microbial metabolite delta-valerobetaine is a diet-dependent obesogen

Ken H. Liu[1†], Joshua A. Owens[2†], Bejan Saeedi[3†], , Catherine E. Cioffi[2], Moriah P. Bellissimo[5], Crystal Naudin[2], Trevor Darby[2], Samuel Druzak[4], Kristal Maner-Smith[4], Michael Orr[1], Xin Hu[1], Jolyn Fernandes[1], Mary Catherine Camacho[3], Sarah Hunter-Chang[3], David van Insberghe[3], Chunyu Ma[1], Thota Ganesh[6], Samantha Yeligar[1,7], Karan Uppal[1], Young-Mi Go[1], Jessica A. Alvarez[5], Miriam B. Vos[2], Thomas R. Ziegler[5], Michael H. Woodworth[8], Colleen S. Kraft[3,8], Rheinallt M. Jones[2], Eric Ortlund[4], Andrew S. Neish[3†], Dean P. Jones[1†]

[1] Division of Pulmonary, Allergy, Critical Care and Sleep Medicine, Department of Medicine, Emory University School of Medicine, Atlanta GA. [2] Department of Pediatrics, Emory University School of Medicine, Atlanta GA. [3] Department of Pathology and Laboratory Medicine, Emory University School of Medicine, Atlanta GA. [4] Department of Biochemistry, Emory University School of Medicine, Atlanta GA. [5] Division of Endocrinology, Metabolism, and Lipids, Department of Medicine, Emory University School of Medicine, Atlanta GA.

[6] Department of Pharmacology and Chemical Biology, Emory University School of Medicine, Atlanta GA. [7]Atlanta Veterans Affairs Health Care System, Decatur GA. [8] Division of Infectious Disease, Department of Medicine, Emory University School of Medicine, Atlanta GA

[†]These authors contributed equally to this work

Synopsis: This chapter is under secondary revision at the journal of Nature Metabolism. This chapter establishes a causative mechanism as to how a metabolite of the microbiome, delta-valerobetaine, can inhibit fatty-acid oxidation resulting in increased adiposity in murine models of obesity and correlates with obesity in humans. Microbial metabolite delta-valerobetaine is a diet-dependent obesogen.

Summary

Obesity and obesity-related metabolic disorders are linked to the intestinal microbiome. Here, we show the microbiome-derived metabolite, δ-valerobetaine (VB) is a diet-dependent obesogen that is increased with phenotypic obesity and is correlated with visceral adipose tissue mass in humans. VB is absent in germ-free mice and their mitochondria but present in conventionalized mice and mitochondria. Mechanistic studies *in vivo* and *in vitro* show VB is produced by diverse bacterial species and suppresses mitochondrial fatty acid oxidation through decreasing cellular carnitine and mitochondrial long-chain acyl-CoAs. VB administration to germ-free and conventional mice increases visceral fat mass and exacerbates hepatic steatosis with Western diet but not control diet. Thus, VB provides a molecular target to understand and potentially manage microbiome-host symbiosis/dysbiosis in diet-dependent obesity.

3.1: Introduction

The ongoing world-wide epidemic of obesity and its comorbidities is a major health challenge.[156,157] While there are multiple contributing factors, emerging evidence links the epidemic to unfavorable changes in the composition and activity of the intestinal microbiota.[158–161] Given the complexity of an individual's interacting genetic background, microbiome, and diet, application of new technologies to study these interactions may be key to personalized obesity management.[162]

Metabolomic profiling complements metagenomic methods by enabling detection and measurement of tens of thousands of small molecule components/products of both the microbiome and diet. In principle, this can be used for monitoring of intestinal microbiota functions in digestion of dietary macromolecules and synthesis of diverse metabolites that may impact human metabolism.[163,164] For example, epidemiological and experimental evidence shows microbial products such as lipopolysaccharide, phenylacetic acid, and methylamines contribute to development of insulin resistance, hepatic steatosis, and cardiovascular disease.[165–169] Intriguingly, untargeted metabolomic analyses of germ-free (GF) and conventional (C) mice with a reconstituted or intact microbiome further reveal approximately 10% of the circulating mammalian metabolome is of microbial origin; the majority of these metabolites are unidentified and without defined functions.[118,170] Therefore, identification and characterization of these microbially-derived metabolites may provide insight into how the microbiome regulates host metabolism and bioenergetics.

Among the known functions of microbiome-derived metabolites, quorum sensing compounds such as N-acyl lactones support communication within and between

prokaryotic members of the microbiota.[171] Interestingly, recent evidence for bi-directional communication between the microbiome and host mitochondria in metabolic health and disease raises the possibility that specific chemical signals also mediate a functional cross-talk between the microbiome and host mitochondria.[172] Bi-directional communication is supported by reports of microbial metabolite effects on host mitochondrial function and metabolism, and mitochondrial genetic effects on the composition of the microbiome.[25,173,174] If the obesity epidemic is a consequence of changes to an evolved microbiome-host symbiosis affecting energy metabolism, then knowledge of the underlying chemical communication mechanisms may be key to remediation.

3.2: Methods

Animals

Germ-free (GF) male and female Swiss-Webster mice (Taconic Biosciences) were raised in germ-free isolators and fed sterilized mouse chow (Envigo 2019S Teklad Global 19% Protein Extruded Rodent Diet) and sterilized water *ad libitum* at the Emory University Gnotobiotic Animal Research Facility. Conventionalized (CV) mice were transferred to bedding from conventional Swiss-Webster (S) mice at three weeks of age and maintained for 3 weeks while paired GF mice were maintained in germ-free isolators. After three weeks, luminal contents from the cecum and colon, portal vein serum, and intact livers were collected for mitochondrial isolation, RNA-sequencing and metabolomics. Data for GF and conventional C57BL6J (jax.org/strain/000664) mice (Jackson laboratories, identical housing as Swiss-Webster) are provided as indicated.

RNA-Sequencing

Analyses were conducted at the Yerkes NHP Genomics Core. RNA was collected and extracted from PAXgene tubes using on-column DNase digestion and assessed for integrity and quantity using an Agilent Bioanalyzer (Agilent Technologies) and a NanoDrop 2000 spectrophotometer (Thermo Fisher Scientific). Libraries were prepared using the Illumina TruSeq mRNA stranded kit. Briefly, 500–1,000 ng of globin-depleted RNA was used for library preparation. ERCC synthetic spike-in controls 1 or 2 (Ambion) were added to each total RNA sample and processed in parallel. Amplified libraries were validated using the Agilent 4200 TapeStation and quantified using a Qubit fluorometer. Libraries were normalized and pooled, followed by clustering on a HiSeq 3000/4000 flowcell using the Illumina cBot. The clustered flowcell was then sequenced

on the Illumina HiSeq 3000 system employing a single-end 101-cycle run, with multiplexing to achieve approximately 20 million reads per sample. Gene IDs were annotated for 41,128 gene IDs (ENSEMBLID) and mapped to 23,568 genes (*mus musculus*) in DAVID. Transcript abundance was estimated using htseq-count v0.6.1p1 and differential expression analyses were performed using DESeq2, with FDR adjustment using Benjamini-Hochberg. A combination of bioinformatics tools was used for data analysis including the molecular signature database (MSigDB – http://software.broadinstitute.org/gsea/msigdb/index.jsp) and Ingenuity Pathway Analysis. Data are publicly available at the Gene Expression Omnibus: GSE145012.

High-resolution metabolomics (HRM)

Cytosolic and mitochondrial fractions from GF (n = 6)/CV (n = 6) liver were prepared by differential centrifugation.[175] Serum and fractionated cytosol and mitochondria were mixed with 2x volume of ice-cold acetonitrile-internal standard solution. Liver and luminal contents were weighed and mixed with 10x volume of ice-cold 20% water/80% acetonitrile-internal standard solution. Tissue samples were homogenized using a pellet pestle prior to the next step. Samples were vortexed, and placed on ice for 30 minutes prior to centrifugation at 14,000*g* for 10 minutes at 4°C to precipitate proteins. Supernatants were transferred to autosampler vials and stored at -70°C prior to instrumental analysis.

Untargeted high-resolution mass spectrometric profiling was performed using a Dionex Ultimate 3000 UHPLC system coupled to a Thermo Scientific Velos LTQ-Orbitrap (metabolite identification studies), Thermo Scientific High-Field Q-Exactive (HFQE) (liver, liver mitochondria, liver cytosol, portal vein) or Thermo Scientific Fusion

(cecum, colon, *ex vivo* incubations, isotope tracer).[176] On the Fusion and HFQE, an LC column switching method using a reversed phase C18 column (Higgins Targa C18 2.1 mm x 50 mm, 3 µM particle size) and a HILIC column (Waters XBridge BEH Amide XP HILIC column 2.1 mm x 50 mm, 2.6 µM particle size) were used for the analytical separation of extracts prior to high-resolution mass spectrometry analysis with HILIC/ESI+ and C18/ESI- at 120k resolution while of ions between 85-1,275 *m/z*. A similar LC column switching method 10 minute and 20-minute reversed phase C18 and HILIC separation methods with 10 cm columns with ESI+ was used on the Velos-Orbitrap for confirmation. Raw files are available on Metabolomics Workbench (doi etc).

Data processing, statistics, and feature selection

Peak detection, noise removal, alignment, and quantification was performed using apLCMS, with downstream quality control performed by xMSanalyzer.[177–179] Each metabolic feature was characterized by its *m/z* ratio, retention time, and peak intensity. Statistical analysis was performed using R-packages *limma* for differential expression analysis and *diffexp* for linear regression implemented in *lm*() function in R 3.4.0.[180] Benjamini-Hochberg FDR-corrections were applied for *limma* and *lmreg* analyses. For pathway enrichment analysis, differentially expressed metabolites with a raw p-value of less than 0.05 were used with *mummichog* software.[181] Pathway enrichment significance in *mummichog 2.0* was based permutation testing with a $p < 0.05$. Metabolite names in *mummichog* were converted to KEGG IDs using http://csbg.cnb.csic.es/mbrole/conversion.jsp. Spearman correlations and heatmaps were performed and prepared using Metaboanalyst 4.0.

Metabolite Identification and Quantification

Detected metabolites were referenced against an in-house reference library established with authentic chemical standards and matched within 5 ppm of the confirmed mass and within 10s of the confirmed retention time.[182] Features of interest were visually inspected to ensure chromatographic and spectral peak quality. When no standard was available, MS isotopic ratios and MS/MS spectra were referenced against online spectral libraries or *in silico* ion dissociation spectra. Tandem MS^2 spectra were collected for target features on either Thermo Scientific Velos-Orbitrap, High-Field Q-Exactive, or Fusion mass spectrometers using collisional induced dissociation (CID) or high-energy collisional induced dissociation (HCD). MS2 spectra were matched to experimental online mass spectral databases mzCloud and METLIN or *in silico* predicted fragmentation patterns from metfrag to identify candidate structures. Standards were purchased when commercially available or synthesized as described below.[183,184] Reference standardization was used for quantification of identified metabolites.

Synthesis of δ-valerobetaine and valine betaine

δ-Valerobetaine (VB) was synthesized as described previously.[185] Briefly, 5-bromovaleric acid (Sigma-Aldrich) and 1 molar equivalent trimethylamine (20% in EtOH) were stirred for 24h under vacuum at room temperature. The precipitate containing trimethylamine HBr salt was removed by filtration and the filtrate was evaporated under vacuum and recrystallized with cold isopropanol and acetonitrile. MS: 160.1332 *m/z* ESI+ (MS2: 101.0597, 60.0809). ^{1}H NMR (*Extended data 3*) (400 MHz, D_2O) δ 3.15 (multiplet, 2H), δ 2.91 (singlet, 9H), δ 2.27 (triplet, 2H), δ 1.64 (quintuplet, 2H), δ 1.46 (quintuplet, 2H). Elemental analysis (as VB-HBr salt) was C 37%, H 8%, N 5%, Br 31%.

Valine betaine was synthesized as previously described.[186] L-Valine and methyl iodide were stirred for 48h in anhydrous methanol in the presence of excess potassium bicarbonate. The precipitate was dried and washed with ice-cold methanol. MS: 160.1332 m/z ESI+ (MS2: 60.0809).

Ex-vivo fermentation

Cecal contents from conventional or GF mice were collected and immediately placed in either De Man, Rogosa, and Sharpe media (MRS broth – Oxoid, CM0359) or degassed Tryptic Soy Broth (Millipore 22092) in oxygen evacuated headspace vials. Samples were incubated at 37°C were collected in triplicate over a 24-h time period and prepared for metabolomics analysis as above.

Ex-vivo microbial metabolism assays

Bacteria were purchased from ATCC and/or isolated in our laboratory and were cultured in specified liquid media. Samples were collected at baseline and again at 18 hours after incubation at 37°C. *Lactococcus lactis Subsp. cremoris* (LC, ATCC 19257), *Lactobacillus rhamnosus GG* (LGG, ATCC 53103), *Lactobacillus paracasei* (HA274), and *Lactobacillus rhamnosus* (HA-114, HA-111, R0011) were grown in MRS broth (Oxoid, CM0359). *Bacillus cereus*, *Listeria monocytogenes* (LM), and *Streptococcus salivarius* (ATCC13419) were grown in brain heart infusion (BHI) media. *E. coli* (K12) and *Salmonella typhimurium* (SL1344) were grown in Luria Broth (LB). *Bifidobacterium longum* (BL, ATCC15707) was grown anaerobically using Oxyrase for Broth (Sigma, SAE0013) in reinforced clostridial media.

VB dose response experiments in HepG2 cells: metabolomics analysis

HepG2 cells (ATCC) were used between passages 8-15 and grown in EMEM (ATCC) supplemented with 10% FBS and 0.5% Penicillin/Streptomycin (P/S). Cells were grown to 90% confluence in 3.5 cm cell culture dishes and treated with experimental compounds (VB, meldonium, propionylcholine, carnitine) in EMEM supplemented with 0.5% FBS and 0.5% penicillin/streptomycin. Cells were washed with ice cold Hank's Buffered Salt Solution (HBSS) and harvested by scraping on ice using 200 µL of ice-cold 20:80 water:acetonitrile containing 9 stable isotope internal standards and centrifuged at 14,000*g* for 10 minutes at 4°C. Supernatants were transferred to autosampler vials and maintained at 4°C until instrumental analysis.

VB dose response experiments in HepG2 cells: Stable Isotope Palmitate Tracer Assay

$^{13}C_{16}$-palmitic acid (Sigma-Aldrich 605573) was dissolved in 150 mM NaCl after heating to 70°C and slowly mixed with prewarmed (37°C) FFA-free BSA (Sigma-Aldrich A4602) solution in 150 mM NaCl with stirring to produce a 1 mM palmitate to 0.17 mM BSA ratio. HepG2 cells were grown in 12-well cell culture plates to 80% confluence. Cell media was replaced with EMEM containing 0.5% FBS for 12 h ± VB prior to treatment with labeled palmitic acid. Cells were washed twice with pre-warmed HBSS and media was replaced with EMEM containing 0.5% FBS, 200 µM labeled palmitate, and either vehicle, 50 µM VB, 40 µM etomoxir, or 50 µM carnitine. At each time point, cells were washed once with ice cold HBSS and harvested by scraping on ice using 200 µL of ice-cold 20:80 water:acetonitrile containing 9 stable isotope internal standards and centrifuged at 14,000*g* for 10 min at 4°C. Supernatants were transferred to autosampler vials and maintained at 4°C until analysis. Data were analyzed using xCalibur

QuanBrowser for carnitine and labeled palmitate, palmitoyl-CoA, palmitoylcarnitine, acetyl-CoA, and acetylcarnitine.

VB dose response experiments in HepG2 cells: Mitochondrial Respiration Assays

Oxygen consumption (OCR) was measured in the human hepatoma HepG2 cell line using a Seahorse XFe96 analyzer (Agilent Technologies). For assessments of respiration linked to oxidation of glucose and glutamine, cells were cultured on 96-well cell culture microplates and treated overnight with 0, 1, 3, 10, 30, 100 μM VB in DMEM with 0.5% FBS. Cells were then washed 1x with 100 μM pH 7.4 Seahorse XF DMEM (Agilent Technologies) in 0.5% FBS and media was replaced with XF DMEM supplemented with fuel substrates and VB or vehicle. The media was supplemented with 10 mM glucose, 2 mM GlutaMAX, and 1 mM pyruvate ± VB.

For assessments of fatty acid oxidation, cells were serum-starved overnight with or without VB. After washing, media was replaced with Krebs Heinseleit Buffer (KHB) containing 200 μM BSA-conjugated palmitate (Agilent Technologies) in the absence of supplemental glucose, GlutaMAX, pyruvate, or carnitine. KHB was prepared from pH 7.4 sterile filtered water containing 111 mM NaCl, 4.7 mM KCl, 2 mM $MgSO_4$, and 1.2 mM NaH_2PO_4. VB (0, 10, 50 μM final concentration) or etomoxir (40 μM final concentration) were added to the assay medium prior to assessments of oxygen consumption (OCR) and extracellular acidification rate (ECAR).

To evaluate mitochondrial function, a MitoStress test kit (Agilent Technologies) was used with respiration assays. Three consecutive respiration measurements were acquired every 10 minutes for every experimental condition prior to and after injections of Oligomycin (1.5 μM final concentration), FCCP (1 μM final concentration), and

Rotenone/Antimycin A (0.5 μM final concentration). Basal respiration (OCR prior to injection of mitochondrial inhibitors), ATP production (difference in OCR after addition of oligomycin), maximal respiration (OCR after addition of FCCP) and spare capacity (difference in OCR between basal and maximal respiration) were calculated using the Seahorse XF Cell Mito Stress Test Report Generator (https://www.agilent.com/en/products/cell-analysis/cell-analysis-software/data-analysis/seahorse-xf-cell-mito-stress-test-report-generators).

Animal VB model

Animal experiments were performed under approved Emory University IACUC animal protocols. For experiments with fed mice, conventional C57BL6J mice (Jackson laboratories) were injected IP with 100 μL saline vehicle, 100 μL 10 mM VB (10 mg/kg), or 100 μL 100 mM VB (100 mg/kg) once a day for one week. For experiments in fasted conventional mice, animals were treated with the same doses for three days and then fasted for 12 hours prior to sample collection. For the 8-week study in conventional mice (C57BL6J), 8-week old mice were given a Western Diet (Research diets D12079b) or standard chow ad libitum and injected IP daily with 50 mg/kg VB or PBS vehicle. For the 6-week study in GF mice (C57BL6J), animals were maintained in the Emory Gnotobiotic Animal Core (EGAC) within Emory's Health Science Research Building Vivarium. At 6 weeks old, GF mice were transferred into hermetically sealed IsoCage bioexclusion systems (Techniplast) and given a Western Diet (Research diets D12079b) or standard show (Labdiet Rodent 5001) ad libitum and injected IP with 25 mg/kg VB or PBS vehicle. The diets were doubly irradiated and vacuum sealed to prevent contamination. None of the diets used for conventional or GF mouse experiments

contained VB. Information on the diet composition is provided in supplemental information. All manipulation of mice were performed under BSL-2 conditions in a sterile laminar flow hood. Mice were periodically monitored by microbial fecal testing to ensure GF status. At the end of each treatment period liver, heart, brain, adipose, cecal and colonic contents and serum were collected for characterization. Fasting plasma insulin, resistin, glucagon, IL-6, TNF-alpha, and MCP-1 was measured via Milliplex Mouse metabolic hormone panel (Millipore, Burlington, MA) on the Luminex 200 instrument (Millipore).

Histology (Oil Red O, Hematoxylin and Eosin) analysis

Oil red O staining for neutral lipids was performed on 8-10-micron mouse liver sections prepared using a Cryostat. Images were taken on a Nikon Eclipse 50i at 20x magnification and red density was quantified in ImageJ software.

Liver samples were removed upon sacrifice and fixed in 10% formalin overnight followed by transfer to 70% ethanol with subsequent processing and embedding into paraffin. 5-micron sections were cut and underwent H&E staining as performed by the Emory University Cancer Tissue and Pathology core. Stained slides with a minimum of 3 sections were examined in a blinded fashion by a board-certified pathologist for hepatic steatosis. Scoring was as follows: 0 = 0-5% steatosis, 1 = 5-33% steatosis, 2 = 33-66% steatosis, 3 = >66% steatosis. Average scores were taken from multiple sections per sample.

Triglyceride quantification

Triglycerides were quantified in tissues using a triglyceride assay kit (Abcam 65336). 50 mg of liver tissue was homogenized in 1 mL of assay buffer and diluted

100x prior to addition of lipase. After 20 minutes, the triglyceride probe was added. After incubation for 30 minutes, the plate was read fluorometrically (535/587 nm) and quantified using the provided standard calibration curve.

Lipidomics analysis

Chemical reagents and HPLC grade organic solvents (methanol, chloroform, acetonitrile, isopropanol, butylated hydroxytoluene, ammonium formate, and formic acid) were purchased from Sigma Aldrich (St. Louis, MO, USA). A mixture of deuterated synthetic lipid standards, SplashMix (Avanti Polar Lipids, Alabaster, AL, USA) was used as an internal calibrant.

Lipids were extracted according to a modified Bligh and Dyer lipid extraction protocol. Briefly, 50 µL plasma or 100 mg tissue sample was homogenized in 1 mL methanol:chloroform (2:1). 10 µl of each sample was reserved and used to create a tissue specific pooled quality control (QC) sample. To the remaining homogenate, 10 µL internal standard was added. Samples were vortexed for 30 minutes and subsequently centrifuged for 10 minutes at 4000 rpm to pellet any precipitated protein. The supernatant was collected and phases were separated by the addition of 500 µL 100 mM sodium chloride solution. Addition of sodium chloride in lieu of water was used to aid the complete partition of amphiphilic lipids to the organic phase. The organic phase was retained, dried under nitrogen gas, and the weight of recovered lipids was recorded. The extracted lipids were reconstituted in 500 µL methanol:chloroform (1:1) prior to injection into the mass spectrometer. Blank samples were prepared by diluting SplashMix 1:100 (Avanti Polar Lipids Inc. Alabaster, AL, USA) in 1:1 v/v methanol:chloroform. QC samples were prepared in the same manner as samples.

Ten microliters of reconstituted lipid extract was injected into a Thermo ID-X (Waltham, MA, USA) equipped with a Vanquish Duo UHPLC System (Thermo; Waltham, MA) for LC/MS analysis. Chromatographic separation of lipids was achieved using a Thermo Accucore C18 (100 x 4.6mm; 2.6 µm) using a 10 minute linear gradient of the following binary solvent system: Solvent A water: acetonitrile (40:60 v/v; mobile phase A) and Solvent B isopropanol: acetonitrile (90:10 v/v; mobile phase B) containing 10 mM ammonium formate and 0.1% formic acid. Data dependent MS/MS (DDA) were performed in both positive and negative ionization modes for monitoring diagnostic ions for identification. Full MS scans were collected at 120,000 resolution while MS/MS data was collected using 30,000 resolution.

Lipidomics data were processed using proprietary software LipidSearch (Tokyo, Japan), permitting the alignment and identification of lipid species from the DDA, MS/MS fragment data. First, full scan MS data was searched for monoisotopic precursor ions. Second, MS/MS fragment ion data was then scanned against a database for identification of lipids. Finally, MS/MS quality filters were used to provide headgroup specificity and fatty acyl chain information to identify specific lipid classes and species.

VB dose response experiments in HepG2 cells: Luciferase Reporter

To test the effect of VB on PPAR-alpha driven gene regulation, we performed luciferase reporter assays. HepG2 cells, grown in DMEM containing 10 % stripped-FBS, were passed into 96- well clear bottom TC-treated microplates. Cells were transfected at ~60 % confluence per manufacturer instruction. Briefly, 1 ng well^{-1} of pSG5 vector containing full-length human PPARa receptor, 100 ng well−1 PPAR-

response element-driven firefly luciferase reporter (PPAR-response element X3-TK-luc), and 50 ng well^{-1} constitutive *Renilla* luciferase reporter (phRLtk) were mixed with Optimem and Fugene. Twenty-four hours following transfection, media was changed to DMEM containing 0.5 % FBS in the absence of glutamine, glucose or pyruvate. Cells were treated with either VB or PPARa agonist WY14643. One day post-treatment, firefly and *Renilla* luciferase activity was detected using the Dual-Glo Luciferase Assay system (Promega) and read on a BioTek Synergy 4. Data were plotted as bioluminescence generated from firefly luciferase divided by bioluminescence generated from *Renilla* luciferase, normalized to vehicle treatment for each well, and plotted using GraphPad Prism (v8).

Emory Pediatric Liver Biopsy Data Repository

The Emory Pediatric Liver Biopsy Data Biorepository is an ongoing cross-sectional cohort study of children who provided data and biospecimens prior to undergoing a clinically-indicated liver biopsy for suspected liver disease or monitoring of a liver disease, as previously described.[187] Exclusion criteria were fever with in the past two weeks, renal disease or insufficiency, or pregnancy. The analytical sample was a sub-group of 74 participants ages 7-19 years old who were enrolled between 2007 to 2015, had a clinical diagnosis of NAFLD after exclusion of other liver diseases. A physical examination and fasting blood collection were performed prior to liver biopsy. Liver biopsies were reviewed by pathologists in a blinded manner, and were scored based on grade of steatosis (<5% = 0, 5-33% = 1, 34-66% = 2, >66% = 3), steatosis location (Zone 1, Zone 3, azonal, panacinar), lobular inflammation (0 = No foci, 1 = < 2 foci per 200 x field, 2 = 2-4 foci per 200 x field, 3 = > 4 foci per 200 x field), portal

inflammation (0 = none, 1 = mild, 2 = more than mild), hepatocyte ballooning (0 = none, 1 = few, 2 = many), and fibrosis stage (0 = none, 1 = periportal or perisinusoidal, 2 = perisinusoidal and portal/periportal, 3 = bridging fibrosis, 4 = cirrhosis). All study protocols were approved by the Emory University and Children's Healthcare of Atlanta Institutional Review Boards and written informed consent and assent were obtained.

Multiple linear regression adjusted for age (years), sex, and race/ethnicity were used to examine associations of steatosis grade, based on liver biopsy scores, with plasma VB levels. This was done with steatosis grade as a continuous variable (1, 2, or 3) to assess the dose response, and as a categorical variable to compare VB levels in those with moderate and severe steatosis compared to mild steatosis. VB was log-transformed for analysis. Regression analysis was conducted in R Statistical Software (v3.5.3).

Center for Health Discovery and Well-Being (CHDWB) Cohort

This cohort includes adults who were primarily employed by Emory University or Emory Healthcare systems at the time of enrollment. Individuals employed for greater than two years were invited to join the study from an alphabetized list and underwent extensive phenotyping as previously described.[188] General exclusion criteria were presence of a poorly controlled chronic disease, an acute illness within 12 weeks of study visit, currently pregnant or breastfeeding, or a history of malignancy within the previous five years.[189] Two subsets of the cohort (n = 179 and 214) with high-resolution metabolomics data were included in this study.[190] Body composition and visceral adipose tissue (VAT) were determined using a Lunar iDXA densitometer and CoreScan™ software (GE Healthcare, Madison, WI, USA), which automatically

quantifies VAT and has been validated against computed tomography [64]. Peripheral blood samples were drawn by trained nurses and fasting insulin and glucose levels were measured commercially (Quest Diagnostics, Valencia, CA). The homeostatic model assessment of insulin resistance (HOMA-IR) was calculated as fasting insulin (μIU/mL) x fasting glucose (mg/dL) divided by 405.[191]

Multiple linear regression analyses, adjusting for age, race, and sex, were used to test for associations between VB with VAT and HOMA-IR. VAT and HOMA-IR were log-transformed for analyses. Analyses were conducted in JMP Pro (version 14, SAS Inc, Cary, NC).

PREMIX Fecal Microbiota Transplantation Clinical Trial Cohort

All participants enrolled in PREMIX (ClinicalTrials.gov identifier: NCT02922816) had at least one clinical infection with a target multi-drug resistant organism (MDRO) as well as demonstration of persistent post-infection colonization by MDRO positive stool culture on differential and selective media. To minimize potential variability in donor-specific effects, all FMT doses were sourced from a single stool donor, who was well known to the investigators. The donor was thoroughly screened with questionnaires, blood, urine, and stool testing for behavioral risk factors and potentially transmissible pathogens including MDROs and E. coli pathotypes. Study visits were conducted in 36-day cycles with visits on Days 1, 15, and 36, with additional stool sample collection on Day 2. Participants were randomized 1:1 to an observation cycle (Cycle 0) with administration of polyethylene glycol prep alone or an FMT cycle (Cycle 1) with prep followed by FMT delivered as retention enema (**Fig. 5a**). Most participant characteristics were balanced by randomization with exception of sex. Participants with growth of any

MDRO in stool culture at Day 36 of Cycle 0 or Cycle 1 proceeded to Cycle 1 or Cycle 2 respectively, with intent to allow all participants to be treated with up to two FMTs and half of participants to serve as their own controls. Of the 16 participants enrolled, 11 completed at least one full visit cycle. Ten participants received at least one FMT and were evaluable for response. Of these ten, eight individuals had samples available for plasma metabolomics with samples collected at day 1, 15, and 36). Of these eight individuals, 6/8 (75%) were female, 7/8 (88%) were white, 3/8 (38%) were Hispanic and their median age was 62 years old (IQR 53-70).

Data availability

The data that support the findings of this study are available on request from the corresponding authors.

3.3: Results

δ-Valerobetaine (VB) is a microbiome-derived mitochondrial metabolite

To identify microbial metabolites that could impact mitochondrial function, we split a cohort of germ-free (GF) mice into two groups at three weeks of age. For the next three weeks, one group remained GF while the other group was conventionalized (CV) by exposure to bedding from conventional (C) mice (animals with an intact microbiome). We compared the metabolome of liver and liver mitochondria from CV mice compared to GF mice (**Figure 3.1**). The top discriminatory metabolite had an accurate mass *m/z* of 160.1332 by ultra-high-resolution mass spectrometry (**Figure 3.1a**), corresponding to predicted elemental composition $C_8H_{18}NO_2$. This metabolite was found in liver and other tissues, portal and peripheral circulation, and cecal contents of conventional but consistently absent in germ-free mice (**Figure 3.1b; Figure 3.2a**). Authentic standard co-elution and MS/MS experiments show the identity of 160.1332 *m/z* to be δ-valerobetaine (VB) (**Figure 3.1c**). Concurrent analyses of propionylcholine and valine betaine, similar molecules with identical elemental compositions, conclusively excluded these structures (**Figure 3.3**). VB was not present in the mouse diet and was not detectable in other samples collected from GF mice (**Figure 3.2b**). Concentrations of VB in conventional mice were in the millimolar range in the cecum, with somewhat lower concentrations in the colon (**Figure 3.1d**). Concentrations were 9-26 μM in the portal vein, with higher concentrations in the liver (75-190 μmol/kg wet weight) and lower concentrations in the peripheral plasma (2-10 μM) indicating tissue accumulation (**Figure 3.1d**).

To determine whether intestinal microbes produce VB, we performed *ex vivo* incubations of cecal contents from conventional and GF mice. LC-MS/MS analyses show only conventional cecal contents produced VB whereas GF cecum contents did not (**Figure 3.1e**). Incubations of candidate microbes from diverse taxa of gram positive and gram negative pathogenic and commensal bacteria, including *lactobacilli*, *E. coli*, *Salmonella typhimurium* (SL1344), anaerobic *Bifidobacterium longum*, and others showed that VB is produced by monocultures of different and diverse microbes (**Figure 3.1f**). The presence of VB in different tissues and isolated mitochondria of mice with an intact microbiome therefore reflects microbial production, followed by absorption and distribution.

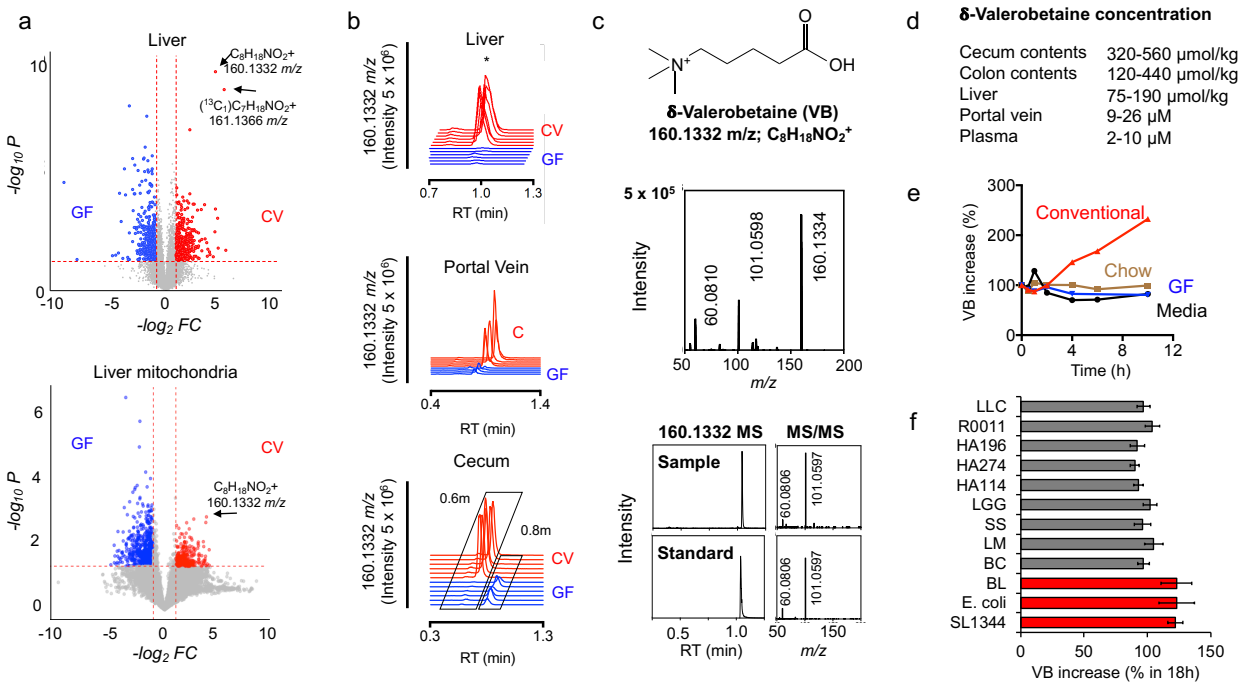

Figure 3.1: δ-Valerobetaine (VB) is a microbiome-derived mitochondrial metabolite. **a)** Volcano-plots of ultra-high-resolution mass spectrometry of extracts from germ-free (GF, blue, n = 6) and conventionalized (CV, red, n = 6) mouse liver and liver mitochondria show a metabolite with accurate mass *m/z* 160.1332 is higher in CV mouse liver and liver mitochondria. The accurate mass allows prediction of an elemental composition $C_8H_{18}NO_2$. The horizontal broken line is at limma *p*-FDR = 0.05, and the vertical broken line is at fold-change (FC) equal two. A list of differentially expressed annotated features is provided in Supplementary Table 1. **b)** Targeted analysis of *m/z* 160.1332 shows the presence of this metabolite in liver, portal vein, and cecum of mice with intact microbiome (red extracted ion chromatograms) but not in germ-free mice (blue extracted ion chromatograms). Other tissues are shown in Supplemental Fig. 1. **c)** Experimental confirmation that the chemical structure of *m/z* 160.1332 is VB is provided by co-elution and fragmentation pattern of *m/z* 160.1332 for experimental sample and synthesized standard. High-resolution tandem mass spectral

analysis shows the characteristic fragmentation pattern of *m/z* 160.1332 includes the trimethyl ammonium product ion, *m/z* 60.061. VB standard was synthesized and structure confirmed by ^{1}H-nuclear magnetic resonance spectroscopy. Other metabolites with elemental composition identical to valerobetaine, i.e., valine betaine and propionylcholine, are excluded by criteria for co-elution and fragmentation. **d)** Concentration of valerobetaine is highest in cecum and colon, with concentrations in portal vein, peripheral plasma and liver showing transport and tissue uptake. **e)** Proof that VB is generated by the microbiome is obtained by mass spectrometry detection of time-dependent increase in *m/z* 160.1332 in *ex vivo* incubation of cecum contents of mice with intact microbiome. Cecum contents from germ-free mice did not generate VB, and control incubation of mouse food showed no generation of VB. **f)** Multiple species of commensal and pathogenic bacteria generate VB as shown by time dependent increase in VB (*m/z* 160.1332) in monocultures. Species included *Lactococcus lactis Subsp. cremoris* (LC, ATCC 19257), *Lactobacillus rhamnosus GG* (LGG, ATCC 53103), *Lactobacillus rhamnosus* (HA-114, R0011), *Bacillus cereus* (BC), *E. coli* (K12), *Streptococcus salivarius* (SS), *Listeria monocytogenes (LM)*, *Salmonella typhimurium* (SL1344), and *Bifidobacterium longum* (LM). At least 4 replicates of each monoculture were generated for sample analysis. This experiment was designed to test for generation of VB and used different culture conditions for different species; consequently, the relative productions may not be representative of enteric generation.

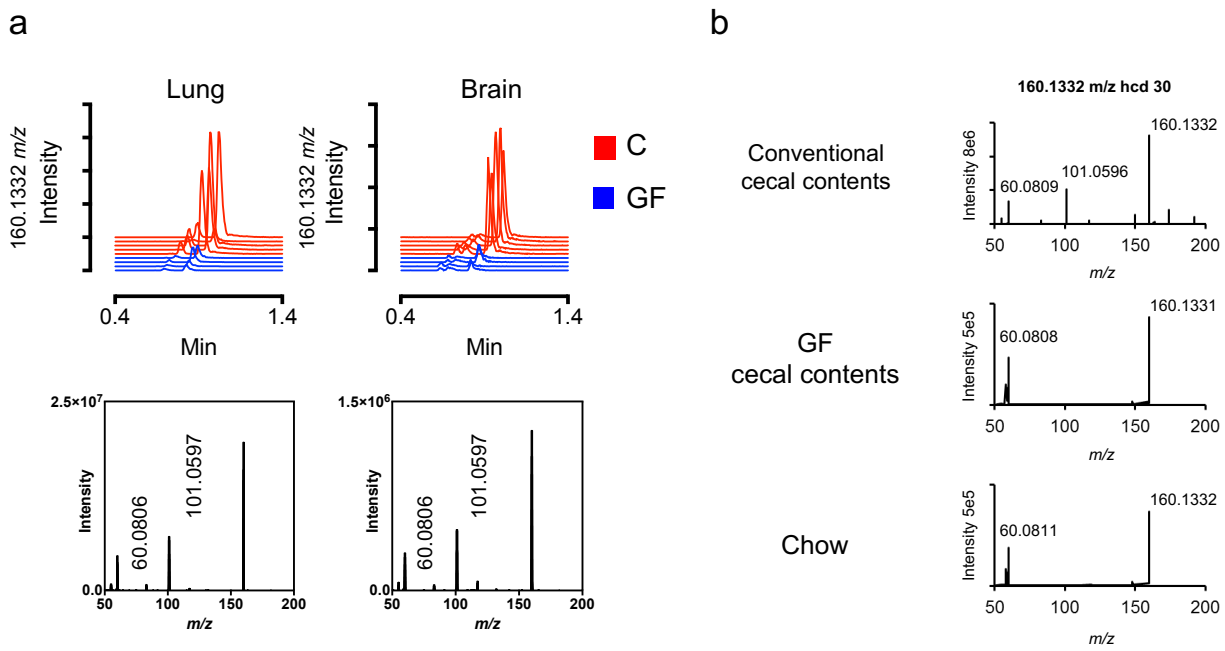

Figure 3.2 Valerobetaine (VB) is present in the lung and brain of conventional mice but not germ-free mice. Mass spectrometric analysis of VB in a) lung and brain of conventional (C) and germ-free (GF) mice and b) Ion dissociation spectra (MS/MS) analysis of 160.1332 *m/z* in cecal contents and mouse diet. VB was not present in GF cecal contents or chow diet.

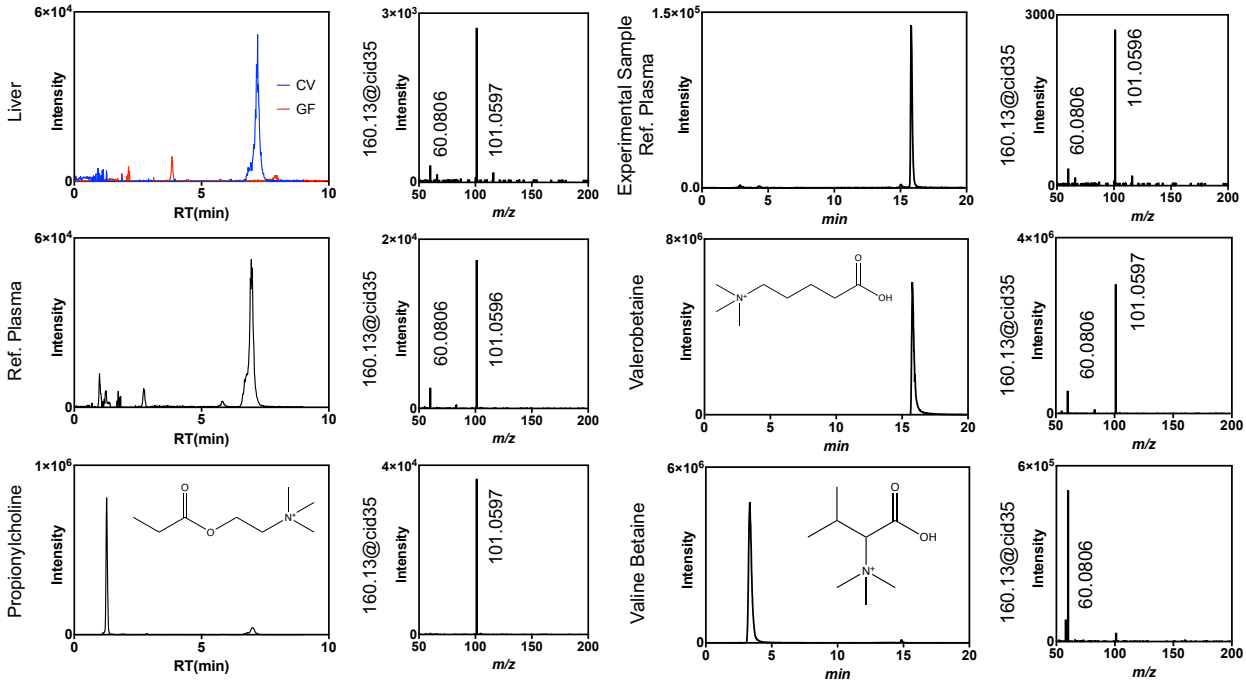

Figure 3.3: **Confirmation of metabolite identity for 160.1332 *m/z***. Co-elution of experimental samples with authentic standard shows 160.1332 *m/z* observed in conventional and conventionalized mouse tissues and human plasma is δ-valerobetaine (VB). Propionylcholine (retention time 2 minutes) and valine betaine (retention time 4 minutes) standards did not co-elute with the observed peak that is present only in CV animals (retention time 7-8 minutes in left panels and 16 minutes in right panels.). Additionally, MS/MS analysis can differentiate propionylcholine (no 60.0809 *m/z* fragment ion) and valine betaine (no 101.0600 *m/z* fragment ion) from VB. VB standard (middle right) produced a peak that co-eluted with the experimental sample (top right) and produced the identical MS/MS spectra as the experimental sample.

VB decreases mitochondrial fatty acid oxidation and increases lipid accumulation in host tissues

We performed dose-response experiments with VB *in vitro* (**Figure 3.4a**) and *in vivo* (**Figure 3.4e**) to examine metabolic effects of VB. The mitochondrial carnitine shuttle was the top metabolic pathway associated with VB in human HepG2 cells (**Figure 3.4a**). At 10 μM, equivalent to VB present in conventional mouse portal circulation, the cell content of carnitine was decreased to half that of control cells. The carnitine shuttle employs carnitine for transport of long-chain fatty acyl chains into mitochondria for fatty acid β-oxidation. Under culture conditions mimicking fasting (no glucose/glutamine), VB elicited a dose-dependent decrease in palmitate-dependent mitochondrial oxygen respiration (**Figure 3.4d**). The effect of VB on inhibition of palmitate-dependent oxygen consumption rate was confirmed by stable isotope tracer studies of palmitate metabolism, which showed that VB inhibits formation of $^{13}C_{16}$ palmitoylcarnitine from $^{13}C_{16}$ palmitate and decreases the formation of $^{13}C_2$ acetyl-CoA (**Figure 3.4e**). Rescue experiments showed that addition of carnitine restores cellular carnitine and formation of palmitoylcarnitine (**Figure 3.5a***).* Thus, VB inhibited mitochondrial long-chain fatty acid metabolism through effects on carnitine and operation of the carnitine shuttle. Control experiments for studies of palmitate-dependent O_2 consumption rate showed that when glucose, glutamine, and pyruvate are present at high concentration in the culture media, VB caused little decrease in basal O_2 consumption rate, ADP-linked O_2 consumption rate, spare capacity, or non-mitochondrial respiration (**Figure 3.5b**). This shows the effect of VB on fatty acid β-oxidation for mitochondrial energy production is dependent on the availability of other (glucose/glutamine) fuel substrates.

To test whether VB treatment could inhibit mitochondrial FA oxidation in vivo, we performed short-term VB treatment experiments in conventional mice. VB treatment increased circulating and hepatic VB (**Figure 3.6a and b**). Similarly, as observed in cells, the carnitine shuttle was the top metabolic pathway associated with VB treatment in mice (**Figure 3.6c and d**). VB treatment decreased circulating (**Figure 3.4b)** and hepatic (**Figure 3.4c**) carnitine (**Figure 3.6e-g**). Decreases in systemic carnitine were accompanied by increased carnitine in the urine (**Figure 3.6h**). Furthermore, VB treatment altered circulating and systemic acylcarnitine and acyl-CoA profiles (**Figure 3.4f**, **Figure 3.6**). In whole tissue, VB increased hepatic palmitoyl-CoA (**Figure 3.4f**) and decreased other short, medium, and long-chain acylcarnitines and CoAs under fasted conditions. In mitochondria, VB decreased the abundance of long-chain fatty acyl-CoAs and carnitines (**Figure 3.4g, Figure 3.6g**), consistent with accumulation of long-chain acyl-CoAs accumulating in cytoplasm and decreased carnitine-dependent transport of long-chain acyl groups into mitochondria for long-chain fatty acid β-oxidation. There was no difference in circulating or hepatic VB between the fasted or fed state (**Figure 3.6i**). VB also decreased circulating and hepatic β-hydroxybutyrate, a product of mitochondrial β-fatty acid oxidation (**Figure 3.7***)*. Additionally, liver triglycerides, the storage form of excess lipids, increased after fasting in both male and female mice (**Figure 3.4h**), and Oil Red O staining of liver showed VB treatment increased macrosteatotic lipid deposits, especially under fasted conditions (**Figure 3.4h**). Finally, lipid profiling showed that VB treatment increases triacylglycerol and diacylglycerol species in liver, heart, and brain (**Figure 3.8**). Taken together, these data

show VB causes systemic carnitine insufficiency, resulting in a decrease in mitochondrial long-chain fatty acid β-oxidation and tissue fat accumulation.

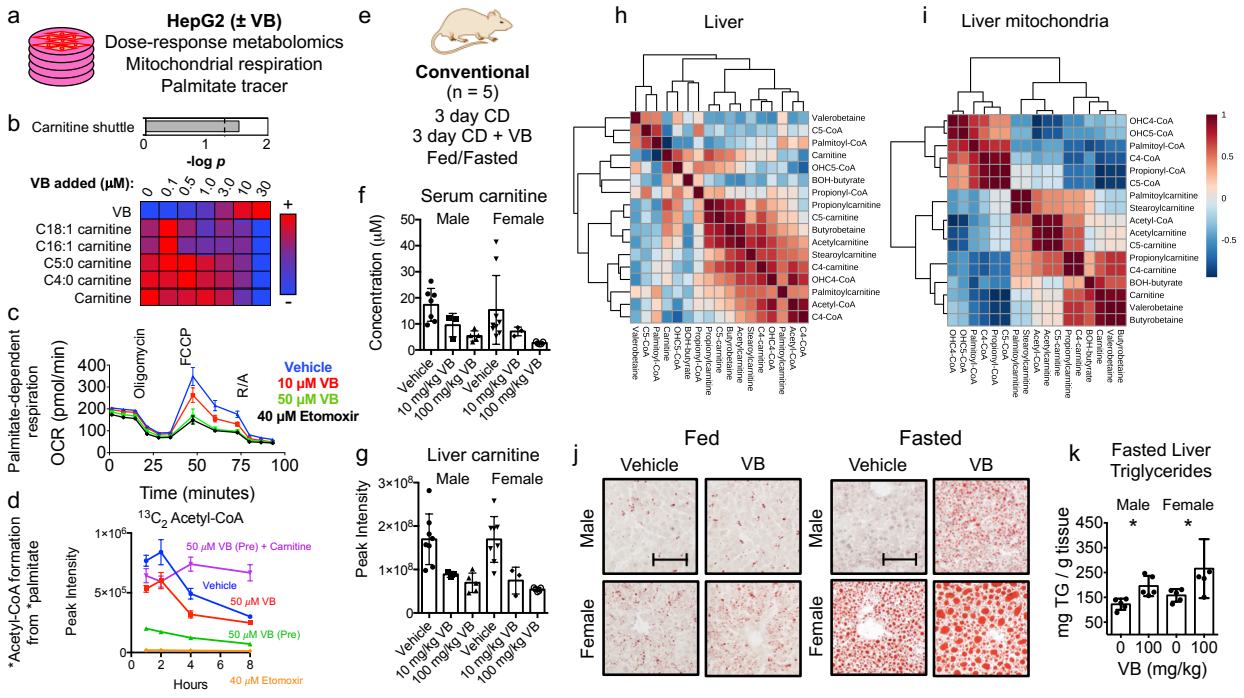

Figure 3.4: Valerobetaine (VB) decreases fatty acid oxidation and increases lipid accumulation in host tissues. a) Experimental *in vitro* characterization of VB activity in HepG2 cells. b) VB alters carnitine shuttle metabolism ($p < 0.05$, mummichog pathway enrichment analysis) and decreases carnitine and acylcarnitines in cultured cells treated with 12h with VB at indicated concentrations (n = 8 each concentration). Spearman correlation analysis with Bejamini-Hochberg FDR corrections were used to identify metabolites with a dose-response relationship with VB-treatment. c) Mitochondrial palmitate-dependent O_2 consumption rate is inhibited by VB. HepG2 cells were incubated for 12 h without glucose, glutamine and pyruvate and studied with either vehicle or VB at 10 or 50 μM. Effect of VB is most pronounced in the spare capacity measured after addition of the uncoupler FCCP. Data presented are 6-8 technical replicates ± standard error of the mean. d) VB decreases formation of labeled acetyl-CoA from labeled palmitate in cultured cells (n = 3). e) Experimental *in vivo*

characterization of VB activity in mice. Mice of each sex were given daily intraperitoneal injection with saline (n = 5), VB at 10 mg/kg (n = 3), or VB at 100 mg/kg (n = 8) for 1 week. f, g) VB decreases circulating and hepatic carnitine in mice. Mice of each sex were given daily intraperitoneal injection with saline (n = 5), VB at 10 mg/kg (n = 3) or VB at 100 mg/kg (n = 8) for 1 week. Kruskal-Wallis test with Dunn's multiple comparisons test to identify pairwise differences s in GraphPad Prism 6.0. Serum male (KW statistic – 9.021, $p = 0.0029$); female serum carnitine (KW statistic 10.98, $p = 0.0004$); male liver carnitine (KW statistic 11, $p = 0.0003$); female liver carnitine (KW statistic 10.83, $p = 0.0004$). h) VB is correlated with increased hepatic palmitoyl-CoA and palmitoylcarnitine in the fasted state. Spearman correlations for selected metabolites in carnitine shuttle metabolism and VB for f and g. i) VB is correlated with decreased mitochondrial long chain acylcarnitine and CoAs. j. k) VB exacerbates hepatic steatosis in male and female mice under fasted conditions as measured by Oil Red O staining ($p < 0.05$, 1-tailed t-test) and triglyceride analysis ($p < 0.05$, 1-tailed t-test). Mice of each sex were given daily intraperitoneal injection with saline (n = 5) or VB at 100 mg/kg (n = 5) for 3 days ± fasting. Scale bar represents 100 μm.

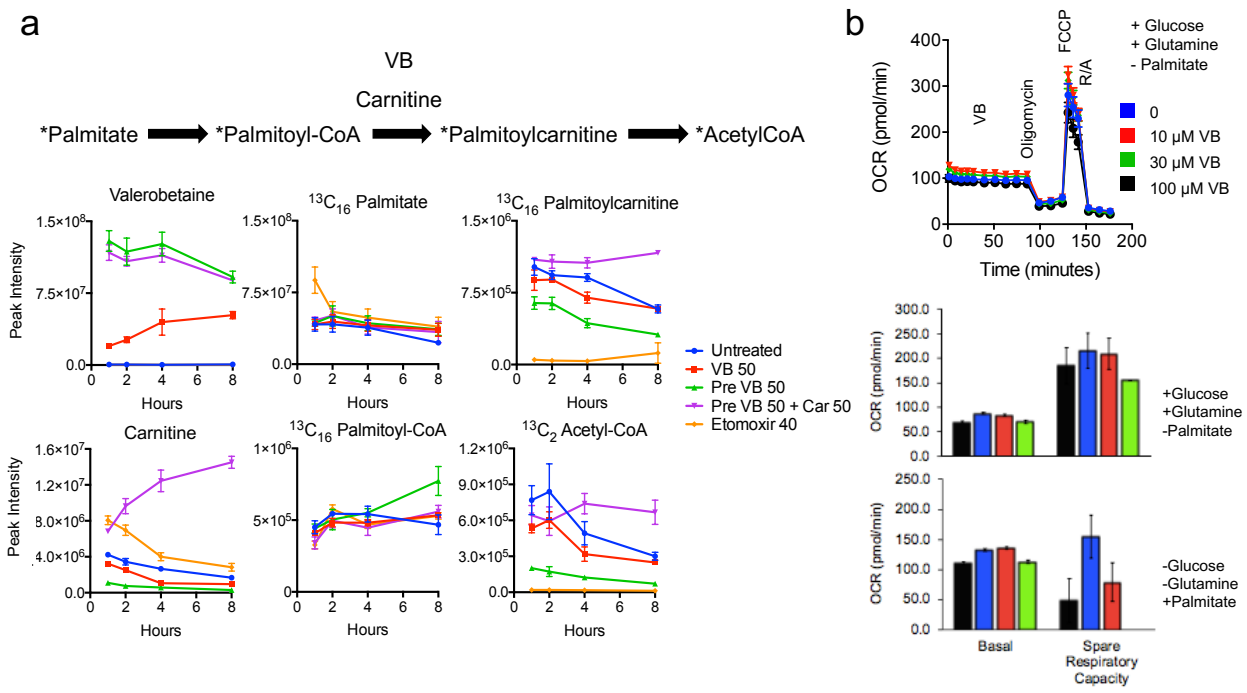

Figure 3.5: VB inhibits mitochondrial fatty acid oxidation. a) Stable isotope tracer study to examine the immediate effect of VB treatment on cellular mitochondrial fatty acid oxidation. 12 hour pretreatment with VB (green) decreased the formation of labeled acetyl-CoA (bottom right) by approximately 75% compared to vehicle (blue). Addition of carnitine back to cells pretreated with VB for 12 hours (purple) restored the carnitine-dependent formation of mitochondrial acetyl-CoA. Co-treatment of VB with the addition of stable isotope-labeled palmitate (red) decreased the formation of labeled acetyl-CoA by approximately 25% compared to vehicle. Data for VB, carnitine, and other metabolites are shown to illustrate VB treatment does not affect uptake of labeled $^{13}C_{16}$ palmitate (top middle), or the conjugation of labeled palmitate to CoA (bottom middle). VB treatment decreased carnitine approximately 20% after one hour (bottom left) and these changes drive decreased formation of labeled palmitoylcarnitine (top right) and labeled acetyl-CoA (bottom right). Each data point represents the average of

3 biological replicates ± standard deviation. b) The effects of VB on mitochondrial respiration is dependent on the availability of fuel substrates. In the presence of glucose and glutamine, VB does not decrease basal respiration or spare respiratory capacity.

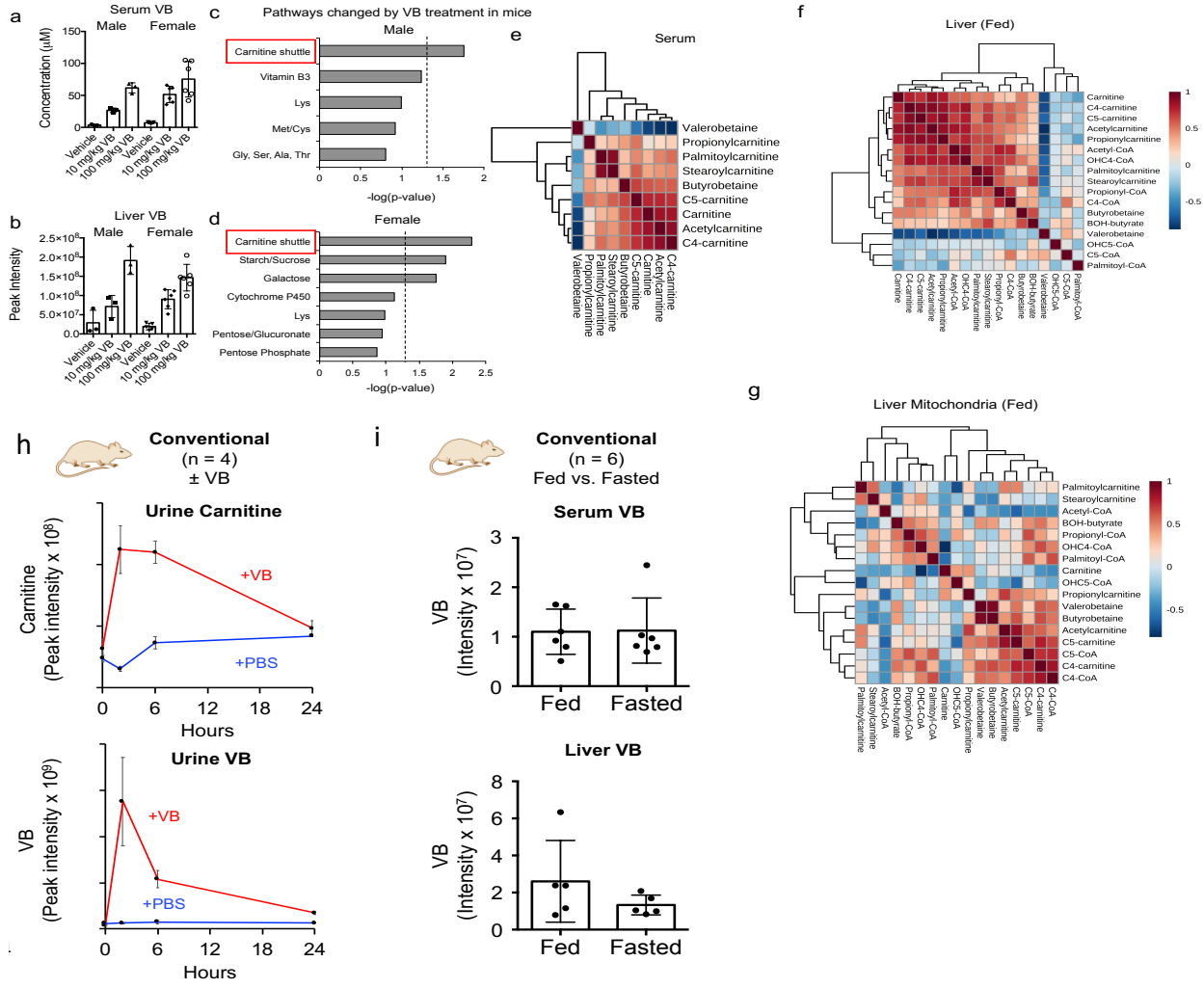

Figure 3.6: VB causes systemic alterations to carnitine metabolism in mice. a, b) Increases in circulating and hepatic VB following VB treatment in conventional mice. c, d) Metabolomics analysis shows VB alters carnitine shuttle metabolism in male and female mice ($p < 0.05$, mummichog pathway enrichment analysis). e-g) VB elicits a

systemic carnitine deficiency in fasted and fed mice and decreases circulating and tissue carnitine and acylcarnitines. VB elicits differential effects on acylcarnitine and acyl-CoA metabolism in different tissues depending on fasted or fed status. Correlation heatmaps are based on Spearman's correlation values. H) Time course of urinary carnitine and VB following VB treatment (at time 0) in conventional mice. VB treatment increases urinary carnitine at 2h and 6h. Urinary VB is stable at 0, 2, 6, 24h time points in PBS-treated mice. i) Fasting does not change circulating and hepatic VB compared to fed mice.

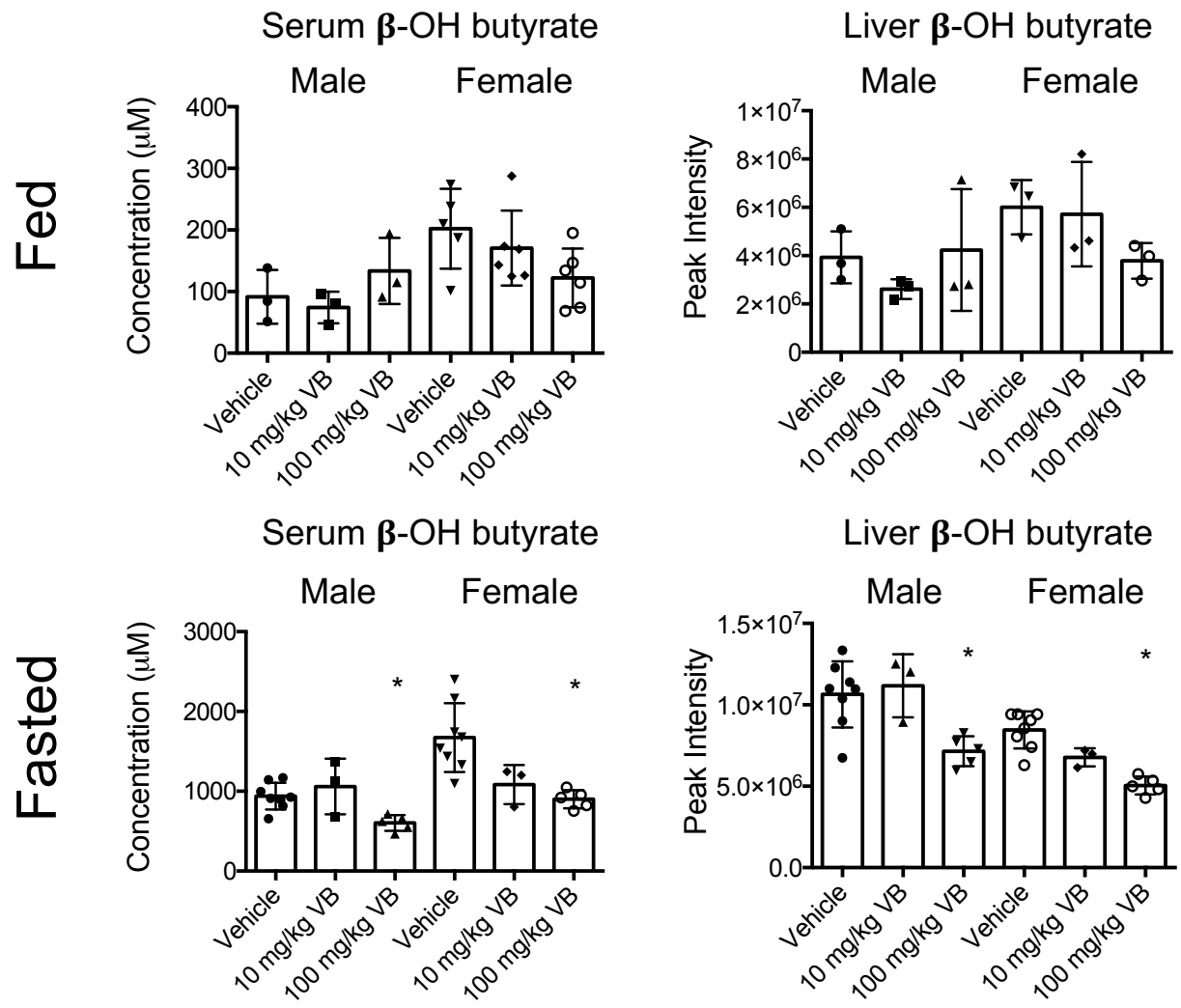

Figure 3.7 Valerobetaine (VB) decreases circulating and hepatic beta-hydroxbuyrate. a) Mass Spectrometry was performed on both serum and liver samples for both male and female mice with either vehicle or VB at two different concentrations. Statistical analysis was performed through Kruskal-Wallis analysis with Dunn's multiple comparisons tests.

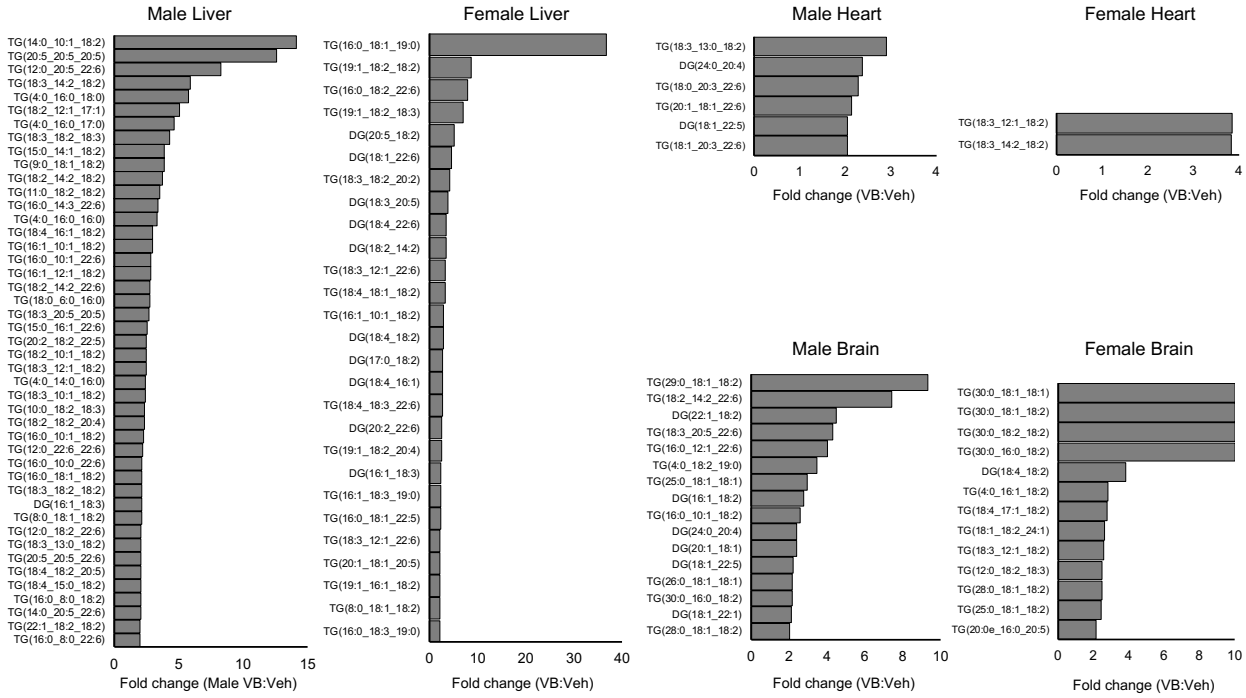

Figure 3.8: VB alters neutral lipid profiles liver, heart, and brain of male and female mice. a) Samples of heart, liver, and brain from both male and female mice were analyzed for neutral lipids by untargeted lipidomic profiling.

VB treatment increased adiposity in GF and conventional mice on a Western Diet

VB effects in fasting are particularly intriguing as a mechanism causing obesity because decreasing mitochondrial β-oxidation of lipids mobilized from adipose tissue during fasting could cause a long-term increase in fat deposition. Therefore, we tested whether long-term VB treatment could increase weight gain and adiposity in mice. We tested this in both GF and conventional mice, with or without a high fat/sugar Western diet (WD), since previous studies showed that GF-mice were protected from WD induced obesity.[192] In GF-mice, VB was dosed parenterally to achieve concentrations similar to VB concentrations observed in untreated conventional mice which also resulted in carnitine concentrations equivalent to conventional mice (**Fig 3.9a,b**). Six weeks of VB treatment increased weight gain in GF mice fed a WD (**Fig. 3.10a**), characterized by increased adipose tissue fat mass (**Fig. 3.10b-d**), with substantial increases in perigonadal visceral (VAT), posterior subcutaneous (SubQ), and interscapular brown adipose (BAT) compartments compared to GF mice administered a WD alone. Furthermore, VB treatment exacerbated the development of hepatic steatosis in these mice (**Fig. 3.10e, f**). Similarly, we found that VB increased adipose tissue fat mass (VAT, SubQ, BAT) in conventional mice after 8-weeks (**Fig. 3.10h-j**) with the WD. The relative increases were most pronounced in white adipose compartments (VAT, SubQ) where fat mass in VB-treated GF and conventional mice on a WD was increased over 80% compared to WD alone. We also observed trends for increase in severity of hepatic steatosis and total body mass in VB-treated conventional mice with the WD, but these did not reach a significant difference after 8 weeks (**Fig. 3.10g, k, l**). Although WD-fed mice gained more weight than control-fed mice, no

differences in circulating VB were observed between WD or control diet-fed mice (**Fig 3.9c**). These effects were not observed in GF or conventional mice fed the control diet, and were not associated with increased inflammatory markers (IL-6, TNF-α, MCP-1) changes to insulin signaling (insulin, glucagon, resistin) either with the WD or the addition of VB to the WD in conventional mice (**Fig 3.11**). Thus, the long-term consequences of VB inhibition of mitochondrial β-oxidation of fatty acids in conjunction with a WD causes pronounced effects on increasing visceral adipose tissue mass in both GF and conventional mice.

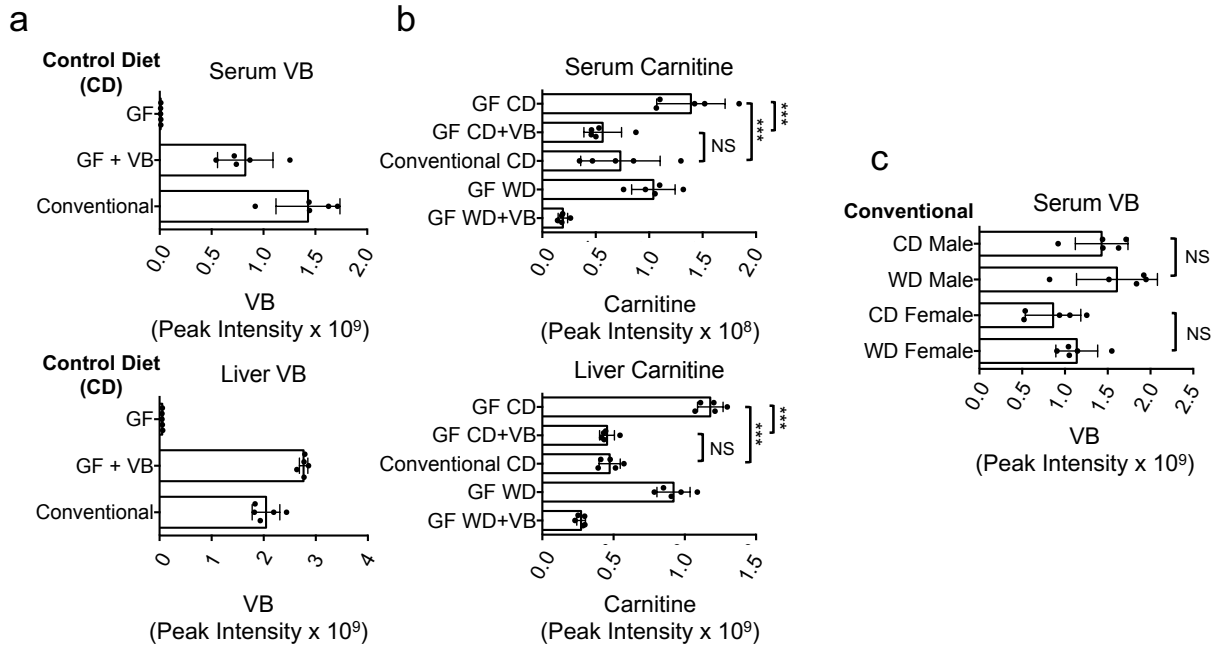

Figure 3.9: a) Comparison of VB in GF mouse serum and liver after treatment with 25 mg/kg VB with conventional mice (control chow diet). Samples were analyzed after 6 week treatment with VB and normal conventional mice. b) Comparison of carnitine in mouse serum and liver after treatment with 25 mg/kg in GF mice with conventional mouse (control diet) data for comparison. Carnitine is decreased in conventional mice compared to GF mice. VB treatment to GF mice led to serum and liver carnitine concentrations equivalent to conventional mice. (Two-tailed unpaired student t-tests: Serum GFCD vs. GFCD+VB $p = 0.0001$, GFCD vs. Conventional CD $p < 0.0001$, GFCD+VB vs. Conventional CD $p = 0.395$; Liver GFCD vs. GFCD+VB $p < 0.0001$, GFCD vs. Conventional CD $p < 0.0001$, GFCD+VB vs. Conventional CD $p = 0.6559$) c) Comparison of circulating VB in conventional mice (male M, female F) between Western diet (WD) and control chow (Two-tailed unpaired student t-tests: CD male vs. WD male $p = 0.4982$; CD female vs. WD female $p = 0.1653$).

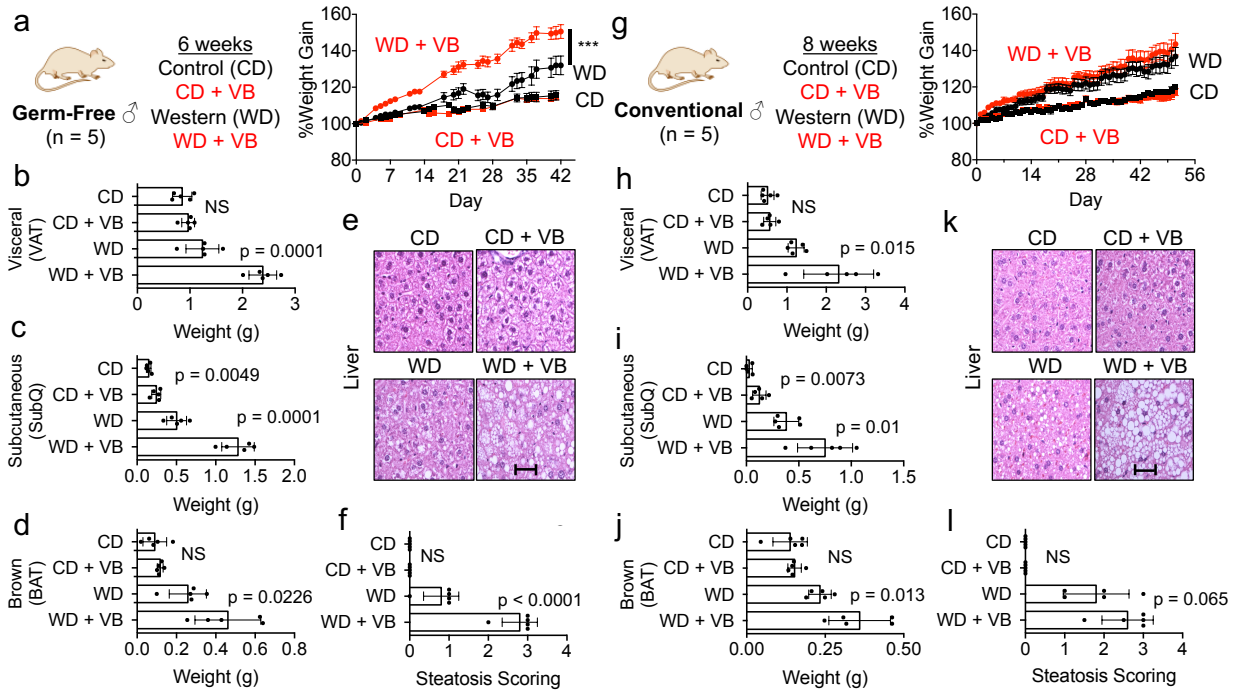

Figure 3.10: Long-term valerobetaine (VB) treatment in GF and conventional mice

a) GF mice were administered PBS or VB in conjunction with a control diet (CD) or western diet (WD) for 6 weeks with body weight recorded as percent weight gain. (2-way repeat measures ANOVA with multiple comparisons per day, VB treatment with WD $F = 17.19$, $p = 0.0032$, AUC p-value = 0.0028; VB treatment with CD $F = 0.4609$, $p = 0.5164$, AUC p-value = 0.5164) Weight of b) visceral adipose tissue (VAT), c) Subcutaneous white adipose tissue (SubQ), d) brown-adipose tissue (BAT) in GF mice after 6 weeks. e) Representative liver hematoxylin and eosin (H&E) stains for each GF group under 40x magnification. Scale bar represents 50 μm. f) Scoring of hepatic steatosis from H&E from GF mice. g) Conventional mice were administered PBS or VB in conjunction with a CD or WD for 8 weeks with body weight recorded as percent weight gain. Weight of h) VAT, i) SubQ, j) BAT in conventional mice after 8 weeks. (2-way repeat measures ANOVA with multiple comparisons per day, VB treatment with

WD F = 1.218, p = 0.3019, AUC p-value = 0.1462; VB treatment with CD F = 0.4609, p = 0.5164, AUC p-value = 0.4917) k) Representative liver H&E stains for each conventional group under 40x magnification. Scale bar represents 50 μm. l) Scoring of hepatic steatosis from H&E from conventional mice. One-way student's t-test (n = 5, $p < 0.05$) used for comparisons unless otherwise noted.

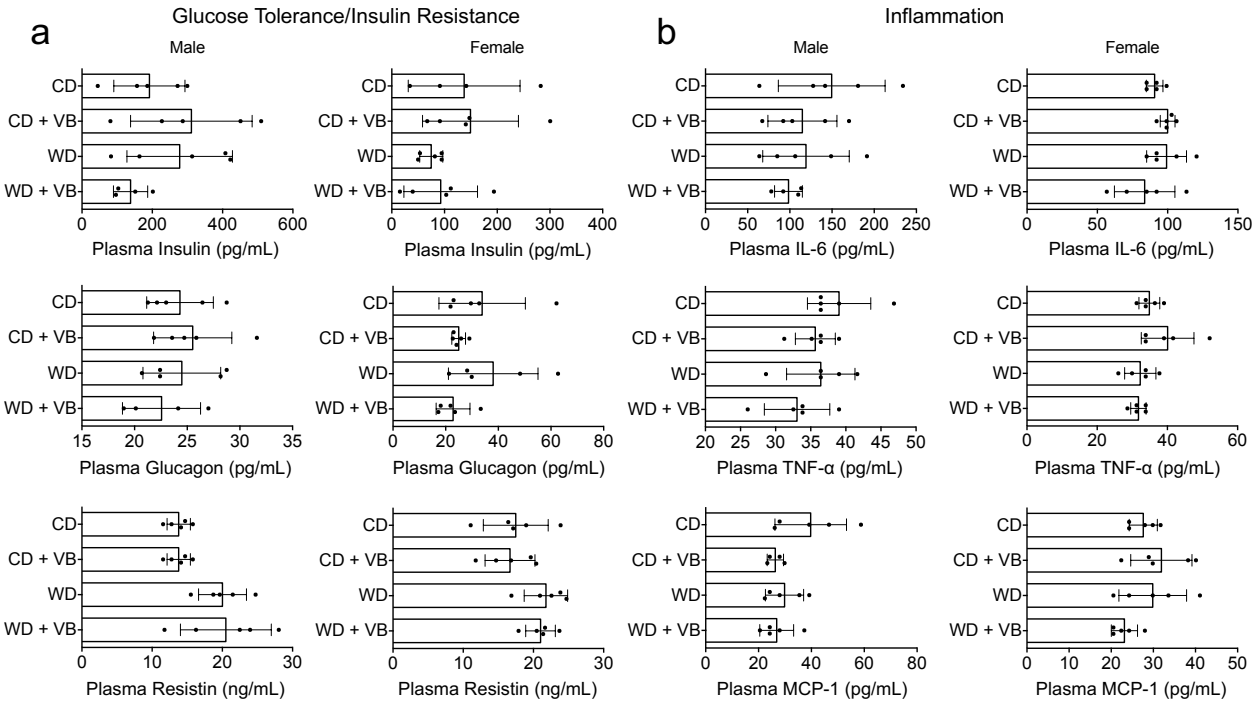

Fig 3.11: Glucose Intolerance and Inflammatory markers in VB treated animals. a) Plasma biomarkers of glucose tolerance/insulin resistance (insulin, glucagon, resistin) in conventional mice after 8 weeks of VB treatment. (One-way ANOVA with Sidak's multiple comparisons: Insulin male F = 1.648, p = 0.2205; Insulin female F = 1.034, p = 0.4059; Glucagon male F = 0.5165, p = 0.6772; Glucagon female F = 1.723, p = 0.2025; Resistin male F = 4.747, p = 0.0149 [CD vs. CDVB not significant, WD vs. WDVB not significant]; Resistin female F = 2.687, p = 0.0814) b) Plasma biomarkers of inflammation (IL-6, TNF-alpha, MCP-1) in conventional mice after 8 weeks of VB treatment. (One-way ANOVA with Sidak's multiple comparisons: IL-6 male F = 0.9316, p = 0.4497; IL-6 female F = 1.646, p = 0.2185; TNF-alpha male F = 1.645, p = 0.2186; TNF-alpha female F = 3.241, p = 0.0499 [CD vs. CDVB not significant, WD vs. WDVB not significant]; MCP-1 male F = 2.467, p = 0.1021; MCP-1 female F = 2.048, p = 0.1477)

VB drives transcriptional regulation of lipid and mitochondrial metabolism in liver

To further elucidate VB orchestration of microbiome-mitochondria interactions regulating host metabolism, we compared transcriptional responses in GF mice to microbiome acquisition (CV) with transcriptional responses to VB treatment. Since VB was the top microbiome-derived metabolite identified in CV mouse liver, we predicted that transcriptional responses observed in conventionalized mouse liver could be directly attributed to the introduction of VB into GF mice. RNA-seq analysis showed that microbiome acquisition in GF mice upregulated mitochondria and lipid metabolism/transport pathways linked to activation of Ppar-α (**Fig. 3.12a, Fig 3.13a**). More specifically, genes encoding mitochondrial energy production and fatty acid oxidation [Sdh, Nduf, Atp5f, Cyc1, Cox5a, Vdac, Hadh, Acsl, Eci, Acaa], TAG biosynthesis [Agpat, Dgat2, Gpat3], and lipoprotein export [Apoa, Apob, Apoc, Apoe, Mttp, Pdia3,4,6] were increased in CV mice (**Fig. 3.12b**). Upregulation of many of these genes is linked to transcriptional activation of Ppar-α (Agpat2, Apoc2, Acot1, Acsl5, Sdhd, Hmgcl, Crat, Cyp4a14). As VB elicited a dose-dependent increase in PPAR-α response element-linked luciferase activity in cultured cells (**Fig. 3.12c**), we expected VB to elicit similar responses in mice. Indeed, VB-treatment in control diet fed GF mice altered the expression of mitochondria associated genes, and increased expression of genes related to lipid metabolism linked to activation of Ppar-α (**Fig. 3.12d, e**). More specifically, genes encoding for transcription factors important for regulation of fatty acid metabolism [Ppara, Pparg, Rxra, Crebbp, Fxr, Sirt1, Ppargc1b], mitochondrial energy production and fatty acid metabolism [Sdha, Hadha, Hadhb, Slc27a5, Cpt1a, Acox1, Acadl, Eci2, Fads, Acadl], TAG biosynthesis [Agpat3, Dgat2], and lipoprotein export

[Apob, Apoa5] were upregulated by VB treatment with the control diet. Furthermore, many of these changes were linked to activation of Ppar-α regulated genes [Cyp4a14, Ncoa2, Cpt1a, Crebbp, Chd9, Nr1d1, Apoa5, Med17, Rxra, Pparg, Hmgcs2, Ppara, Ppgargc1b, Tead3] (**Fig. 3.12e**). Conversely, VB treatment in WD-fed GF mice downregulated mitochondria, lipid, and Ppar-α related genes (**Fig. 3.12f**, **Fig 3.13b**) – illustrating how diet quality impacts transcriptional responses to VB. Taken together, these data show how microbially-derived VB interacts with dietary factors to drive transcriptional regulation of lipid processing and mitochondrial energy metabolism in the liver.

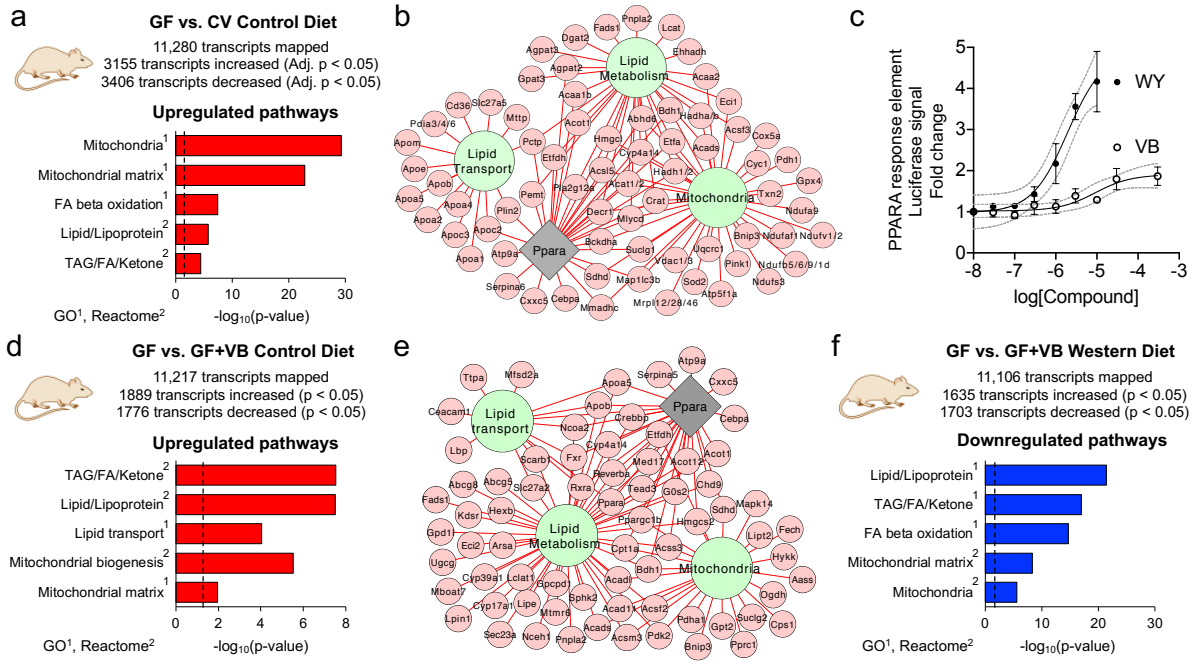

Fig. 3.12: VB participates in microbiome-mitochondria communication to reprogram host lipid metabolism. a) Mitochondria and lipid pathways are the top transcriptome pathways upregulated in conventionalized (CV) mice (n = 6 per group). Pathway analysis of transcripts increased (p-FDR < 0.05, FC > 2) in CV mouse liver. Results from differential expression analysis were filtered with a FDR < 0.05 and increased by 2-fold in CV mice over GF and overrepresentation analysis performed using Enrichr and MSigDB. b) Gene expression for mitochondrial energy metabolism, FA uptake, FA oxidation, TAG biosynthesis, and lipoprotein assembly and export are increased in CV mice. Many of these changes were linked to activation of Ppar-α. Green nodes indicate Reactome pathways or gene ontologies, grey node represents transcription factor enrichment and red edges/nodes indicate increased transcript abundance in CV mice. c) VB treatment elicits a dose-dependent increase in PPAR-response element linked luciferase activity in HepG2 cells. The calculated EC_{50} for VB

is 14 μM, similar to concentrations observed in the portal circulation of conventional mice. Data for Wy14643, a synthetic PPAR-alpha agonist (EC_{50} = 1.9 μM), shown for comparison. Data are displayed as the mean ± standard deviation of 3 biological replicates. d) Mitochondria and lipid pathways are upregulated in GF mice treated with VB (n = 5 per group). Pathway analysis of transcripts increased (raw p-value < 0.05, FC > 2) in CV mouse liver. Overrepresentation analysis was performed using Enrichr and MSigDB. e) Gene expression for mitochondria and lipid pathways linked to Ppar-α activation are upregulated by VB treatment in GF mice with the control diet. Green nodes indicate Reactome pathways or gene ontologies, grey node represents transcription factor enrichment and red edges/nodes indicate increased transcript abundance in VB treated mice (control diet). Network plots prepared in Cytoscape 3.7.1. f) Mitochondria and lipid pathways were downregulated by VB treatment in GF mice with the Western diet.

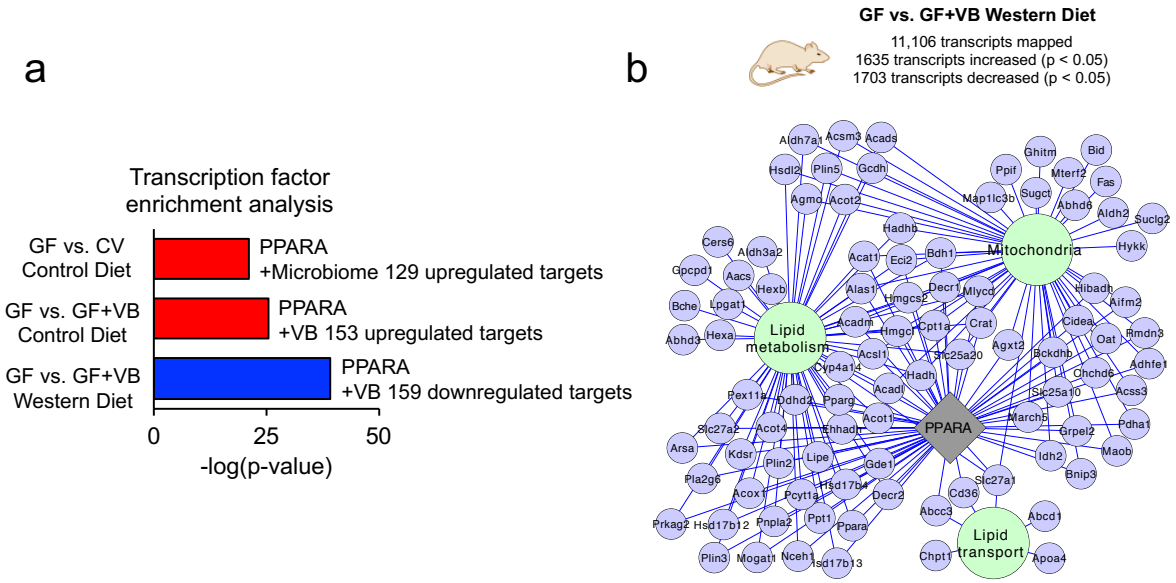

Fig 3.13: Ppar alpha targets are transcriptionally changed by VB. Transcription factor enrichment analysis shows that Ppara target genes are upregulated by a) microbiome acquisition and VB treatment in control diet fed GF mice. Ppara target genes are downregulated by VB treatment in Western diet (WD) fed GF mice. b) VB treatment in WD fed mice downregulates genes linked to Ppara which function in mitochondria and lipid processing pathways.

Clinical associations of plasma VB with microbiome transplantation and obesity-related phenotypes in people

To test whether qualitative changes in the microbiome could impact circulating VB in humans, we measured circulating VB in participants of a clinical trial of fecal microbiome transplantation (FMT) at Emory University Hospital. Participants were randomized 1:1 to initial bowel purge with polyethylene glycol (prep) or prep plus fecal enema (FMT) (**Fig. 3.14a**), with longitudinal follow-up. In both randomization groups, circulating VB increased in most individuals after the procedure (**Fig. 3.14b**). We also observed increases in plasma short-chain acylcarnitines (**Fig. 3.14c**) and decreases in long-chain acylcarnitines (**Fig. 3.14d**).

To test whether VB was associated with obesity-related phenotypes in humans, we measured plasma VB in 130 obese individuals [Body Mass Index (BMI) > 30 kg/m^2] without overt disease compared to 84 individuals from the same cohort with BMI < 30. The results show that average VB concentrations in the obese individuals is 40% higher than non-obese individuals (**Fig. 3.14e**). Extraction of plasma VB concentrations from a previously published dataset[23] of adults (n = 179, mean age 50 years, males = 63, females = 116) with measures of visceral adipose tissue mass (VAT) shows a positive correlation of plasma VB with VAT (β = 3.7E+04 ± 1.1E+04, p = 0.0006), independent of age, race, and sex (**Fig. 3.14f**). This relationship is also maintained when controlling for total body fat, suggesting that VB association in humans occurs with both adipose tissue mass and BMI. Similarly, a study of serum VB in youth with biopsy-proven NAFLD (n = 74, mean age 14 y, males = 54, females = 20) [24] shows an association of plasma VB with hepatic steatosis (**Fig. 3.14g**). Circulating VB levels were 40% higher

with severe steatosis (>66% steatosis) compared to mild steatosis (<33% steatosis; β = 0.328, $p = 0.03$, linear regression adjusted for age, sex, and race).

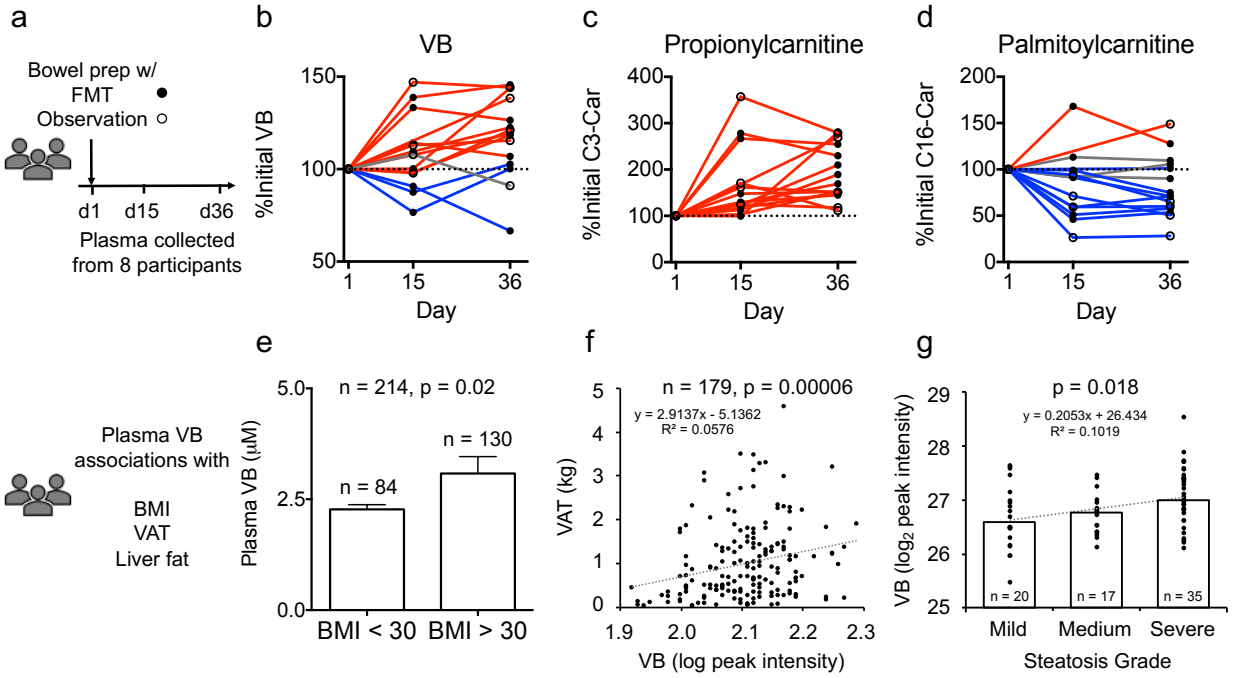

Figure 3.14. Clinical associations of plasma VB with microbiome manipulation and obesity-related phenotypes in people. a) Fecal microbiota transplantation (FMT) clinical trial design at Emory University Hospital. b) Circulating VB increases in 11 out of 15 cycles following treatment. c) Circulating propionycarnitine increases in all cycles following treatment. d) Circulating palmitoylcarnitine decreases in 10 out of 15 cycles following treatment. e) In a subclinical population of individuals without diagnosis of disease, obese individuals (n = 130) have higher VB concentration than non-obese individuals (n=84) (One-tailed t-test ($p = 0.0213$) with Welch's correction, F, DFn, Dfd: 20.79, 129, 83, $p < 0.0001$). f) Plasma VB is correlated with increased central adiposity in adults (Visceral Adipose Tissue mass, n = 179, $p = 0.00006$). g) Plasma VB is positively associated with severity of hepatic steatosis in adolescents (n = 74, $\beta = 0.345$, $p < 0.02$).

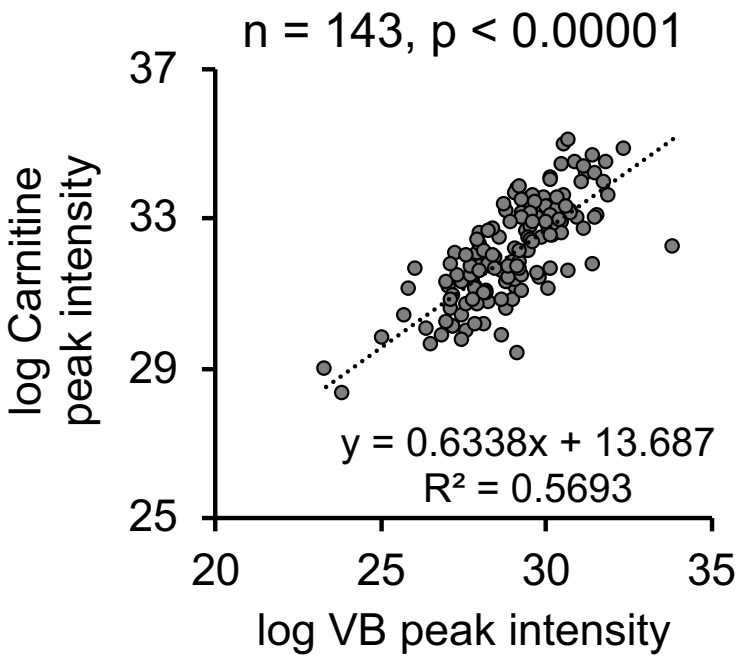

Fig 3.15: Urinary carnitine is correlated with urinary VB in humans (n = 143, Pearson's R 0.754, p < 0.00001).

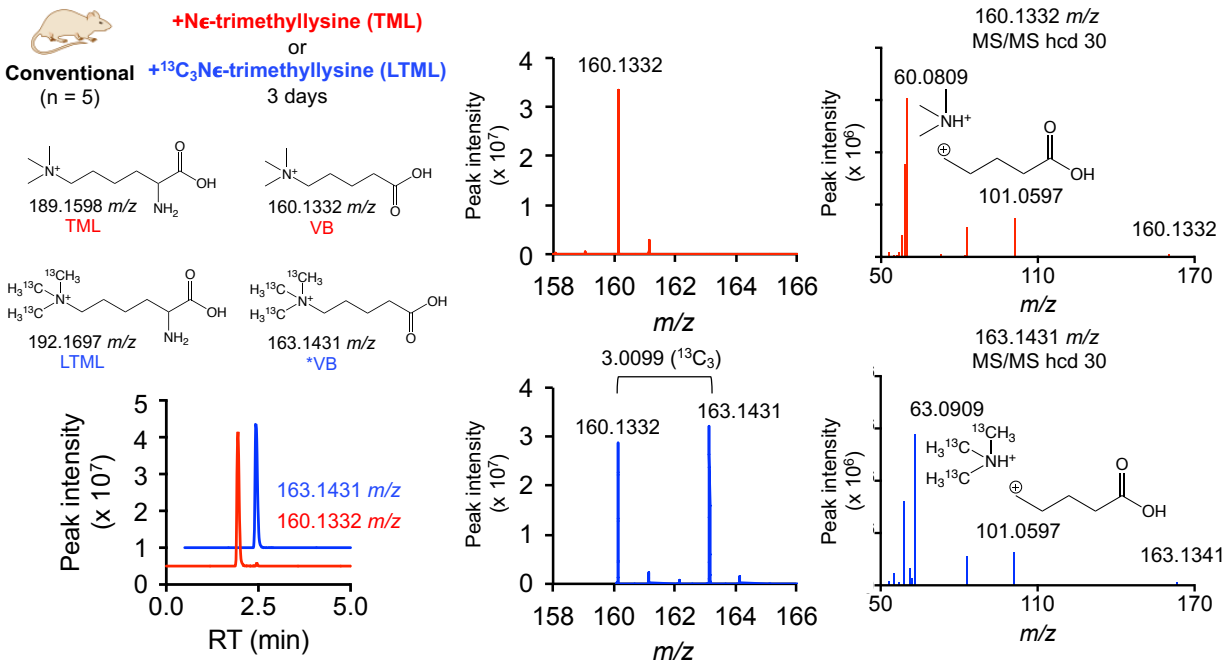

Fig 3.16: (Nε, Nε, Nε)-trimethyllysine (TML) is a precursor to δ-valerobetaine (VB). (Nε, Nε, Nε)-trimethyllysine (100 mg/kg) or (^{13}C Nε, ^{13}C Nε, ^{13}C Nε)-trimethyllysine (25 mg/kg) was orally gavaged into conventional mice. The formation of unlabeled VB (160.1332 *m/z*) from TML and labeled VB (163.1431 *m/z*) from isotopically labeled TML is shown here along with accurate mass MS1 and ion fragmentation spectra consistent with VB and labeled VB. Chromatograms and spectral peaks corresponding to serum sample collected from mice treated with TML (red) or LTML (blue) for three days.

3.4: Discussion

Here, we describe the discovery of a single microbiome-derived metabolite, delta-valerobetaine (VB), absent in GF-mice, which regulates host metabolism by decreasing systemic carnitine and suppressing mitochondrial fatty acid oxidation. GF and conventional mice treated with VB were more susceptible to diet-induced obesity, as they gained more weight, had increased adipose tissue mass and hepatic steatosis when fed a WD. VB treatment in control diet fed GF and conventional mice did not result in these changes. With the control diet, VB treatment caused upregulation of genes related to lipid metabolism and transport. However, with the WD, VB treatment led to downregulation of genes related to lipid metabolism and fatty acid oxidation. Circulating VB increased in people following microbiome manipulation procedures that replenished the microbiota, and increased circulating VB was positively associated with obesity-related phenotypes in humans (BMI, central adiposity, and severe fatty liver). Taken together, the results of this present study shows that VB is a microbially-derived molecule that causes diet-dependent obesity in mice and may be a causal factor driving obesogenic mechanisms in humans.

The possible dependence of the relationships upon diet, as found in mice, cannot be directly tested in these retrospective human studies. Evidence for common mechanisms is provided, however, by correlations between urinary VB and urinary carnitine as well as increases in circulating VB following microbiome manipulation in humans. There was a positive correlation between urinary VB and carnitine in human populations (**Fig 3.15**), consistent with our data showing that VB treatment increased urinary carnitine elimination in mice. Previous studies showed that VB is a substrate for

the carnitine transporter (OCTN2), which is highly expressed in the kidney.[193] Therefore, VB decreases the efficiency of renal carnitine reuptake and increases in VB likely increase urinary carnitine elimination in humans. Furthermore, patterns observed in VB-treated mice were mirrored in humans undergoing microbiome manipulation with FMT. Circulating VB increased following FMT with associated changes to circulating acylcarnitine profiles. These data show that microbiome manipulation in humans can alter circulating VB concentrations with potential downstream effects on lipid metabolism.

The mechanistic basis for VB effects through the carnitine shuttle has widespread implications for human health. Carnitine regulates glucose and lipid metabolism, and declines in free carnitine are accompanied by an accumulation of medium and long-chain acylcarnitines in muscle and obesity in aging.[194–196] Carnitine supplementation is beneficial for obesity, fatty liver and glucose utilization.[197–200] Accumulation of incompletely oxidized acylcarnitines is associated with obesity and insulin resistance, potentially exacerbated by chemicals that decrease cellular carnitine, cause mitochondrial dysfunction and decrease hepatic fatty acid oxidation.[201,202] Therefore, assessment of interactions of VB with the carnitine system may provide a way to simplify use of VB measures for management of obesity.

Use of clinical VB measures to guide diet and health management will require consideration of complex interactions between diet and microbiome composition. VB from dietary sources has both positive and negative health implications.[203,204] VB from ruminant microbes is relatively high in ruminants and improves nutritional value of milk by increasing acylcarnitine content.[205] Conversely, trimethyllysine, a precursor to VB

(**Fig 3.16**), is high in foods (e.g. red meat) associated with poor metabolic health and increased in people at risk for cardiovascular diseases.[206,207] Whole grain diets, which do not contain VB but increase circulating VB in humans through pre-biotic effects on gut microbial composition such as increasing *Lactobacillus* and increasing the *Bacteroidetes/Firmicutes* ratio, are associated with decreased risk of cardiometabolic disorders, type 2 diabetes, and weight gain.[208] Therefore, effective use of VB measures in management of obesity will require evaluation in the context of diet and microbiome. This interpretation is consistent with potential use for NAFLD, where circulating VB is increased and hepatosteatosis is potentiated by a high-fat diet.[209]

There is increasing recognition that the eukaryotic host and its associated microbiome function as a biological unit, termed holobiont, and are subject to evolutionary pressures, which include agricultural shifts and changes in dietary patterns. Phylogenetic and evolutionary evidence show eukaryotic mitochondria are descendent from an ancient bacterial endosymbiont.[210] Thus, VB modulation of carnitine-dependent fatty acid oxidation may reflect an evolutionarily conserved phenomenon linking the microbiome to mitochondrial function. The results of our study show that VB participates in mitohormesis, a process by which a minor impairment increases gene expression of mitochondrial systems which improve metabolic function of mitochondria.[211] Comparative analysis of GF/CV mouse liver transcriptomes shows that microbiome increases expression of many genes for mitochondrial bioenergetics and lipid homeostasis. With this interpretation, lipid accumulation caused by the presence of VB in CV animals drives activity of Ppar-α pathways, which control mitochondrial bioenergetics and lipid metabolism.[212,213] Indeed, in control diet fed GF mice, VB

treatment increased expression of Ppar-α linked genes regulating mitochondrial function and lipid processes. This can explain why VB did not augment body composition phenotypes with the control diet (and even decreased weight gain in control diet female mice. However, in the context of excess fats and sugars characteristic of a WD, this microbiome-mitochondria axis is overwhelmed with the addition of VB. As a result, VB worsens the effects of a WD on body composition (increased weight gain and adiposity), with associated downregulation downregulation of Ppar-α linked genes regulating mitochondrial bioenergetics and lipid metabolism. Since the addition of VB to WD-fed GF mice caused GF mice to gain weight similar to WD-fed conventional mice, our data show that the lack of microbially-derived VB in GF mice is a factor that protects them from WD-induced obesity. This is further supported by our observation that circulating and hepatic carnitine is increased in GF mice compared to conventional mice, and the addition of VB to GF mice caused serum and liver carnitine to be equivalent to carnitine levels observed in conventional mice. The effects on body weight are more pronounced in GF mice since C/CV mice are adapted to the presence of VB (as evidenced by comparative transcriptome analysis of GF and CV liver) and potential effects of other microbial metabolites on host bioenergetics. In recognition of this, it cannot pass without notice that improved quality of maize with high lysine content,[214] which is helping to erase global malnutrition, may have contributed to the global obesity epidemic through increased content of the VB precursor, trimethyllysine, which could further shift the intricate balance between microbially derived VB and mitochondrial bioenergetics beyond what homeostatic mechanisms can compensate for.

3.5: Conclusion

In conclusion, δ-valerobetaine (VB), a gut microbe-derived molecule, orchestrates microbiome-mitochondrial communication to control energy metabolism and augment visceral adiposity in the context of a Western diet. Measures of VB, along with carnitine, may provide a key approach to guide use of prebiotic and probiotic interventions and dietary management for excessive adiposity. Such an approach may be unavoidable if the obesity epidemic is a consequence of an evolved microbiome-human symbiotic relationship that is shifting due to global agricultural or environmental change.

Chapter 4

General Discussion

Synopsis: This chapter serves as a discussion for the thesis in its entirety. First, we will summarize the findings reported in both chapter 2 and chapter 3. Then, we will begin to dissect the immediate questions raised from these results and how they pertain to their respective fields. From chapter 2, we will discuss the role the microbiome will play in immunotherapy and immune responses as well as the future approach to the microbiome in cancer treatment. From chapter 3, we will dissect the role of gut microbiome-derived metabolites in metabolic disease treatment as well as the evolutionary foundation for these interactions. Finally, we will extrapolate our data as well as other reports to speculate about the gut microbiome field as a whole and its future.

4.1: Immunotherapy and the Gut Microbiome

First, in chapter 2, we showed that the bacteria, *Lactobacillus rhamnosus* GG (LGG), could modulate a mucosal CD8 T-cell immune response. This modulation occurred through a novel microbiome-mediated TLR2:DC axis. This was shown through utilization of knockout mice to illustrate the requirement for both DCs and the presence of TLR2 on DCs for LGG to be able to induce CD8 T-cells. Furthermore, we were able to use this modulation of CD8 T-cell activation in settings of colorectal cancers to reduce tumor burden and increase intra-tumoral CD8 T-cells. This modulation was critical to tumor reduction as depletion of CD8 T-cells removed the majority of LGG's effect on tumor burden. Altogether, we showed that LGG could attenuate colonic tumor burden through its orchestration of the mucosal immune response (**Figure 4.1**).

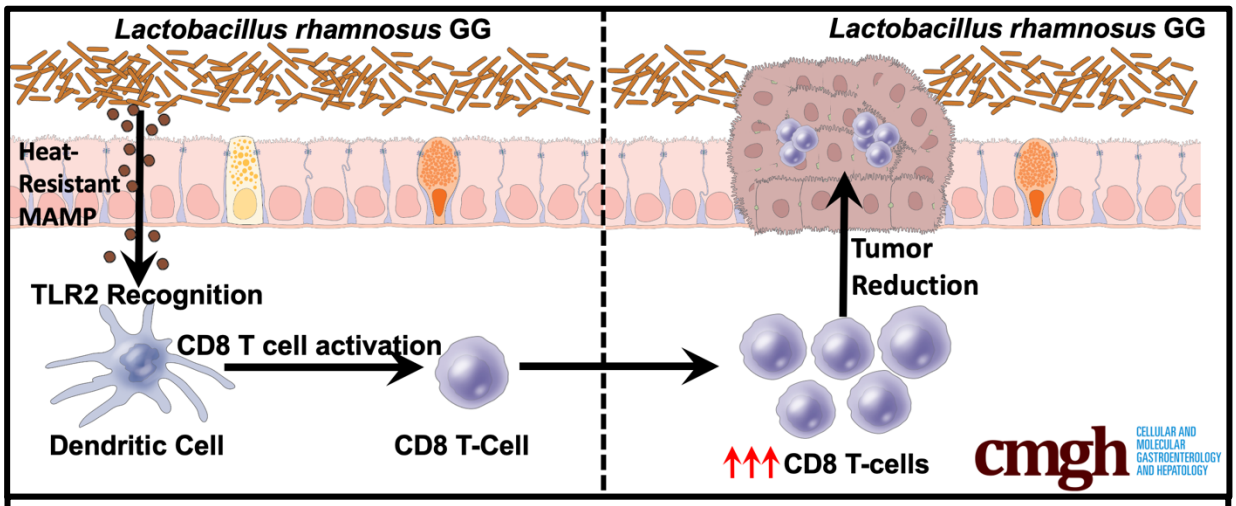

Figure 4.1: Graphical abstract depicting Lactobacillus rhamnosus GG effects on CD8 T-cells and colorectal cancer as published in CMGH.[201]

After illustrating the robust ability of the microbiome to initiate immune responses and reduce tumor burden in an immune-mediated manner, one main question is whether microbial interventions should be used in conjunction with cancer immunotherapy. Though not tested in this thesis, other groups have illustrated that there is indeed a relationship between the gut microbiome and immunotherapy responses.[75–77] Furthermore, recent groups has shown that indeed LGG can synergize with immunotherapy in models of melanoma and that TLR2 is important for immunotherapy.[81,152] Because of these reports and our data, it is reasonable to discuss the role that supplementation or microbial interventions that enhance CD8 T-cells responses may enhance immunotherapy efficacy and breadth. Due to heterogeneity between individuals and their particular microbiome community structures across different cultural and ethnic populations, utilization of a 16S rDNA sequencing or shotgun metagenomic approaches may prove difficult. Indeed, this is further confounded by the report that a consortium of different bacteria may be necessary to expand CD8 T-cell responses.[78] Until the particular consortium or individual bacteria that expand CD8 T-cells has been identified and can be easily detected, the gap in knowledge of a clearly defined microbiome that expands CD8 T-cell responses will be a barrier to the cancer immunotherapy field.

However, administration of probiotics, their lysates or products, and even potentially fecal-microbial transfers (FMTs) may hold promise in removing the need for sequencing of the microbiome if these approaches can faithfully produce the desired response. As we report in this thesis, we have shown that single administration of the bacteria, *Lactobacillus rhamnosus* GG, can induce CD8 T-cells and mount an anti-

tumor immune response. Many other groups have reported that single administration of other bacteria can have similar anti-tumor effects but through different epithelial mechanisms.[101,102,215,216] However, there may be a potential risk in administering large doses of live bacteria to cancer patients though in our opinion the risk is relatively small. For proof of this small risk, studies and clinical trials have shown that despite a dramatic increase of probiotic usage by the general public over the past twenty years there has been no increase in lactobacilli-induced bacteremia and no documented adverse events in at-risk groups.[155,217]

Despite any form of risk, there may not be a need to administer live bacteria. Indeed, our results suggest that LGG does not need to be viable to induce its immunomodulatory activity. Though we did not directly test if heat-killed LGG could reduce tumor burden, another group has shown that lysates from *Lactobacillus acidophilus* could enhance CTLA-4 targeted immunotherapy.[154] Administering heat-killed bacteria or only one particular product of bacteria would reduce the risk of adverse events while still promoting a microenvironment that increases immunotherapy efficacy. Furthermore, the field is moving to discover potential metabolites that are produced by the microbiome that may be mediating increased immunotherapy rates. For example, a recent study has shown that the bacterial metabolite inosine can increase T-cell responses *in vitro* and *in vivo* and can synergize with immunotherapy.[218] These reports and our data suggest that bacterial products or metabolites could be administered in conjunction with immunotherapy without risk of unintentional harm or unnecessary signal transduction of different pathways that needed for immunotherapy.

Finally, if finding potential metabolites or products proves too challenging, another alternative could be fecal-microbial transfers (FMTs). Utilizing microbiome sequencing, the ideal microbiome community structure for immunotherapy could be discovered. Once known, administration of the microbiome to cancer patients using a FMT in conjunction with immunotherapy could improve response rates. In agreement with this logic, a recent phase one clinical trial concluded that FMTs held promise in increasing patient immunotherapy rates in melanoma patients that had previously been refractory to immunotherapy. In addition, they observed increased immune cell numbers and upregulated pro-inflammatory immune pathways.[217] Now, large scale usage of this approach may prove difficult and the microbiome that produces the best immunotherapy response rates may not be beneficial after cancer remission. Alternatively, as we have proposed single administration of a probiotic in this thesis, it is important to note that exogenous administration of LGG does not cause colonization of the microbiome. Indeed, after three weeks, LGG is no longer detectable in the colon of mice and can only become a permanent member of the microbiome if administered early in life.[219] This allows administration of LGG to occur through immunotherapy treatment, and after remission, LGG administration can be discontinued with no long-term risks.

In this thesis, we proposed the utilization of a single probiotic administration that expands CD8 T-cells through the well-known bacterial sensing toll-like receptors. However, we do not discount the possibility that other known and unknown pathways might be a target of the microbiome, but the TLR2 pathway is indeed shaping the mucosal immune environment and aiding in anti-tumor immune responses. As previously mentioned, many bacterial metabolites are unknown in structure and function

and should be the intense investigative focus as another way the microbiome is shaping immunotherapy responses. Indeed, the entirety of the microbiome and its targets should be considered and investigated as the field continues to move forward in dissecting the role of the microbiome and immunotherapy.

Now, what will the future of immunotherapy and the gut microbiome look like? As the cost for sequencing continues to decrease, there is a renewed sense in the healthcare and biotechnology fields of personalized or precision medicine.[220] Television and internet advertisements are already trying to convince recently diagnosed cancer patients to get their tumors sequenced. Indeed, recent publications have focused on utilization of RNA-sequencing to predict patient outcomes to immunotherapy as well as to predict the right combination of treatment to prevent reoccurrence of disease.[221–223] Therefore, is the next logical step to begin sequencing the tumor and the microbiome to move the field into personalized medicine? We would argue that one more -omic approach is necessary which is metabolomics. With the combination of sequencing and metabolomics, not only will we know which pathways to target and what the microbiome community structure to potentially modify, we will know which microbial metabolites are present and how they may be modifying the tumor microenvironment, immune cells, and the tumor

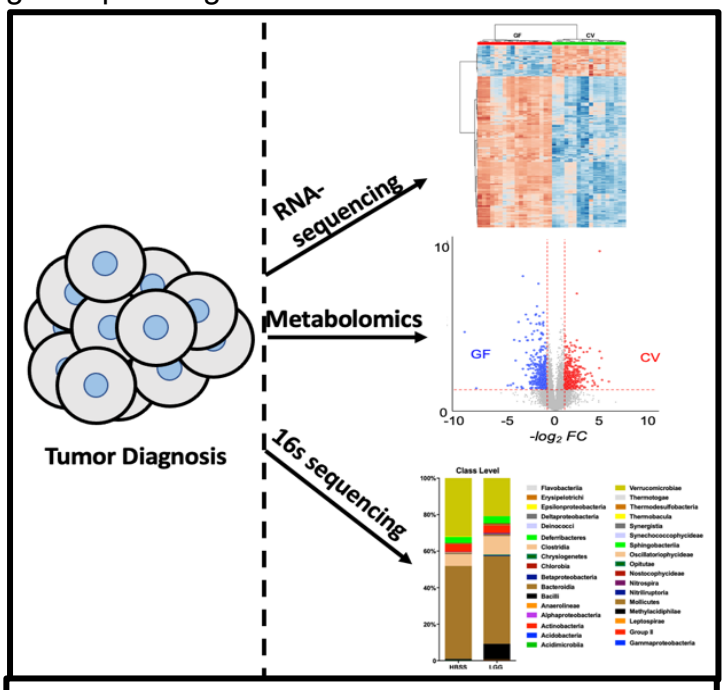

Figure 4.2: Cross-Disciplinary approach for the future of personalized tumor treatment

itself. Utilization of cross-disciplinary approaches will give greater knowledge into the right treatment course for a particular patient as well as continue research in the multitude of unknown metabolites coming from the microbiome and how they are affecting host physiology **(Figure 4.2)**.

4.2: Microbiome-derived metabolites, metabolic disease, and evolution

In chapter 3, we reported that the microbiome produces a metabolite known as valerobetaine (VB). Interestingly, increasing concentration of VB to cells correlated with a decrease in the molecule, carnitine. Through depletion of carnitine, VB effectively inhibits long-chain fatty acid oxidation. Indeed, VB administration to mice alters the metabolome as well as altering metabolic-related transcripts that align with a reduction in oxidation of fatty acids. Furthermore, VB administration to germ-free or conventional mice in conjunction with a high fat diet resulted in increased weight gain, adiposity, and

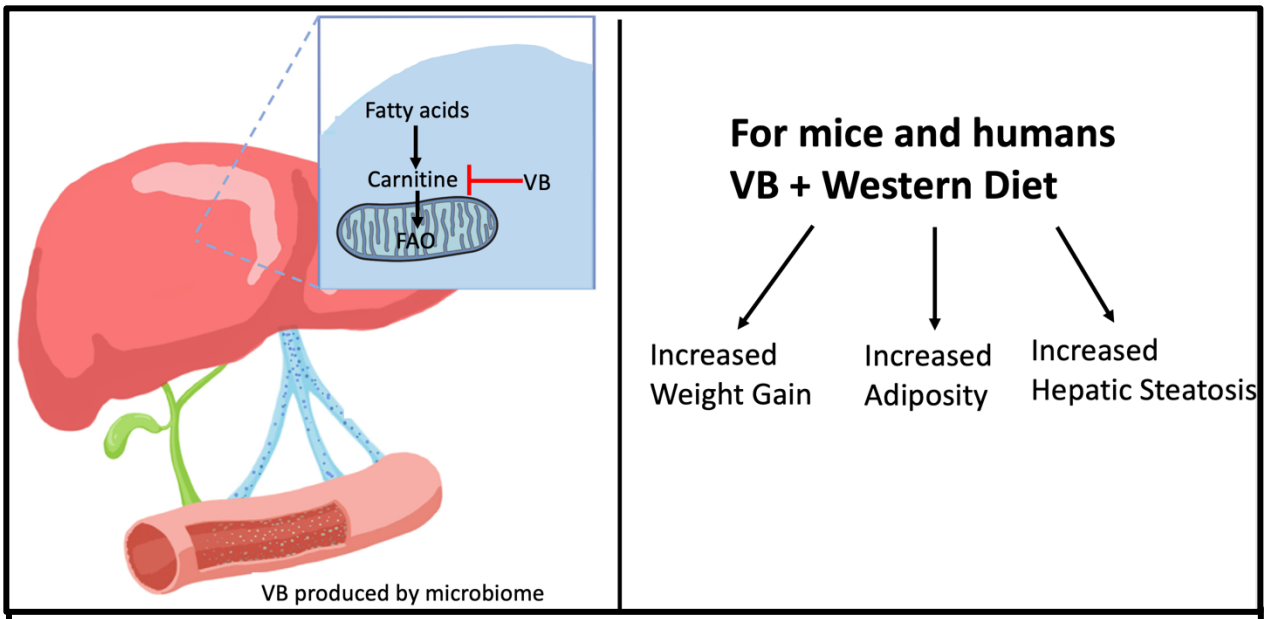

Figure 4.3: Graphical Abstract depicting delta-Valerobetaine (VB) effects on carnitine and host physiology.

hepatic steatosis. Most importantly, VB correlates with increased visceral fat, obesity, and hepatic steatosis in humans illustrating that the effects we see in the murine models are true in human physiology as well. Altogether, VB is a diet-dependent obesogen that causes increased weight gain and adiposity when on a high-fat diet due to its depletion of carnitine (**Figure 4.3**).

These results raise very interesting scientific as well as societal questions. As previously discussed in chapter 3, almost 10% of host metabolites are microbial in origin.[118] If one metabolite can significantly worsen metabolic disease then there should be an intense investigative focus on this wave of hundreds of unknown metabolites that are coming from the gut microbiome. However, this proves difficult as many different disciplines are needed to identify, produce, evaluate, and test these microbially-derived metabolites. As mentioned above, one potentially easier way to analyze these metabolites is through cross-platform analysis. This approach combines different -omic technologies such as genomic, proteomic, lipidomic, and metabolomic technologies. In combination, these approaches could reveal individual, unknown metabolites and then map these metabolites to different pathway changes. These *in silica* pathway analyses could then be analyzed and verified functionally through both *in vitro* and *in vivo* model systems. Indeed, this cutting-edge approach is beginning to be used in different settings to predict metabolite changes and their role in disease though this approach for gut microbiome derived metabolites is still in its infancy.[224–227] In our case, identification of VB and its potential targets occurred relatively quickly. However, testing of VB in both cell culture and mouse models as well as validation of our mechanism took much longer. Altogether, a cross-platform analysis as well as *in vivo* testing and validation

could help to identify this wave of microbially produced metabolites and what their roles are in different metabolic diseases.

With the identification of VB and its drastic effect on fatty-acid oxidation by the mitochondria, it raised the question as to the evolutionary reason for this occurrence. Though we do not have empirical evidence, one potential evolutionary pressure in inhibiting long-chain fatty acid is to give preferential beta-oxidation of short-chain fatty acids. Short-chain fatty acids are produced by the gut microbiome, and to force a symbiotic relationship, microbes could produce VB in conjunction with short-chain fatty acids (SCFAs) to force the preferential burning of their products over long-chain fatty acids. If true, microbes that produced both SCFAs and VB would exist in greater symbiosis with their host possibly increasing survival and replication of these microbes. In support of this, we tested *Bifidobacterium longum* which produces SCFAs, and discovered that it produced high levels of VB. This theory could be one possibility of the evolutionary pressure for the microbiome to produce VB.

Another potential evolutionary reason for the production of VB is due to cross-talk between the gut microbiome and its ancestral cousin, the mitochondria. Production of VB could be the result of the battle over nutrients. Production of VB by certain microbes could prevent neighboring bacteria species to utilize fatty acids as energy this gives a greater chance of survival to the bacteria that produce VB. As a consequence of this billions of year old battle, modern-day mitochondria are still susceptible to VB and potentially other bacterial metabolites coming from the microbiome which this phenomenon being termed the mitochondria-microbiome axis.[106,228–230] Indeed, the

microbiome-mitochondria axis is beginning to be further researched and needs to be considered as a possibility of metabolic disease.

Outside of basic science questions, our results raise certain societal questions. Corn is the most produced crop in the United States and due to hybrid varieties as well as genetic modification is now high in lysine.[231] The result of high-lysine crops has improved the nutritional values of these crops and increased the caloric count of these crops. However, we have evidence that the precursor for VB is a methylated derivative of lysine known as tri-methyl lysine. This means that by modifying our crops to contain more lysine, we have also increased the amount of the precursor for VB.

However, throughout our data, we show that VB has minimal or zero detrimental effects if on a standard diet. The negative ramifications of VB can only be observed when the mice are placed on a high fat diet. Accordingly in humans, we detected a higher concentration of VB in obese individuals compared to lean individuals. This suggests that VB does indeed correlate with increased adiposity in humans. But if humans are similar to our murine experiments, the diet of the obese individuals would need to be high in fat for detrimental effects by VB to be observed. However, this does not explain why obese individuals have greater concentration of VB than lean individuals. In our opinion, there are two simple answers to explain this observation. One, the diet of obese individuals is not only high in fat but also high in the precursor for VB, trimethyl lysine. Secondly, obese individuals could have a microbiome that produces more VB than lean individuals as the microbiome has been document to be different between these two populations.[106,113] Though both explanations are reasonable, if the first answer plays a greater role in the increase in VB, it raises

questions on the benefits of increasing lysine in crops if this act is exacerbating the obesity epidemic.

4.3 The Future of Gut Microbiome Research

Over the past decade, there has been a dramatic evolution in gut microbiome research. Initially, investigators could simply report on changes in the community structure between populations, knockout mice, or different disease settings and this was considered ground-breaking. Some of the most highly cited papers published in the late 2000's investigated the microbiomes between obese and lean individuals, the "average" microbiome, and how diet or age effects the microbiome.[27,229,232,233] In the past five years, the most highly cited paper have shown the effects of the microbiome on immunotherapy.[75–77] In the most recent years, this has shifted to the microbiome and everyone's organ of interest such as the gut-brain axis, gut-bone axis, gut-liver axis, and others.[9,234,235] All of these reports demonstrate the enormous potential of the gut microbiome and its products to impact host physiology and disease but what will the future of gut microbiome research look like?

Like many other fields, the microbiome research space will continue to advance through utilization of multiple -omic approaches. The combination of these large dataset producing tools will enable a greater analysis and understanding of the gut microbiome. Additionally, more investigators will try to remove the microbiome as a potential confounding factor in their experiments. To do this, littermate controls as well as gnotobiotic approaches will become standard across all fields. Though utilization of germ-free mice is an extremely powerful tool, the germ-free system is inherently artificial

as no animals exist in a germ-free state naturally. However, mice with a defined microbiome will become more commonplace and utilized to ensure the effects reported are not due to shifts in the microbiome between experimental and control groups.

It is our opinion that the microbiome field will begin to exert much of its investigative focus on microbially derived metabolites. For a decade, many groups have focused on the well-known microbially-derived products such as SCFAs and indoles. However, similar to our discovery of the effects of VB, more groups will try to decipher the wave of unknown metabolites that are being produced. These metabolites may positively or negative impact dozens of different disease states and may hold clinical promise in the treatment of those diseases.

To close, the gut microbiome and its complex relationship with the host continues to be investigated and refined. We report that administration of a single bacteria, *Lactobacillus rhamnosus* GG, can modify CD8 T-cell responses and exert anti-tumor immunity in settings of CRC. Additionally, one microbially-derived metabolite, delta-valerobetaine, can inhibit fatty acid oxidation culminating in increased obesity. These two examples add to the growing body of evidence of ways in which the gut microbiome impacts host physiology. The mystery of the microbiome has only begun to be solved and many more opportunities for research and many more questions still exist.

References:

1 Neish AS. Microbes in gastrointestinal health and disease. *Gastroenterology* 2009;**136**:65–80. https://doi.org/10.1053/j.gastro.2008.10.080.

2 Vyas U, Ranganathan N. Probiotics, prebiotics, and synbiotics: gut and beyond. *Gastroenterol Res Pract* 2012;**2012**:872716. https://doi.org/10.1155/2012/872716.

3 Hollister EB, Gao C, Versalovic J. Compositional and functional features of the gastrointestinal microbiome and their effects on human health. *Gastroenterology* 2014;**146**:1449–58. https://doi.org/10.1053/j.gastro.2014.01.052.

4 Gilbert JA, Quinn RA, Debelius J, Xu ZZ, Morton J, Garg N, *et al.* Microbiome-wide association studies link dynamic microbial consortia to disease. *Nature* 2016;**535**:94–103. https://doi.org/10.1038/nature18850.

5 Macpherson AJ, McCoy KD. Standardised animal models of host microbial mutualism. *Mucosal Immunol* 2015;**8**:476–86. https://doi.org/10.1038/mi.2014.113.

6 Falk PG, Hooper LV, Midtvedt T, Gordon JI. Creating and maintaining the gastrointestinal ecosystem: what we know and need to know from gnotobiology. *Microbiol Mol Biol Rev* 1998;**62**:1157–70. https://doi.org/10.1128/MMBR.62.4.1157-1170.1998.

7 Qin J, Li Y, Cai Z, Li S, Zhu J, Zhang F, *et al.* A metagenome-wide association study of gut microbiota in type 2 diabetes. *Nature* 2012;**490**:55–60. https://doi.org/10.1038/nature11450.

8 Frank DN, St Amand AL, Feldman RA, Boedeker EC, Harpaz N, Pace NR. Molecular-phylogenetic characterization of microbial community imbalances in human inflammatory bowel diseases. *Proc Natl Acad Sci U S A* 2007;**104**:13780–5. https://doi.org/10.1073/pnas.0706625104.

9 Tyagi AM, Yu M, Darby TM, Vaccaro C, Li J-Y, Owens JA, *et al.* The Microbial Metabolite Butyrate Stimulates Bone Formation via T Regulatory Cell-Mediated Regulation of WNT10B Expression. *Immunity* 2018;**49**:1116-1131.e7. https://doi.org/10.1016/j.immuni.2018.10.013.

10 Jones RM, Desai C, Darby TM, Luo L, Wolfarth AA, Scharer CD, *et al.* Lactobacilli Modulate Epithelial Cytoprotection through the Nrf2 Pathway. *Cell Rep* 2015;**12**:1217–25. https://doi.org/10.1016/j.celrep.2015.07.042.

11 Sekirov I, Russell SL, Antunes LCM, Finlay BB. Gut microbiota in health and disease. *Physiol Rev* 2010;**90**:859–904. https://doi.org/10.1152/physrev.00045.2009.

12 Pelzer E, Gomez-Arango LF, Barrett HL, Nitert MD. Review: Maternal health and the placental microbiome. *Placenta* 2017;**54**:30–7. https://doi.org/10.1016/j.placenta.2016.12.003.

13 Goedicke-Fritz S, Härtel C, Krasteva-Christ G, Kopp MV, Meyer S, Zemlin M. Preterm Birth Affects the Risk of Developing Immune-Mediated Diseases. *Front Immunol* 2017;**8**:1266. https://doi.org/10.3389/fimmu.2017.01266.

14 Mishra A, Lai GC, Yao LJ, Aung TT, Shental N, Rotter-Maskowitz A, *et al.* Microbial exposure during early human development primes fetal immune cells. *Cell* 2021:S0092-8674(21)00574-2. https://doi.org/10.1016/j.cell.2021.04.039.

15 Stinson LF, Boyce MC, Payne MS, Keelan JA. The Not-so-Sterile Womb: Evidence That the Human Fetus Is Exposed to Bacteria Prior to Birth. *Front Microbiol* 2019;**10**:1124. https://doi.org/10.3389/fmicb.2019.01124.

16 Kundu P, Blacher E, Elinav E, Pettersson S. Our Gut Microbiome: The Evolving Inner Self. *Cell* 2017;**171**:1481–93. https://doi.org/10.1016/j.cell.2017.11.024.

17 Zachariassen LF, Krych L, Rasmussen SH, Nielsen DS, Kot W, Holm TL, *et al.* Cesarean Section Induces Microbiota-Regulated Immune Disturbances in C57BL/6 Mice. *J Immunol* 2019;**202**:142–50. https://doi.org/10.4049/jimmunol.1800666.

18 Gomez de Agüero M, Ganal-Vonarburg SC, Fuhrer T, Rupp S, Uchimura Y, Li H, *et al.* The maternal microbiota drives early postnatal innate immune development. *Science* 2016;**351**:1296–302. https://doi.org/10.1126/science.aad2571.

19 Renz-Polster H, David MR, Buist AS, Vollmer WM, O'Connor EA, Frazier EA, *et al.* Caesarean section delivery and the risk of allergic disorders in childhood. *Clin Exp Allergy* 2005;**35**:1466–72. https://doi.org/10.1111/j.1365-2222.2005.02356.x.
20 Wang R, Wiemels JL, Metayer C, Morimoto L, Francis SS, Kadan-Lottick N, *et al.* Cesarean Section and Risk of Childhood Acute Lymphoblastic Leukemia in a Population-Based, Record-Linkage Study in California. *Am J Epidemiol* 2017;**185**:96–105. https://doi.org/10.1093/aje/kww153.
21 Meng X, Dunsmore G, Koleva P, Elloumi Y, Wu RY, Sutton RT, *et al.* The Profile of Human Milk Metabolome, Cytokines, and Antibodies in Inflammatory Bowel Diseases Versus Healthy Mothers, and Potential Impact on the Newborn. *J Crohns Colitis* 2019;**13**:431–41. https://doi.org/10.1093/ecco-jcc/jjy186.
22 Ramani S, Stewart CJ, Laucirica DR, Ajami NJ, Robertson B, Autran CA, *et al.* Human milk oligosaccharides, milk microbiome and infant gut microbiome modulate neonatal rotavirus infection. *Nat Commun* 2018;**9**:5010. https://doi.org/10.1038/s41467-018-07476-4.
23 Ward RE, Niñonuevo M, Mills DA, Lebrilla CB, German JB. In vitro fermentation of breast milk oligosaccharides by Bifidobacterium infantis and Lactobacillus gasseri. *Appl Environ Microbiol* 2006;**72**:4497–9. https://doi.org/10.1128/AEM.02515-05.
24 Lawson MAE, O'Neill IJ, Kujawska M, Gowrinadh Javvadi S, Wijeyesekera A, Flegg Z, *et al.* Breast milk-derived human milk oligosaccharides promote Bifidobacterium interactions within a single ecosystem. *ISME J* 2020;**14**:635–48. https://doi.org/10.1038/s41396-019-0553-2.
25 Donohoe DR, Garge N, Zhang X, Sun W, O'Connell TM, Bunger MK, *et al.* The microbiome and butyrate regulate energy metabolism and autophagy in the mammalian colon. *Cell Metab* 2011;**13**:517–26. https://doi.org/10.1016/j.cmet.2011.02.018.
26 Furusawa Y, Obata Y, Fukuda S, Endo TA, Nakato G, Takahashi D, *et al.* Commensal microbe-derived butyrate induces the differentiation of colonic regulatory T cells. *Nature* 2013;**504**:446–50. https://doi.org/10.1038/nature12721.
27 Human Microbiome Project Consortium. Structure, function and diversity of the healthy human microbiome. *Nature* 2012;**486**:207–14. https://doi.org/10.1038/nature11234.
28 Johansson MEV, Sjövall H, Hansson GC. The gastrointestinal mucus system in health and disease. *Nat Rev Gastroenterol Hepatol* 2013;**10**:352–61. https://doi.org/10.1038/nrgastro.2013.35.
29 Johansson MEV, Phillipson M, Petersson J, Velcich A, Holm L, Hansson GC. The inner of the two Muc2 mucin-dependent mucus layers in colon is devoid of bacteria. *Proc Natl Acad Sci U S A* 2008;**105**:15064–9. https://doi.org/10.1073/pnas.0803124105.
30 Desai MS, Seekatz AM, Koropatkin NM, Kamada N, Hickey CA, Wolter M, *et al.* A Dietary Fiber-Deprived Gut Microbiota Degrades the Colonic Mucus Barrier and Enhances Pathogen Susceptibility. *Cell* 2016;**167**:1339-1353.e21. https://doi.org/10.1016/j.cell.2016.10.043.
31 Johansson MEV, Jakobsson HE, Holmén-Larsson J, Schütte A, Ermund A, Rodríguez-Piñeiro AM, *et al.* Normalization of Host Intestinal Mucus Layers Requires Long-Term Microbial Colonization. *Cell Host Microbe* 2015;**18**:582–92. https://doi.org/10.1016/j.chom.2015.10.007.
32 Powell DN, Swimm A, Sonowal R, Bretin A, Gewirtz AT, Jones RM, *et al.* Indoles from the commensal microbiota act via the AHR and IL-10 to tune the cellular composition of the colonic epithelium during aging. *Proc Natl Acad Sci U S A* 2020;**117**:21519–26. https://doi.org/10.1073/pnas.2003004117.
33 Feng Y, Huang Y, Wang Y, Wang P, Song H, Wang F. Antibiotics induced intestinal tight junction barrier dysfunction is associated with microbiota dysbiosis, activated NLRP3 inflammasome and autophagy. *PLoS One* 2019;**14**:e0218384. https://doi.org/10.1371/journal.pone.0218384.

34 Hayes CL, Dong J, Galipeau HJ, Jury J, McCarville J, Huang X, *et al.* Commensal microbiota induces colonic barrier structure and functions that contribute to homeostasis. *Sci Rep* 2018;**8**:14184. https://doi.org/10.1038/s41598-018-32366-6.
35 Cario E, Gerken G, Podolsky DK. Toll-like receptor 2 enhances ZO-1-associated intestinal epithelial barrier integrity via protein kinase C. *Gastroenterology* 2004;**127**:224–38. https://doi.org/10.1053/j.gastro.2004.04.015.
36 Ewaschuk JB, Diaz H, Meddings L, Diederichs B, Dmytrash A, Backer J, *et al.* Secreted bioactive factors from Bifidobacterium infantis enhance epithelial cell barrier function. *Am J Physiol Gastrointest Liver Physiol* 2008;**295**:G1025-1034. https://doi.org/10.1152/ajpgi.90227.2008.
37 Ukena SN, Singh A, Dringenberg U, Engelhardt R, Seidler U, Hansen W, *et al.* Probiotic Escherichia coli Nissle 1917 inhibits leaky gut by enhancing mucosal integrity. *PLoS One* 2007;**2**:e1308. https://doi.org/10.1371/journal.pone.0001308.
38 Karczewski J, Troost FJ, Konings I, Dekker J, Kleerebezem M, Brummer R-JM, *et al.* Regulation of human epithelial tight junction proteins by Lactobacillus plantarum in vivo and protective effects on the epithelial barrier. *Am J Physiol Gastrointest Liver Physiol* 2010;**298**:G851-859. https://doi.org/10.1152/ajpgi.00327.2009.
39 Takiishi T, Fenero CIM, Câmara NOS. Intestinal barrier and gut microbiota: Shaping our immune responses throughout life. *Tissue Barriers* 2017;**5**:e1373208. https://doi.org/10.1080/21688370.2017.1373208.
40 Wong SH, Zhao L, Zhang X, Nakatsu G, Han J, Xu W, *et al.* Gavage of Fecal Samples From Patients With Colorectal Cancer Promotes Intestinal Carcinogenesis in Germ-Free and Conventional Mice. *Gastroenterology* 2017;**153**:1621-1633.e6. https://doi.org/10.1053/j.gastro.2017.08.022.
41 Stevens CE, Leblond CP. Rate of renewal of the cells of the intestinal epithelium in the rat. *Anat Rec* 1947;**97**:373.
42 Jadhav U, Saxena M, O'Neill NK, Saadatpour A, Yuan G-C, Herbert Z, *et al.* Dynamic Reorganization of Chromatin Accessibility Signatures during Dedifferentiation of Secretory Precursors into Lgr5+ Intestinal Stem Cells. *Cell Stem Cell* 2017;**21**:65-77.e5. https://doi.org/10.1016/j.stem.2017.05.001.
43 Kelly CJ, Zheng L, Campbell EL, Saeedi B, Scholz CC, Bayless AJ, *et al.* Crosstalk between Microbiota-Derived Short-Chain Fatty Acids and Intestinal Epithelial HIF Augments Tissue Barrier Function. *Cell Host Microbe* 2015;**17**:662–71. https://doi.org/10.1016/j.chom.2015.03.005.
44 Kaiko GE, Ryu SH, Koues OI, Collins PL, Solnica-Krezel L, Pearce EJ, *et al.* The Colonic Crypt Protects Stem Cells from Microbiota-Derived Metabolites. *Cell* 2016;**165**:1708–20. https://doi.org/10.1016/j.cell.2016.05.018.
45 Wu X, Wu Y, He L, Wu L, Wang X, Liu Z. Effects of the intestinal microbial metabolite butyrate on the development of colorectal cancer. *J Cancer* 2018;**9**:2510–7. https://doi.org/10.7150/jca.25324.
46 Li Q, Ding C, Meng T, Lu W, Liu W, Hao H, *et al.* Butyrate suppresses motility of colorectal cancer cells via deactivating Akt/ERK signaling in histone deacetylase dependent manner. *J Pharmacol Sci* 2017;**135**:148–55. https://doi.org/10.1016/j.jphs.2017.11.004.
47 Xi Y, Jing Z, Wei W, Chun Z, Quan Q, Qing Z, *et al.* Inhibitory effect of sodium butyrate on colorectal cancer cells and construction of the related molecular network. *BMC Cancer* 2021;**21**:127. https://doi.org/10.1186/s12885-021-07845-1.
48 Lee Y-S, Kim T-Y, Kim Y, Lee S-H, Kim S, Kang SW, *et al.* Microbiota-Derived Lactate Accelerates Intestinal Stem-Cell-Mediated Epithelial Development. *Cell Host Microbe* 2018;**24**:833-846.e6. https://doi.org/10.1016/j.chom.2018.11.002.
49 Metidji A, Omenetti S, Crotta S, Li Y, Nye E, Ross E, *et al.* The Environmental Sensor AHR Protects from Inflammatory Damage by Maintaining Intestinal Stem Cell Homeostasis

and Barrier Integrity. *Immunity* 2018;**49**:353-362.e5. https://doi.org/10.1016/j.immuni.2018.07.010.
50 Megna BW, Carney PR, Nukaya M, Geiger P, Kennedy GD. Indole-3-carbinol induces tumor cell death: function follows form. *J Surg Res* 2016;**204**:47–54. https://doi.org/10.1016/j.jss.2016.04.021.
51 Belizário JE, Faintuch J. Microbiome and Gut Dysbiosis. *Exp Suppl* 2018;**109**:459–76. https://doi.org/10.1007/978-3-319-74932-7_13.
52 Yang JH, Bhargava P, McCloskey D, Mao N, Palsson BO, Collins JJ. Antibiotic-Induced Changes to the Host Metabolic Environment Inhibit Drug Efficacy and Alter Immune Function. *Cell Host Microbe* 2017;**22**:757-765.e3. https://doi.org/10.1016/j.chom.2017.10.020.
53 Belkaid Y, Hand TW. Role of the microbiota in immunity and inflammation. *Cell* 2014;**157**:121–41. https://doi.org/10.1016/j.cell.2014.03.011.
54 Zhan Y, Chen P-J, Sadler WD, Wang F, Poe S, Núñez G, *et al.* Gut microbiota protects against gastrointestinal tumorigenesis caused by epithelial injury. *Cancer Res* 2013;**73**:7199–210. https://doi.org/10.1158/0008-5472.CAN-13-0827.
55 Robinson CM, Pfeiffer JK. Viruses and the Microbiota. *Annu Rev Virol* 2014;**1**:55–69. https://doi.org/10.1146/annurev-virology-031413-085550.
56 Stecher B, Macpherson AJ, Hapfelmeier S, Kremer M, Stallmach T, Hardt W-D. Comparison of Salmonella enterica serovar Typhimurium colitis in germfree mice and mice pretreated with streptomycin. *Infect Immun* 2005;**73**:3228–41. https://doi.org/10.1128/IAI.73.6.3228-3241.2005.
57 Harrison CA, Laubitz D, Ohland CL, Midura-Kiela MT, Patil K, Besselsen DG, *et al.* Microbial dysbiosis associated with impaired intestinal Na+/H+ exchange accelerates and exacerbates colitis in ex-germ free mice. *Mucosal Immunol* 2018;**11**:1329–41. https://doi.org/10.1038/s41385-018-0035-2.
58 Lundberg R, Toft MF, Metzdorff SB, Hansen CHF, Licht TR, Bahl MI, *et al.* Human microbiota-transplanted C57BL/6 mice and offspring display reduced establishment of key bacteria and reduced immune stimulation compared to mouse microbiota-transplantation. *Sci Rep* 2020;**10**:7805. https://doi.org/10.1038/s41598-020-64703-z.
59 Jin C, Lagoudas GK, Zhao C, Bullman S, Bhutkar A, Hu B, *et al.* Commensal Microbiota Promote Lung Cancer Development via γδ T Cells. *Cell* 2019;**176**:998-1013.e16. https://doi.org/10.1016/j.cell.2018.12.040.
60 Khosravi A, Yáñez A, Price JG, Chow A, Merad M, Goodridge HS, *et al.* Gut microbiota promote hematopoiesis to control bacterial infection. *Cell Host Microbe* 2014;**15**:374–81. https://doi.org/10.1016/j.chom.2014.02.006.
61 Trompette A, Gollwitzer ES, Yadava K, Sichelstiel AK, Sprenger N, Ngom-Bru C, *et al.* Gut microbiota metabolism of dietary fiber influences allergic airway disease and hematopoiesis. *Nat Med* 2014;**20**:159–66. https://doi.org/10.1038/nm.3444.
62 Balmer ML, Schürch CM, Saito Y, Geuking MB, Li H, Cuenca M, *et al.* Microbiota-derived compounds drive steady-state granulopoiesis via MyD88/TICAM signaling. *J Immunol* 2014;**193**:5273–83. https://doi.org/10.4049/jimmunol.1400762.
63 Singh N, Gurav A, Sivaprakasam S, Brady E, Padia R, Shi H, *et al.* Activation of Gpr109a, receptor for niacin and the commensal metabolite butyrate, suppresses colonic inflammation and carcinogenesis. *Immunity* 2014;**40**:128–39. https://doi.org/10.1016/j.immuni.2013.12.007.
64 Chang PV, Hao L, Offermanns S, Medzhitov R. The microbial metabolite butyrate regulates intestinal macrophage function via histone deacetylase inhibition. *Proc Natl Acad Sci U S A* 2014;**111**:2247–52. https://doi.org/10.1073/pnas.1322269111.
65 Bain CC, Bravo-Blas A, Scott CL, Perdiguero EG, Geissmann F, Henri S, *et al.* Constant replenishment from circulating monocytes maintains the macrophage pool in the intestine of adult mice. *Nat Immunol* 2014;**15**:929–37. https://doi.org/10.1038/ni.2967.

66 Kang B, Alvarado LJ, Kim T, Lehmann ML, Cho H, He J, *et al.* Commensal microbiota drive the functional diversification of colon macrophages. *Mucosal Immunol* 2020;**13**:216–29. https://doi.org/10.1038/s41385-019-0228-3.
67 Riehl TE, Alvarado D, Ee X, Zuckerman A, Foster L, Kapoor V, *et al.* Lactobacillus rhamnosus GG protects the intestinal epithelium from radiation injury through release of lipoteichoic acid, macrophage activation and the migration of mesenchymal stem cells. *Gut* 2019;**68**:1003–13. https://doi.org/10.1136/gutjnl-2018-316226.
68 Kaji R, Kiyoshima-Shibata J, Nagaoka M, Nanno M, Shida K. Bacterial teichoic acids reverse predominant IL-12 production induced by certain lactobacillus strains into predominant IL-10 production via TLR2-dependent ERK activation in macrophages. *J Immunol* 2010;**184**:3505–13. https://doi.org/10.4049/jimmunol.0901569.
69 Platt AM, Bain CC, Bordon Y, Sester DP, Mowat AM. An independent subset of TLR expressing CCR2-dependent macrophages promotes colonic inflammation. *J Immunol* 2010;**184**:6843–54. https://doi.org/10.4049/jimmunol.0903987.
70 Ichikawa S, Miyake M, Fujii R, Konishi Y. MyD88 associated ROS generation is crucial for Lactobacillus induced IL-12 production in macrophage. *PLoS One* 2012;**7**:e35880. https://doi.org/10.1371/journal.pone.0035880.
71 Bakdash G, Vogelpoel LTC, van Capel TMM, Kapsenberg ML, de Jong EC. Retinoic acid primes human dendritic cells to induce gut-homing, IL-10-producing regulatory T cells. *Mucosal Immunol* 2015;**8**:265–78. https://doi.org/10.1038/mi.2014.64.
72 Qiang Y, Xu J, Yan C, Jin H, Xiao T, Yan N, *et al.* Butyrate and retinoic acid imprint mucosal-like dendritic cell development synergistically from bone marrow cells. *Clin Exp Immunol* 2017;**189**:290–7. https://doi.org/10.1111/cei.12990.
73 Kaisar MMM, Pelgrom LR, van der Ham AJ, Yazdanbakhsh M, Everts B. Butyrate Conditions Human Dendritic Cells to Prime Type 1 Regulatory T Cells via both Histone Deacetylase Inhibition and G Protein-Coupled Receptor 109A Signaling. *Front Immunol* 2017;**8**:1429. https://doi.org/10.3389/fimmu.2017.01429.
74 Uribe-Herranz M, Rafail S, Beghi S, Gil-de-Gómez L, Verginadis I, Bittinger K, *et al.* Gut microbiota modulate dendritic cell antigen presentation and radiotherapy-induced antitumor immune response. *J Clin Invest* 2020;**130**:466–79. https://doi.org/10.1172/JCI124332.
75 Gopalakrishnan V, Spencer CN, Nezi L, Reuben A, Andrews MC, Karpinets TV, *et al.* Gut microbiome modulates response to anti-PD-1 immunotherapy in melanoma patients. *Science* 2018;**359**:97–103. https://doi.org/10.1126/science.aan4236.
76 Routy B, Le Chatelier E, Derosa L, Duong CPM, Alou MT, Daillère R, *et al.* Gut microbiome influences efficacy of PD-1-based immunotherapy against epithelial tumors. *Science* 2018;**359**:91–7. https://doi.org/10.1126/science.aan3706.
77 Matson V, Fessler J, Bao R, Chongsuwat T, Zha Y, Alegre M-L, *et al.* The commensal microbiome is associated with anti-PD-1 efficacy in metastatic melanoma patients. *Science* 2018;**359**:104–8. https://doi.org/10.1126/science.aao3290.
78 Tanoue T, Morita S, Plichta DR, Skelly AN, Suda W, Sugiura Y, *et al.* A defined commensal consortium elicits CD8 T cells and anti-cancer immunity. *Nature* 2019;**565**:600–5. https://doi.org/10.1038/s41586-019-0878-z.
79 Sivan A, Corrales L, Hubert N, Williams JB, Aquino-Michaels K, Earley ZM, *et al.* Commensal Bifidobacterium promotes antitumor immunity and facilitates anti-PD-L1 efficacy. *Science* 2015;**350**:1084–9. https://doi.org/10.1126/science.aac4255.
80 Bessell CA, Isser A, Havel JJ, Lee S, Bell DR, Hickey JW, *et al.* Commensal bacteria stimulate antitumor responses via T cell cross-reactivity. *JCI Insight* 2020;**5**:. https://doi.org/10.1172/jci.insight.135597.
81 Si W, Liang H, Bugno J, Xu Q, Ding X, Yang K, *et al.* Lactobacillus rhamnosus GG induces cGAS/STING- dependent type I interferon and improves response to immune checkpoint blockade. *Gut* 2021. https://doi.org/10.1136/gutjnl-2020-323426.

82 Bachem A, Makhlouf C, Binger KJ, de Souza DP, Tull D, Hochheiser K, *et al.* Microbiota-Derived Short-Chain Fatty Acids Promote the Memory Potential of Antigen-Activated CD8+ T Cells. *Immunity* 2019;**51**:285-297.e5. https://doi.org/10.1016/j.immuni.2019.06.002.
83 Atarashi K, Tanoue T, Ando M, Kamada N, Nagano Y, Narushima S, *et al.* Th17 Cell Induction by Adhesion of Microbes to Intestinal Epithelial Cells. *Cell* 2015;**163**:367–80. https://doi.org/10.1016/j.cell.2015.08.058.
84 Ivanov II, Atarashi K, Manel N, Brodie EL, Shima T, Karaoz U, *et al.* Induction of intestinal Th17 cells by segmented filamentous bacteria. *Cell* 2009;**139**:485–98. https://doi.org/10.1016/j.cell.2009.09.033.
85 Wang J, Bhatia A, Krugliak Cleveland N, Gupta N, Dalal S, Rubin DT, *et al.* Rapid Onset of Inflammatory Bowel Disease after Receiving Secukinumab Infusion. *ACG Case Rep J* 2018;**5**:e56. https://doi.org/10.14309/crj.2018.56.
86 Hueber W, Sands BE, Lewitzky S, Vandemeulebroecke M, Reinisch W, Higgins PDR, *et al.* Secukinumab, a human anti-IL-17A monoclonal antibody, for moderate to severe Crohn's disease: unexpected results of a randomised, double-blind placebo-controlled trial. *Gut* 2012;**61**:1693–700. https://doi.org/10.1136/gutjnl-2011-301668.
87 Muranski P, Boni A, Antony PA, Cassard L, Irvine KR, Kaiser A, *et al.* Tumor-specific Th17-polarized cells eradicate large established melanoma. *Blood* 2008;**112**:362–73. https://doi.org/10.1182/blood-2007-11-120998.
88 Imani Fooladi AA, Yazdi MH, Pourmand MR, Mirshafiey A, Hassan ZM, Azizi T, *et al.* Th1 Cytokine Production Induced by Lactobacillus acidophilus in BALB/c Mice Bearing Transplanted Breast Tumor. *Jundishapur J Microbiol* 2015;**8**:e17354. https://doi.org/10.5812/jjm.8(4)2015.17354.
89 Ghadimi D, Fölster-Holst R, de Vrese M, Winkler P, Heller KJ, Schrezenmeir J. Effects of probiotic bacteria and their genomic DNA on TH1/TH2-cytokine production by peripheral blood mononuclear cells (PBMCs) of healthy and allergic subjects. *Immunobiology* 2008;**213**:677–92. https://doi.org/10.1016/j.imbio.2008.02.001.
90 Angelin A, Gil-de-Gómez L, Dahiya S, Jiao J, Guo L, Levine MH, *et al.* Foxp3 Reprograms T Cell Metabolism to Function in Low-Glucose, High-Lactate Environments. *Cell Metab* 2017;**25**:1282-1293.e7. https://doi.org/10.1016/j.cmet.2016.12.018.
91 Zhang X, Kelaria S, Kerstetter J, Wang J. The functional and prognostic implications of regulatory T cells in colorectal carcinoma. *J Gastrointest Oncol* 2015;**6**:307–13. https://doi.org/10.3978/j.issn.2078-6891.2015.017.
92 Cao Y, Wu K, Mehta R, Drew DA, Song M, Lochhead P, *et al.* Long-term use of antibiotics and risk of colorectal adenoma. *Gut* 2018;**67**:672–8. https://doi.org/10.1136/gutjnl-2016-313413.
93 Zhang J, Haines C, Watson AJM, Hart AR, Platt MJ, Pardoll DM, *et al.* Oral antibiotic use and risk of colorectal cancer in the United Kingdom, 1989-2012: a matched case-control study. *Gut* 2019;**68**:1971–8. https://doi.org/10.1136/gutjnl-2019-318593.
94 Gaines S, van Praagh JB, Williamson AJ, Jacobson RA, Hyoju S, Zaborin A, *et al.* Western Diet Promotes Intestinal Colonization by Collagenolytic Microbes and Promotes Tumor Formation After Colorectal Surgery. *Gastroenterology* 2020;**158**:958-970.e2. https://doi.org/10.1053/j.gastro.2019.10.020.
95 Abed J, Emgård JEM, Zamir G, Faroja M, Almogy G, Grenov A, *et al.* Fap2 Mediates Fusobacterium nucleatum Colorectal Adenocarcinoma Enrichment by Binding to Tumor-Expressed Gal-GalNAc. *Cell Host Microbe* 2016;**20**:215–25. https://doi.org/10.1016/j.chom.2016.07.006.
96 Gur C, Ibrahim Y, Isaacson B, Yamin R, Abed J, Gamliel M, *et al.* Binding of the Fap2 protein of Fusobacterium nucleatum to human inhibitory receptor TIGIT protects tumors from immune cell attack. *Immunity* 2015;**42**:344–55. https://doi.org/10.1016/j.immuni.2015.01.010.

97 Kostic AD, Chun E, Robertson L, Glickman JN, Gallini CA, Michaud M, *et al.* Fusobacterium nucleatum potentiates intestinal tumorigenesis and modulates the tumor-immune microenvironment. *Cell Host Microbe* 2013;**14**:207–15. https://doi.org/10.1016/j.chom.2013.07.007.
98 Mima K, Sukawa Y, Nishihara R, Qian ZR, Yamauchi M, Inamura K, *et al.* Fusobacterium nucleatum and T Cells in Colorectal Carcinoma. *JAMA Oncol* 2015;**1**:653–61. https://doi.org/10.1001/jamaoncol.2015.1377.
99 Rubinstein MR, Wang X, Liu W, Hao Y, Cai G, Han YW. Fusobacterium nucleatum promotes colorectal carcinogenesis by modulating E-cadherin/β-catenin signaling via its FadA adhesin. *Cell Host Microbe* 2013;**14**:195–206. https://doi.org/10.1016/j.chom.2013.07.012.
100 Salminen S, Ouwehand A, Benno Y, Lee YK. Probiotics: how should they be defined? *Trends in Food Science & Technology* 1999;**10**:107–10. https://doi.org/10.1016/S0924-2244(99)00027-8.
101 Goldin BR, Gualtieri LJ, Moore RP. The effect of Lactobacillus GG on the initiation and promotion of DMH-induced intestinal tumors in the rat. *Nutr Cancer* 1996;**25**:197–204. https://doi.org/10.1080/01635589609514442.
102 Femia AP, Luceri C, Dolara P, Giannini A, Biggeri A, Salvadori M, *et al.* Antitumorigenic activity of the prebiotic inulin enriched with oligofructose in combination with the probiotics Lactobacillus rhamnosus and Bifidobacterium lactis on azoxymethane-induced colon carcinogenesis in rats. *Carcinogenesis* 2002;**23**:1953–60. https://doi.org/10.1093/carcin/23.11.1953.
103 Lenoir M, Del Carmen S, Cortes-Perez NG, Lozano-Ojalvo D, Muñoz-Provencio D, Chain F, *et al.* Lactobacillus casei BL23 regulates Treg and Th17 T-cell populations and reduces DMH-associated colorectal cancer. *J Gastroenterol* 2016;**51**:862–73. https://doi.org/10.1007/s00535-015-1158-9.
104 McGarry JD, Brown NF. The mitochondrial carnitine palmitoyltransferase system. From concept to molecular analysis. *Eur J Biochem* 1997;**244**:1–14. https://doi.org/10.1111/j.1432-1033.1997.00001.x.
105 McGarry JD, Mannaerts GP, Foster DW. A possible role for malonyl-CoA in the regulation of hepatic fatty acid oxidation and ketogenesis. *J Clin Invest* 1977;**60**:265–70. https://doi.org/10.1172/JCI108764.
106 Ridaura VK, Faith JJ, Rey FE, Cheng J, Duncan AE, Kau AL, *et al.* Gut microbiota from twins discordant for obesity modulate metabolism in mice. *Science* 2013;**341**:1241214. https://doi.org/10.1126/science.1241214.
107 Suárez-Zamorano N, Fabbiano S, Chevalier C, Stojanović O, Colin DJ, Stevanović A, *et al.* Microbiota depletion promotes browning of white adipose tissue and reduces obesity. *Nat Med* 2015;**21**:1497–501. https://doi.org/10.1038/nm.3994.
108 Rabot S, Membrez M, Bruneau A, Gérard P, Harach T, Moser M, *et al.* Germ-free C57BL/6J mice are resistant to high-fat-diet-induced insulin resistance and have altered cholesterol metabolism. *FASEB J* 2010;**24**:4948–59. https://doi.org/10.1096/fj.10-164921.
109 Koh A, De Vadder F, Kovatcheva-Datchary P, Bäckhed F. From Dietary Fiber to Host Physiology: Short-Chain Fatty Acids as Key Bacterial Metabolites. *Cell* 2016;**165**:1332–45. https://doi.org/10.1016/j.cell.2016.05.041.
110 Yamashita H, Fujisawa K, Ito E, Idei S, Kawaguchi N, Kimoto M, *et al.* Improvement of obesity and glucose tolerance by acetate in Type 2 diabetic Otsuka Long-Evans Tokushima Fatty (OLETF) rats. *Biosci Biotechnol Biochem* 2007;**71**:1236–43. https://doi.org/10.1271/bbb.60668.
111 Gao Z, Yin J, Zhang J, Ward RE, Martin RJ, Lefevre M, *et al.* Butyrate improves insulin sensitivity and increases energy expenditure in mice. *Diabetes* 2009;**58**:1509–17. https://doi.org/10.2337/db08-1637.

112 De Vadder F, Kovatcheva-Datchary P, Goncalves D, Vinera J, Zitoun C, Duchampt A, *et al.* Microbiota-generated metabolites promote metabolic benefits via gut-brain neural circuits. *Cell* 2014;**156**:84–96. https://doi.org/10.1016/j.cell.2013.12.016.
113 Schwiertz A, Taras D, Schäfer K, Beijer S, Bos NA, Donus C, *et al.* Microbiota and SCFA in lean and overweight healthy subjects. *Obesity (Silver Spring)* 2010;**18**:190–5. https://doi.org/10.1038/oby.2009.167.
114 Ridlon JM, Kang D-J, Hylemon PB. Bile salt biotransformations by human intestinal bacteria. *J Lipid Res* 2006;**47**:241–59. https://doi.org/10.1194/jlr.R500013-JLR200.
115 Louis P, Flint HJ. Diversity, metabolism and microbial ecology of butyrate-producing bacteria from the human large intestine. *FEMS Microbiol Lett* 2009;**294**:1–8. https://doi.org/10.1111/j.1574-6968.2009.01514.x.
116 Cipriani S, Mencarelli A, Palladino G, Fiorucci S. FXR activation reverses insulin resistance and lipid abnormalities and protects against liver steatosis in Zucker (fa/fa) obese rats. *J Lipid Res* 2010;**51**:771–84. https://doi.org/10.1194/jlr.M001602.
117 Xie C, Jiang C, Shi J, Gao X, Sun D, Sun L, *et al.* An Intestinal Farnesoid X Receptor-Ceramide Signaling Axis Modulates Hepatic Gluconeogenesis in Mice. *Diabetes* 2017;**66**:613–26. https://doi.org/10.2337/db16-0663.
118 Wikoff WR, Anfora AT, Liu J, Schultz PG, Lesley SA, Peters EC, *et al.* Metabolomics analysis reveals large effects of gut microflora on mammalian blood metabolites. *Proc Natl Acad Sci U S A* 2009;**106**:3698–703. https://doi.org/10.1073/pnas.0812874106.
119 Cai S, Kandasamy M, Rahmat JN, Tham SM, Bay BH, Lee YK, *et al.* Lactobacillus rhamnosus GG Activation of Dendritic Cells and Neutrophils Depends on the Dose and Time of Exposure. *J Immunol Res* 2016;**2016**:7402760. https://doi.org/10.1155/2016/7402760.
120 Davidson LE, Fiorino A-M, Snydman DR, Hibberd PL. Lactobacillus GG as an immune adjuvant for live-attenuated influenza vaccine in healthy adults: a randomized double-blind placebo-controlled trial. *Eur J Clin Nutr* 2011;**65**:501–7. https://doi.org/10.1038/ejcn.2010.289.
121 Harata G, He F, Hiruta N, Kawase M, Kubota A, Hiramatsu M, *et al.* Intranasal administration of Lactobacillus rhamnosus GG protects mice from H1N1 influenza virus infection by regulating respiratory immune responses. *Lett Appl Microbiol* 2010;**50**:597–602. https://doi.org/10.1111/j.1472-765X.2010.02844.x.
122 Ni Y, Wong VHY, Tai WCS, Li J, Wong WY, Lee MML, *et al.* A metagenomic study of the preventive effect of Lactobacillus rhamnosus GG on intestinal polyp formation in ApcMin/+ mice. *J Appl Microbiol* 2017;**122**:770–84. https://doi.org/10.1111/jam.13386.
123 Siegel RL, Miller KD, Jemal A. Cancer statistics, 2019. *CA A Cancer J Clin* 2019;**69**:7–34. https://doi.org/10.3322/caac.21551.
124 Torre LA, Bray F, Siegel RL, Ferlay J, Lortet-Tieulent J, Jemal A. Global cancer statistics, 2012: Global Cancer Statistics, 2012. *CA: A Cancer Journal for Clinicians* 2015;**65**:87–108. https://doi.org/10.3322/caac.21262.
125 Arnold M, Sierra MS, Laversanne M, Soerjomataram I, Jemal A, Bray F. Global patterns and trends in colorectal cancer incidence and mortality. *Gut* 2017;**66**:683–91. https://doi.org/10.1136/gutjnl-2015-310912.
126 Overman MJ, Lonardi S, Wong KYM, Lenz H-J, Gelsomino F, Aglietta M, *et al.* Durable Clinical Benefit With Nivolumab Plus Ipilimumab in DNA Mismatch Repair-Deficient/Microsatellite Instability-High Metastatic Colorectal Cancer. *J Clin Oncol* 2018;**36**:773–9. https://doi.org/10.1200/JCO.2017.76.9901.
127 Overman MJ, Ernstoff MS, Morse MA. Where We Stand With Immunotherapy in Colorectal Cancer: Deficient Mismatch Repair, Proficient Mismatch Repair, and Toxicity Management. *Am Soc Clin Oncol Educ Book* 2018;**38**:239–47. https://doi.org/10.1200/EDBK_200821.

128 Brown SD, Warren RL, Gibb EA, Martin SD, Spinelli JJ, Nelson BH, *et al.* Neo-antigens predicted by tumor genome meta-analysis correlate with increased patient survival. *Genome Res* 2014;**24**:743–50. https://doi.org/10.1101/gr.165985.113.
129 Lennerz V, Fatho M, Gentilini C, Frye RA, Lifke A, Ferel D, *et al.* The response of autologous T cells to a human melanoma is dominated by mutated neoantigens. *Proc Natl Acad Sci U S A* 2005;**102**:16013–8. https://doi.org/10.1073/pnas.0500090102.
130 Schumacher TN, Schreiber RD. Neoantigens in cancer immunotherapy. *Science* 2015;**348**:69–74. https://doi.org/10.1126/science.aaa4971.
131 Roxburgh CSD, McMillan DC. The role of the in situ local inflammatory response in predicting recurrence and survival in patients with primary operable colorectal cancer. *Cancer Treat Rev* 2012;**38**:451–66. https://doi.org/10.1016/j.ctrv.2011.09.001.
132 Gryfe R, Kim H, Hsieh ET, Aronson MD, Holowaty EJ, Bull SB, *et al.* Tumor microsatellite instability and clinical outcome in young patients with colorectal cancer. *N Engl J Med* 2000;**342**:69–77. https://doi.org/10.1056/NEJM200001133420201.
133 Galon J, Costes A, Sanchez-Cabo F, Kirilovsky A, Mlecnik B, Lagorce-Pagès C, *et al.* Type, density, and location of immune cells within human colorectal tumors predict clinical outcome. *Science* 2006;**313**:1960–4. https://doi.org/10.1126/science.1129139.
134 Naito Y, Saito K, Shiiba K, Ohuchi A, Saigenji K, Nagura H, *et al.* CD8+ T cells infiltrated within cancer cell nests as a prognostic factor in human colorectal cancer. *Cancer Res* 1998;**58**:3491–4.
135 Jansen CS, Prokhnevska N, Master VA, Sanda MG, Carlisle JW, Bilen MA, *et al.* An intra-tumoral niche maintains and differentiates stem-like CD8 T cells. *Nature* 2019;**576**:465–70. https://doi.org/10.1038/s41586-019-1836-5.
136 Jia L, Wu R, Han N, Fu J, Luo Z, Guo L, *et al.* Porphyromonas gingivalis and Lactobacillus rhamnosus GG regulate the Th17/Treg balance in colitis via TLR4 and TLR2. *Clin Transl Immunology* 2020;**9**:e1213. https://doi.org/10.1002/cti2.1213.
137 Mirpuri J, Sotnikov I, Myers L, Denning TL, Yarovinsky F, Parkos CA, *et al.* Lactobacillus rhamnosus (LGG) regulates IL-10 signaling in the developing murine colon through upregulation of the IL-10R2 receptor subunit. *PLoS One* 2012;**7**:e51955. https://doi.org/10.1371/journal.pone.0051955.
138 Wang B, Wu Y, Liu R, Xu H, Mei X, Shang Q, *et al.* Lactobacillus rhamnosus GG promotes M1 polarization in murine bone marrow-derived macrophages by activating TLR2/MyD88/MAPK signaling pathway. *Anim Sci J* 2020;**91**:e13439. https://doi.org/10.1111/asj.13439.
139 Wang Y, Liu L, Moore DJ, Shen X, Peek RM, Acra SA, *et al.* An LGG-derived protein promotes IgA production through upregulation of APRIL expression in intestinal epithelial cells. *Mucosal Immunol* 2017;**10**:373–84. https://doi.org/10.1038/mi.2016.57.
140 Saeedi BJ, Liu KH, Owens JA, Hunter-Chang S, Camacho MC, Eboka RU, *et al.* Gut-Resident Lactobacilli Activate Hepatic Nrf2 and Protect Against Oxidative Liver Injury. *Cell Metab* 2020. https://doi.org/10.1016/j.cmet.2020.03.006.
141 Darby TM, Owens JA, Saeedi BJ, Luo L, Matthews JD, Robinson BS, *et al.* Lactococcus Lactis Subsp. cremoris Is an Efficacious Beneficial Bacterium that Limits Tissue Injury in the Intestine. *IScience* 2019;**12**:356–67. https://doi.org/10.1016/j.isci.2019.01.030.
142 Owens JA, Jones RM. Immune Cell Isolation from Murine Intestine for Antibody Array Analysis. *Methods Mol Biol* 2021;**2237**:247–56. https://doi.org/10.1007/978-1-0716-1064-0_21.
143 Henry CJ, Grayson JM, Brzoza-Lewis KL, Mitchell LM, Westcott MM, Cook AS, *et al.* The roles of IL-12 and IL-23 in CD8+ T cell-mediated immunity against Listeria monocytogenes: Insights from a DC vaccination model. *Cell Immunol* 2010;**264**:23–31. https://doi.org/10.1016/j.cellimm.2010.04.007.

144 Kucherlapati MH, Lee K, Nguyen AA, Clark AB, Hou H, Rosulek A, *et al.* An Msh2 conditional knockout mouse for studying intestinal cancer and testing anticancer agents. *Gastroenterology* 2010;**138**:993-1002.e1. https://doi.org/10.1053/j.gastro.2009.11.009.
145 Popivanova BK, Kitamura K, Wu Y, Kondo T, Kagaya T, Kaneko S, *et al.* Blocking TNF-alpha in mice reduces colorectal carcinogenesis associated with chronic colitis. *J Clin Invest* 2008;**118**:560–70. https://doi.org/10.1172/JCI32453.
146 Zhang Z, Zhou Z, Li Y, Zhou L, Ding Q, Xu L. Isolated exopolysaccharides from Lactobacillus rhamnosus GG alleviated adipogenesis mediated by TLR2 in mice. *Sci Rep* 2016;**6**:36083. https://doi.org/10.1038/srep36083.
147 Ryu S-H, Park J-H, Choi S-Y, Jeon H-Y, Park J-I, Kim J-Y, *et al.* The Probiotic Lactobacillus Prevents Citrobacter rodentium-Induced Murine Colitis in a TLR2-Dependent Manner. *J Microbiol Biotechnol* 2016;**26**:1333–40. https://doi.org/10.4014/jmb.1602.02004.
148 de Miranda NFCC, Goudkade D, Jordanova ES, Tops CMJ, Hes FJ, Vasen HFA, *et al.* Infiltration of Lynch colorectal cancers by activated immune cells associates with early staging of the primary tumor and absence of lymph node metastases. *Clin Cancer Res* 2012;**18**:1237–45. https://doi.org/10.1158/1078-0432.CCR-11-1997.
149 Femia AP, Luceri C, Dolara P, Giannini A, Biggeri A, Salvadori M, *et al.* Antitumorigenic activity of the prebiotic inulin enriched with oligofructose in combination with the probiotics Lactobacillus rhamnosus and Bifidobacterium lactis on azoxymethane-induced colon carcinogenesis in rats. *Carcinogenesis* 2002;**23**:1953–60. https://doi.org/10.1093/carcin/23.11.1953.
150 Gamallat Y, Meyiah A, Kuugbee ED, Hago AM, Chiwala G, Awadasseid A, *et al.* Lactobacillus rhamnosus induced epithelial cell apoptosis, ameliorates inflammation and prevents colon cancer development in an animal model. *Biomed Pharmacother* 2016;**83**:536–41. https://doi.org/10.1016/j.biopha.2016.07.001.
151 Walia S, Kamal R, Dhawan DK, Kanwar SS. Chemoprevention by Probiotics During 1,2-Dimethylhydrazine-Induced Colon Carcinogenesis in Rats. *Dig Dis Sci* 2018;**63**:900–9. https://doi.org/10.1007/s10620-018-4949-z.
152 Lee S-H, Cho S-Y, Yoon Y, Park C, Sohn J, Jeong J-J, *et al.* Bifidobacterium bifidum strains synergize with immune checkpoint inhibitors to reduce tumour burden in mice. *Nat Microbiol* 2021. https://doi.org/10.1038/s41564-020-00831-6.
153 Ciorba MA, Riehl TE, Rao MS, Moon C, Ee X, Nava GM, *et al.* Lactobacillus probiotic protects intestinal epithelium from radiation injury in a TLR-2/cyclo-oxygenase-2-dependent manner. *Gut* 2012;**61**:829–38. https://doi.org/10.1136/gutjnl-2011-300367.
154 Zhuo Q, Yu B, Zhou J, Zhang J, Zhang R, Xie J, *et al.* Lysates of Lactobacillus acidophilus combined with CTLA-4-blocking antibodies enhance antitumor immunity in a mouse colon cancer model. *Sci Rep* 2019;**9**:20128. https://doi.org/10.1038/s41598-019-56661-y.
155 Salminen MK, Tynkkynen S, Rautelin H, Saxelin M, Vaara M, Ruutu P, *et al.* Lactobacillus bacteremia during a rapid increase in probiotic use of Lactobacillus rhamnosus GG in Finland. *Clin Infect Dis* 2002;**35**:1155–60. https://doi.org/10.1086/342912.
156 Miranda JJ, Barrientos-Gutiérrez T, Corvalan C, Hyder AA, Lazo-Porras M, Oni T, *et al.* Understanding the rise of cardiometabolic diseases in low- and middle-income countries. *Nat Med* 2019;**25**:1667–79. https://doi.org/10.1038/s41591-019-0644-7.
157 Wang Y, Beydoun MA, Min J, Xue H, Kaminsky LA, Cheskin LJ. Has the prevalence of overweight, obesity and central obesity levelled off in the United States? Trends, patterns, disparities, and future projections for the obesity epidemic. *International Journal of Epidemiology* 2020;**49**:810–23. https://doi.org/10.1093/ije/dyz273.
158 Carding S, Verbeke K, Vipond DT, Corfe BM, Owen LJ. Dysbiosis of the gut microbiota in disease. *Microb Ecol Health Dis* 2015;**26**:26191. https://doi.org/10.3402/mehd.v26.26191.

159 Rosenbaum M, Knight R, Leibel RL. The gut microbiota in human energy homeostasis and obesity. *Trends in Endocrinology & Metabolism* 2015;**26**:493–501. https://doi.org/10.1016/j.tem.2015.07.002.
160 Ignacio A, Fernandes MR, Rodrigues VAA, Groppo FC, Cardoso AL, Avila-Campos MJ, *et al.* Correlation between body mass index and faecal microbiota from children. *Clinical Microbiology and Infection* 2016;**22**:258.e1-258.e8. https://doi.org/10.1016/j.cmi.2015.10.031.
161 Gonzalez FJ, Jiang C, Patterson AD. An Intestinal Microbiota–Farnesoid X Receptor Axis Modulates Metabolic Disease. *Gastroenterology* 2016;**151**:845–59. https://doi.org/10.1053/j.gastro.2016.08.057.
162 San-Cristobal R, Navas-Carretero S, Martínez-González MÁ, Ordovas JM, Martínez JA. Contribution of macronutrients to obesity: implications for precision nutrition. *Nat Rev Endocrinol* 2020;**16**:305–20. https://doi.org/10.1038/s41574-020-0346-8.
163 Holmes E, Li JV, Athanasiou T, Ashrafian H, Nicholson JK. Understanding the role of gut microbiome–host metabolic signal disruption in health and disease. *Trends in Microbiology* 2011;**19**:349–59. https://doi.org/10.1016/j.tim.2011.05.006.
164 Spanogiannopoulos P, Bess EN, Carmody RN, Turnbaugh PJ. The microbial pharmacists within us: a metagenomic view of xenobiotic metabolism. *Nat Rev Microbiol* 2016;**14**:273–87. https://doi.org/10.1038/nrmicro.2016.17.
165 Cani PD, Amar J, Iglesias MA, Poggi M, Knauf C, Bastelica D, *et al.* Metabolic Endotoxemia Initiates Obesity and Insulin Resistance. *Diabetes* 2007;**56**:1761–72. https://doi.org/10.2337/db06-1491.
166 Hoyles L, Fernández-Real J-M, Federici M, Serino M, Abbott J, Charpentier J, *et al.* Molecular phenomics and metagenomics of hepatic steatosis in non-diabetic obese women. *Nat Med* 2018;**24**:1070–80. https://doi.org/10.1038/s41591-018-0061-3.
167 Wang Z, Klipfell E, Bennett BJ, Koeth R, Levison BS, DuGar B, *et al.* Gut flora metabolism of phosphatidylcholine promotes cardiovascular disease. *Nature* 2011;**472**:57–63. https://doi.org/10.1038/nature09922.
168 Koeth RA, Wang Z, Levison BS, Buffa JA, Org E, Sheehy BT, *et al.* Intestinal microbiota metabolism of l-carnitine, a nutrient in red meat, promotes atherosclerosis. *Nat Med* 2013;**19**:576–85. https://doi.org/10.1038/nm.3145.
169 Cani PD, Bibiloni R, Knauf C, Waget A, Neyrinck AM, Delzenne NM, *et al.* Changes in Gut Microbiota Control Metabolic Endotoxemia-Induced Inflammation in High-Fat Diet-Induced Obesity and Diabetes in Mice. *Diabetes* 2008;**57**:1470–81. https://doi.org/10.2337/db07-1403.
170 Peisl BYL, Schymanski EL, Wilmes P. Dark matter in host-microbiome metabolomics: Tackling the unknowns–A review. *Analytica Chimica Acta* 2018;**1037**:13–27. https://doi.org/10.1016/j.aca.2017.12.034.
171 Goo E, An JH, Kang Y, Hwang I. Control of bacterial metabolism by quorum sensing. *Trends Microbiol* 2015;**23**:567–76. https://doi.org/10.1016/j.tim.2015.05.007.
172 Bajpai P, Darra A, Agrawal A. Microbe-mitochondrion crosstalk and health: An emerging paradigm. *Mitochondrion* 2018;**39**:20–5. https://doi.org/10.1016/j.mito.2017.08.008.
173 Mollica MP, Mattace Raso G, Cavaliere G, Trinchese G, De Filippo C, Aceto S, *et al.* Butyrate Regulates Liver Mitochondrial Function, Efficiency, and Dynamics in Insulin-Resistant Obese Mice. *Diabetes* 2017;**66**:1405–18. https://doi.org/10.2337/db16-0924.
174 Yardeni T, Tanes CE, Bittinger K, Mattei LM, Schaefer PM, Singh LN, *et al.* Host mitochondria influence gut microbiome diversity: A role for ROS. *Sci Signal* 2019;**12**:eaaw3159. https://doi.org/10.1126/scisignal.aaw3159.
175 Go Y-M, Uppal K, Walker DI, Tran V, Dury L, Strobel FH, *et al.* Mitochondrial Metabolomics Using High-Resolution Fourier-Transform Mass Spectrometry. In: Raftery D, editor. *Mass Spectrometry in Metabolomics*, vol. 1198. New York, NY: Springer New York; 2014. p. 43–73.

176 Liu KH, Walker DI, Uppal K, Tran V, Rohrbeck P, Mallon TM, *et al.* High-Resolution Metabolomics Assessment of Military Personnel: Evaluating Analytical Strategies for Chemical Detection. *Journal of Occupational & Environmental Medicine* 2016;**58**:S53–61. https://doi.org/10.1097/JOM.0000000000000773.
177 Yu T, Jones DP. Improving peak detection in high-resolution LC/MS metabolomics data using preexisting knowledge and machine learning approach. *Bioinformatics* 2014;**30**:2941–8. https://doi.org/10.1093/bioinformatics/btu430.
178 Yu T, Park Y, Johnson JM, Jones DP. apLCMS—adaptive processing of high-resolution LC/MS data. *Bioinformatics* 2009;**25**:1930–6. https://doi.org/10.1093/bioinformatics/btp291.
179 Uppal K, Soltow QA, Strobel FH, Pittard WS, Gernert KM, Yu T, *et al.* xMSanalyzer: automated pipeline for improved feature detection and downstream analysis of large-scale, non-targeted metabolomics data. *BMC Bioinformatics* 2013;**14**:15. https://doi.org/10.1186/1471-2105-14-15.
180 Ritchie ME, Phipson B, Wu D, Hu Y, Law CW, Shi W, *et al.* limma powers differential expression analyses for RNA-sequencing and microarray studies. *Nucleic Acids Research* 2015;**43**:e47–e47. https://doi.org/10.1093/nar/gkv007.
181 Li S, Park Y, Duraisingham S, Strobel FH, Khan N, Soltow QA, *et al.* Predicting Network Activity from High Throughput Metabolomics. *PLoS Comput Biol* 2013;**9**:e1003123. https://doi.org/10.1371/journal.pcbi.1003123.
182 Liu KH, Nellis M, Uppal K, Ma C, Tran V, Liang Y, *et al.* Reference Standardization for Quantification and Harmonization of Large-Scale Metabolomics. *Anal Chem* 2020;**92**:8836–44. https://doi.org/10.1021/acs.analchem.0c00338.
183 Smith CA, O'Maille G, Want EJ, Qin C, Trauger SA, Brandon TR, *et al.* METLIN: a metabolite mass spectral database. *Ther Drug Monit* 2005;**27**:747–51. https://doi.org/10.1097/01.ftd.0000179845.53213.39.
184 Ruttkies C, Schymanski EL, Wolf S, Hollender J, Neumann S. MetFrag relaunched: incorporating strategies beyond in silico fragmentation. *J Cheminform* 2016;**8**:3. https://doi.org/10.1186/s13321-016-0115-9.
185 Tars K, Leitans J, Kazaks A, Zelencova D, Liepinsh E, Kuka J, *et al.* Targeting Carnitine Biosynthesis: Discovery of New Inhibitors against γ-Butyrobetaine Hydroxylase. *J Med Chem* 2014;**57**:2213–36. https://doi.org/10.1021/jm401603e.
186 Chen FCM, Benoiton NL. A new method of quaternizing amines and its use in amino acid and peptide chemistry. *Can J Chem* 1976;**54**:3310–1. https://doi.org/10.1139/v76-475.
187 Cioffi C, Vos MB. Su1506 - Comparison of Plasma Metabolomics Profiles of Pediatric NASH vs. NAFLD. *Gastroenterology* 2018;**154**:S-1161. https://doi.org/10.1016/S0016-5085(18)33847-2.
188 Rask KJ, Brigham KL, Johns MME. Integrating comparative effectiveness research programs into predictive health: a unique role for academic health centers. *Acad Med* 2011;**86**:718–23. https://doi.org/10.1097/ACM.0b013e318217ea6c.
189 Brigham KL. Predictive health: the imminent revolution in health care. *J Am Geriatr Soc* 2010;**58 Suppl 2**:S298-302. https://doi.org/10.1111/j.1532-5415.2010.03107.x.
190 Soltow QA, Strobel FH, Mansfield KG, Wachtman L, Park Y, Jones DP. High-performance metabolic profiling with dual chromatography-Fourier-transform mass spectrometry (DC-FTMS) for study of the exposome. *Metabolomics* 2013;**9**:132–43. https://doi.org/10.1007/s11306-011-0332-1.
191 Matthews DR, Hosker JP, Rudenski AS, Naylor BA, Treacher DF, Turner RC. Homeostasis model assessment: insulin resistance and beta-cell function from fasting plasma glucose and insulin concentrations in man. *Diabetologia* 1985;**28**:412–9. https://doi.org/10.1007/BF00280883.

192 Bäckhed F, Manchester JK, Semenkovich CF, Gordon JI. Mechanisms underlying the resistance to diet-induced obesity in germ-free mice. *Proc Natl Acad Sci U S A* 2007;**104**:979–84. https://doi.org/10.1073/pnas.0605374104.
193 Mølstad P. The efflux of L-carnitine from cells in culture (CCL 27). *Biochim Biophys Acta* 1980;**597**:166–73. https://doi.org/10.1016/0005-2736(80)90160-1.
194 Ringseis R, Keller J, Eder K. Role of carnitine in the regulation of glucose homeostasis and insulin sensitivity: evidence from in vivo and in vitro studies with carnitine supplementation and carnitine deficiency. *Eur J Nutr* 2012;**51**:1–18. https://doi.org/10.1007/s00394-011-0284-2.
195 Fritz IB. Action of carnitine on long chain fatty acid oxidation by liver. *Am J Physiol* 1959;**197**:297–304. https://doi.org/10.1152/ajplegacy.1959.197.2.297.
196 Noland RC, Koves TR, Seiler SE, Lum H, Lust RM, Ilkayeva O, *et al.* Carnitine insufficiency caused by aging and overnutrition compromises mitochondrial performance and metabolic control. *J Biol Chem* 2009;**284**:22840–52. https://doi.org/10.1074/jbc.M109.032888.
197 Bianchi PB, Lehotay DC, Davis AT. Carnitine supplementation ameliorates the steatosis and ketosis induced by pivalate in rats. *J Nutr* 1996;**126**:2873–9. https://doi.org/10.1093/jn/126.11.2873.
198 Asai T, Okumura K, Takahashi R, Matsui H, Numaguchi Y, Murakami H, *et al.* Combined therapy with PPARα agonist and l-carnitine rescues lipotoxic cardiomyopathy due to systemic carnitine deficiency. *Cardiovascular Research* 2006;**70**:566–77. https://doi.org/10.1016/j.cardiores.2006.02.005.
199 Jiang F, Zhang Z, Zhang Y, Wu J, Yu L, Liu S. L-carnitine ameliorates the liver inflammatory response by regulating carnitine palmitoyltransferase I-dependent PPARγ signaling. *Molecular Medicine Reports* 2016;**13**:1320–8. https://doi.org/10.3892/mmr.2015.4639.
200 Libert DM, Nowacki AS, Natowicz MR. Metabolomic analysis of obesity, metabolic syndrome, and type 2 diabetes: amino acid and acylcarnitine levels change along a spectrum of metabolic wellness. *PeerJ* 2018;**6**:e5410. https://doi.org/10.7717/peerj.5410.
201 Koves TR, Ussher JR, Noland RC, Slentz D, Mosedale M, Ilkayeva O, *et al.* Mitochondrial Overload and Incomplete Fatty Acid Oxidation Contribute to Skeletal Muscle Insulin Resistance. *Cell Metabolism* 2008;**7**:45–56. https://doi.org/10.1016/j.cmet.2007.10.013.
202 Spaniol M, Kaufmann P, Beier K, Wüthrich J, Török M, Scharnagl H, *et al.* Mechanisms of liver steatosis in rats with systemic carnitine deficiency due to treatment with trimethylhydraziniumpropionate. *Journal of Lipid Research* 2003;**44**:144–53. https://doi.org/10.1194/jlr.M200200-JLR200.
203 Kärkkäinen O, Lankinen MA, Vitale M, Jokkala J, Leppänen J, Koistinen V, *et al.* Diets rich in whole grains increase betainized compounds associated with glucose metabolism. *Am J Clin Nutr* 2018;**108**:971–9. https://doi.org/10.1093/ajcn/nqy169.
204 Servillo L, D'Onofrio N, Giovane A, Casale R, Cautela D, Castaldo D, *et al.* Ruminant meat and milk contain δ-valerobetaine, another precursor of trimethylamine N-oxide (TMAO) like γ-butyrobetaine. *Food Chemistry* 2018;**260**:193–9. https://doi.org/10.1016/j.foodchem.2018.03.114.
205 Servillo L, D'Onofrio N, Neglia G, Casale R, Cautela D, Marrelli M, *et al.* Carnitine Precursors and Short-Chain Acylcarnitines in Water Buffalo Milk. *J Agric Food Chem* 2018;**66**:8142–9. https://doi.org/10.1021/acs.jafc.8b02963.
206 Wang Y, Beydoun MA. Meat consumption is associated with obesity and central obesity among US adults. *Int J Obes* 2009;**33**:621–8. https://doi.org/10.1038/ijo.2009.45.
207 Li XS, Wang Z, Cajka T, Buffa JA, Nemet I, Hurd AG, *et al.* Untargeted metabolomics identifies trimethyllysine, a TMAO-producing nutrient precursor, as a predictor of incident cardiovascular disease risk. *JCI Insight* 2018;**3**:e99096. https://doi.org/10.1172/jci.insight.99096.

208 Ye EQ, Chacko SA, Chou EL, Kugizaki M, Liu S. Greater whole-grain intake is associated with lower risk of type 2 diabetes, cardiovascular disease, and weight gain. *J Nutr* 2012;**142**:1304–13. https://doi.org/10.3945/jn.111.155325.
209 Zhao M, Zhao L, Xiong X, He Y, Huang W, Liu Z, *et al.* TMAVA, a Metabolite of Intestinal Microbes, Is Increased in Plasma From Patients With Liver Steatosis, Inhibits γ-Butyrobetaine Hydroxylase, and Exacerbates Fatty Liver in Mice. *Gastroenterology* 2020;**158**:2266-2281.e27. https://doi.org/10.1053/j.gastro.2020.02.033.
210 Sagan L. On the origin of mitosing cells. *J Theor Biol* 1967;**14**:255–74. https://doi.org/10.1016/0022-5193(67)90079-3.
211 Ristow M. Unraveling the Truth About Antioxidants: Mitohormesis explains ROS-induced health benefits. *Nat Med* 2014;**20**:709–11. https://doi.org/10.1038/nm.3624.
212 Khan SA, Sathyanarayan A, Mashek MT, Ong KT, Wollaston-Hayden EE, Mashek DG. ATGL-Catalyzed Lipolysis Regulates SIRT1 to Control PGC-1α/PPAR-α Signaling. *Diabetes* 2015;**64**:418–26. https://doi.org/10.2337/db14-0325.
213 Montagner A, Polizzi A, Fouché E, Ducheix S, Lippi Y, Lasserre F, *et al.* Liver PPARα is crucial for whole-body fatty acid homeostasis and is protective against NAFLD. *Gut* 2016;**65**:1202–14. https://doi.org/10.1136/gutjnl-2015-310798.
214 Azevedo RA, Arruda P. High-lysine maize: the key discoveries that have made it possible. *Amino Acids* 2010;**39**:979–89. https://doi.org/10.1007/s00726-010-0576-5.
215 Escamilla J, Lane MA, Maitin V. Cell-free supernatants from probiotic Lactobacillus casei and Lactobacillus rhamnosus GG decrease colon cancer cell invasion in vitro. *Nutr Cancer* 2012;**64**:871–8. https://doi.org/10.1080/01635581.2012.700758.
216 Roller M, Clune Y, Collins K, Rechkemmer G, Watzl B. Consumption of prebiotic inulin enriched with oligofructose in combination with the probiotics Lactobacillus rhamnosus and Bifidobacterium lactis has minor effects on selected immune parameters in polypectomised and colon cancer patients. *Br J Nutr* 2007;**97**:676–84. https://doi.org/10.1017/S0007114507450292.
217 Baruch EN, Youngster I, Ben-Betzalel G, Ortenberg R, Lahat A, Katz L, *et al.* Fecal microbiota transplant promotes response in immunotherapy-refractory melanoma patients. *Science* 2021;**371**:602–9. https://doi.org/10.1126/science.abb5920.
218 Mager LF, Burkhard R, Pett N, Cooke NCA, Brown K, Ramay H, *et al.* Microbiome-derived inosine modulates response to checkpoint inhibitor immunotherapy. *Science* 2020;**369**:1481–9. https://doi.org/10.1126/science.abc3421.
219 Yan F, Liu L, Cao H, Moore DJ, Washington MK, Wang B, *et al.* Neonatal colonization of mice with LGG promotes intestinal development and decreases susceptibility to colitis in adulthood. *Mucosal Immunol* 2017;**10**:117–27. https://doi.org/10.1038/mi.2016.43.
220 Schwarze K, Buchanan J, Fermont JM, Dreau H, Tilley MW, Taylor JM, *et al.* The complete costs of genome sequencing: a microcosting study in cancer and rare diseases from a single center in the United Kingdom. *Genet Med* 2020;**22**:85–94. https://doi.org/10.1038/s41436-019-0618-7.
221 Hwang S, Kwon A-Y, Jeong J-Y, Kim S, Kang H, Park J, *et al.* Immune gene signatures for predicting durable clinical benefit of anti-PD-1 immunotherapy in patients with non-small cell lung cancer. *Sci Rep* 2020;**10**:643. https://doi.org/10.1038/s41598-019-57218-9.
222 Sehgal K, Portell A, Ivanova EV, Lizotte PH, Mahadevan NR, Greene JR, *et al.* Dynamic single-cell RNA sequencing identifies immunotherapy persister cells following PD-1 blockade. *J Clin Invest* 2021;**131**:. https://doi.org/10.1172/JCI135038.
223 Wisdom AJ, Mowery YM, Hong CS, Himes JE, Nabet BY, Qin X, *et al.* Single cell analysis reveals distinct immune landscapes in transplant and primary sarcomas that determine response or resistance to immunotherapy. *Nat Commun* 2020;**11**:6410. https://doi.org/10.1038/s41467-020-19917-0.

224 Tang Z-Z, Chen G, Hong Q, Huang S, Smith HM, Shah RD, *et al.* Multi-Omic Analysis of the Microbiome and Metabolome in Healthy Subjects Reveals Microbiome-Dependent Relationships Between Diet and Metabolites. *Front Genet* 2019;**10**:454. https://doi.org/10.3389/fgene.2019.00454.
225 Kurilshikov A, van den Munckhof ICL, Chen L, Bonder MJ, Schraa K, Rutten JHW, *et al.* Gut Microbial Associations to Plasma Metabolites Linked to Cardiovascular Phenotypes and Risk. *Circ Res* 2019;**124**:1808–20. https://doi.org/10.1161/CIRCRESAHA.118.314642.
226 Agus A, Clément K, Sokol H. Gut microbiota-derived metabolites as central regulators in metabolic disorders. *Gut* 2021;**70**:1174–82. https://doi.org/10.1136/gutjnl-2020-323071.
227 Mallick H, Franzosa EA, Mclver LJ, Banerjee S, Sirota-Madi A, Kostic AD, *et al.* Predictive metabolomic profiling of microbial communities using amplicon or metagenomic sequences. *Nat Commun* 2019;**10**:3136. https://doi.org/10.1038/s41467-019-10927-1.
228 Piya MK, McTernan PG, Kumar S. Adipokine inflammation and insulin resistance: the role of glucose, lipids and endotoxin. *Journal of Endocrinology* 2013;**216**:T1–15. https://doi.org/10.1530/JOE-12-0498.
229 Turnbaugh PJ, Ley RE, Mahowald MA, Magrini V, Mardis ER, Gordon JI. An obesity-associated gut microbiome with increased capacity for energy harvest. *Nature* 2006;**444**:1027–31. https://doi.org/10.1038/nature05414.
230 Samuel BS, Shaito A, Motoike T, Rey FE, Backhed F, Manchester JK, *et al.* Effects of the gut microbiota on host adiposity are modulated by the short-chain fatty-acid binding G protein-coupled receptor, Gpr41. *Proceedings of the National Academy of Sciences* 2008;**105**:16767–72. https://doi.org/10.1073/pnas.0808567105.
231 Huang S, Frizzi A, Florida CA, Kruger DE, Luethy MH. High lysine and high tryptophan transgenic maize resulting from the reduction of both 19- and 22-kD alpha-zeins. *Plant Mol Biol* 2006;**61**:525–35. https://doi.org/10.1007/s11103-006-0027-6.
232 Yatsunenko T, Rey FE, Manary MJ, Trehan I, Dominguez-Bello MG, Contreras M, *et al.* Human gut microbiome viewed across age and geography. *Nature* 2012;**486**:222–7. https://doi.org/10.1038/nature11053.
233 David LA, Maurice CF, Carmody RN, Gootenberg DB, Button JE, Wolfe BE, *et al.* Diet rapidly and reproducibly alters the human gut microbiome. *Nature* 2014;**505**:559–63. https://doi.org/10.1038/nature12820.
234 Saeedi BJ, Liu KH, Owens JA, Hunter-Chang S, Camacho MC, Eboka RU, *et al.* Gut-Resident Lactobacilli Activate Hepatic Nrf2 and Protect Against Oxidative Liver Injury. *Cell Metab* 2020;**31**:956-968.e5. https://doi.org/10.1016/j.cmet.2020.03.006.
235 Valles-Colomer M, Falony G, Darzi Y, Tigchelaar EF, Wang J, Tito RY, *et al.* The neuroactive potential of the human gut microbiota in quality of life and depression. *Nat Microbiol* 2019;**4**:623–32. https://doi.org/10.1038/s41564-018-0337-x.